Advances in Anatomy Embryology and Cell Biology

Vol. 70

Walter Pfaller

Structure Function Correlation on Rat Kidney

Quantitative Correlation of Structure and Function in the Normal and Injured Rat Kidney

With 23 Figures

Springer-Verlag
Berlin Heidelberg New York 1982

Dr. Walter Pfaller
Institut für Physiologie und
Balneologie der Universität Innsbruck
Fritz-Pregl-Straße 3
A-6010 Innsbruck
Österreich

ISBN-13:978-3-540-11074-3 e-ISBN-13:978-3-642-68287-2
DOI: 10.1007/978-3-642-68287-2

Composition: Schreibsatz Service Weihrauch, Würzburg

2121/3321-543210

Contents

Abbreviations Used in Figures

BB – brush border (microvilli)
BL – basolateral membrane
ECS – extracellular space
Gly – glycogen
Gol – golgi apparatus
LD – lipid droplets
LM – luminal membrane
Mi – mitochondria
MF – myelin figures
Nuc – nucleus
Per – peroxisomes
PNC – perinuclear cisternae
rER – rough endoplasmic reticulum
sER – smooth endoplasmic reticulum
V – vacuoles

1 Introduction

Over the past few decades an exceedingly large number of experimental and clinical investigations have been performed in an attempt to analyze the way in which the kidney functions. The basis for all this work was established during the nineteenth and the early twentieth century by morphologists (Bowman 1842; Hyrtl 1863, 1872; Heidenhain 1874; Peter 1909; von Möllendorf 1930). All these investigators clearly outlined the extremely heterogeneous assembly of renal tissue and also defined the nephron as the smallest morphological unit. It was further the merit of these anatomists and histologists to preclude quite a number of nephron functions based merely on their careful observations. Contemporary histologists have been able to add little to these observations. Unfortunately with the introduction of physiologic in vivo et situ studies on kidneys the interest in heterogeneity waned. This lack of attention was aggravated by the introduction of the clearance techniques which cannot account for regional differences in the function of the smallest unit, the nephron. That anatomic heterogeneity has a functional correlate was strongly suggested by Trueta et al. (1947) and vigorously stimulated a number of studies. The development of physiologic microtechniques, like micropuncture and microperfusion of single nephrons, or the perfusion of isolated nephron portions and electrophysiologic studies, enormously expanded our knowledge concerning details regarding nephron and total renal function. The possibility of applying biochemical technology to dissected single nephrons, or portions of them, provided insight into the enzymatic and metabolic machinery responsible for specific functions. New basic discoveries regarding renal function, and the demand for knowledge of their structural correlates, have incited morphologists to be more precise about renal structure, segmentation of nephrons and the topography of nephrons and vasculature. The application of modern morphological tools such as electron microscopy, histo- and cytochemistry have thrown new light upon some of the older and classical descriptions of renal structure, and quite a number of well-known morphological characteristics have assumed new significance. In context with new data on renal function it became clear fairly soon that specific subcellular features are linked to certain functional characteristics. For example, nephron portions with different reabsorptive or secretory capacity are characterized by differences in their subcellular architecture with regard to the number of mitochondria they possess or the differentiation of their cell surfaces. These investigations strengthen the opinion that function, if not following directly from structure, must at least be consistent with structure. Despite the fact that a large amount of excellent morphological work carried out on renal and nephron structure has been published over the last decade, the conclusions regarding the interrelationship between structure and function are based upon classical qualitative morphology. Since nearly all functional studies, especially those dealing with transport across cells, are expressed quantitatively, it is of extreme importance that the exact measures for the various cellular "barriers", across which the transport process takes place, are supplied. In addition, transport mechanisms described in the past incorporate measures, areas or thickness of the specific barriers whose real dimensions have not been determined. All statements about structure-function interrelationships are therefore lacking a direct comparison on a quanti-

tative basis. This latter fact has stimulated the present investigation, which is aimed at obtaining quantitative data on structures which comprise the normal rat kidney tissue and the various nephron cells. Those structures and compartments have been quantified which represent either barriers for transcellular transport or which are known to bear enzymes, metabolites, or solutes essential for renal function and which have been carefully exploited by physiologic or biochemical methods. To investigate more closely the statement that "function directly follows, or at least is consistent with structure", kidneys have been damaged by toxins and ischemia. The subsequent change in quantitative morphology, and the changes in those functions known to be directly linked to definite structures, were followed in order to prove the direct interrelationship between structure and function, also under abnormal conditions.

2 Organization of the Rat Kidney

The kidney contains for basic components: blood, intercellular space, tissue, and urine. Blood and urine are transients. Blood enters and leaves the organ, while urine is being formed and continuously modified when leaving the kidney in the direction of the renal pelvis. The tissue, and to a certain extent the extracellular space, is comparatively stationary. The tissue confines urine once it has been formed by glomerular filtration, blood, and the extracellular space to separate compartments and builds channel systems for urine, blood, and extracellular fluid. This tissue "framework" also ensures adequate conditions for the interrelationship between urine and blood which is modulated by the fourth compartment, the extracellular space. The close relationship between vasculature and the uriniferous system can be appreciated by studying the development of the kidney. During embryonal development three bilateral excretory systems are formed from the nephrogenic cord, the pronephros, the mesonephros, and the metanephros. While the pronephros and mesonephros undergo regression, the metanephros forms the final kidney. There exist two regions from which the organ formation starts: the nephrogenic ridge and a specialized structure of the mesonephric duct called the ureteric bud. The ureteric bud grows cranially and contacts the nephrogenic ridge from which renal corpuscles and tubules start to develop. The renal vasculature, on the other hand, is assumed to develop in situ by first forming sinusoid-like structures intermingled between the nephrons spreading out from the condensed mesenchyme, which is located close to the ampullae of the ureteric bud. The tubules, together with the renal corpuscle originating from the nephrogenic ridge, finally develop into what is called a nephron. This term was first introduced by Braus (1929) who denoted these structures as being the smallest architectural and functional units of the kidney. A rat kidney, for example, is composed of 30 000–35 000 nephrons. For the purpose of comparison about 1 300 000 have been estimated for one human kidney. The nephron can be subdivided into several segments or parts. It includes the renal corpuscle (glomerulus and Bowman's capsule), the proximal tubule, the thin limb of Henle's loop, the distal tubule, and the connecting tubule or early part of the cortical collecting duct. Whether or not this initial segment of the collecting duct is derived from the metanephric blastema (v. Möllendorf 1930; Potter 1952) seems to be a matter of dispute (Tisher 1976). Strictly

speaking the cortical, outer and inner medullary collecting duct does not belong to the nephron since it develops from the ureteric bud. For ease of description, and also since this part is interrelated functionally to other parts of the nephron, the collecting duct will be included within the term "nephron" although it is not correct with regard to embryologic notation. Each nephron contains a part referred to as the straight part of the proximal tubule, the thin limb, which together with the ascending early part of the distal tubule forms the so-called loop of Henle. The length of these loops depends on the position of the corresponding renal corpuscle (glomerulum). Two populations of nephrons can be discriminated, one with corpuscles closer to the surface of the kidney and one with renal corpuscles located in deeper regions of the tissue, the so-called corticomedullary region. The hairpin tips of the latter population, also named "juxtamedullary", reach the part of the kidney exposed to the pelvis – the papilla – whereas the loops of the superficial population bend earlier. On the basis of the arrangement of the nephron population we may describe several tissue regions or zones within the kidney (Fig. 1). This was first performed in a systematic manner by v. Möllendorf (1930).

2.1 Cortex

The cortex contains the arterial vessels supplying and draining the renal corpuscles, and the proximal tubules which are wound up in an irregular manner (cortical labyrinth) for both the superficial and the deep (juxtamedullary) nephrons. In addition the cortex includes the regions called "medullary rays" where, at least in the case of most mammals including the rat, the convolution of proximal tubules disappears and the tubules become straightened. Furthermore we find within the cortex, the straight cortical and the convoluted portion of the distal tubules, the connecting tubules, and the cortical portion of the collecting ducts. The cortex contains superficial and deep nephrons, the supplying vascular system, a peritubular capillary plexus, and of course interstitial cells. The demarcation between cortex and medulla is a thought line connecting the most basal points of the cortical labyrinth (Fig. 1).

2.2 Outer Zone of Renal Medulla

a) Outer stripe (OSOM): This zone contains the "downward"-orientated straight proximal tubules and collecting ducts, and the "upward"-orientated distal tubules. It also includes the vascular compartment arising from the vasa efferentia leaving the renal corpuscles and forming vascular bundles around which the collecting ducts are arranged (v. Möllendorf 1930; Rollhäuser et al. 1964; Kriz 1967). The border line is defined by the transition of the proximal straight tubules of deep nephrons into thin limbs.

b) Inner stripe (ISOM): The inner stripe contains thin limbs of the superficial nephrons, collecting ducts and the ascending loop components, the ascending straight distal tubules of both superficial and juxtamedullary nephrons, descending vessels in the form of vascular bundles also known as vasa recta, and a capillary plexus arranged around the nephron segments. The border against the inner zone of the medulla is defined as the layer where no more ascending distal tubules are present.

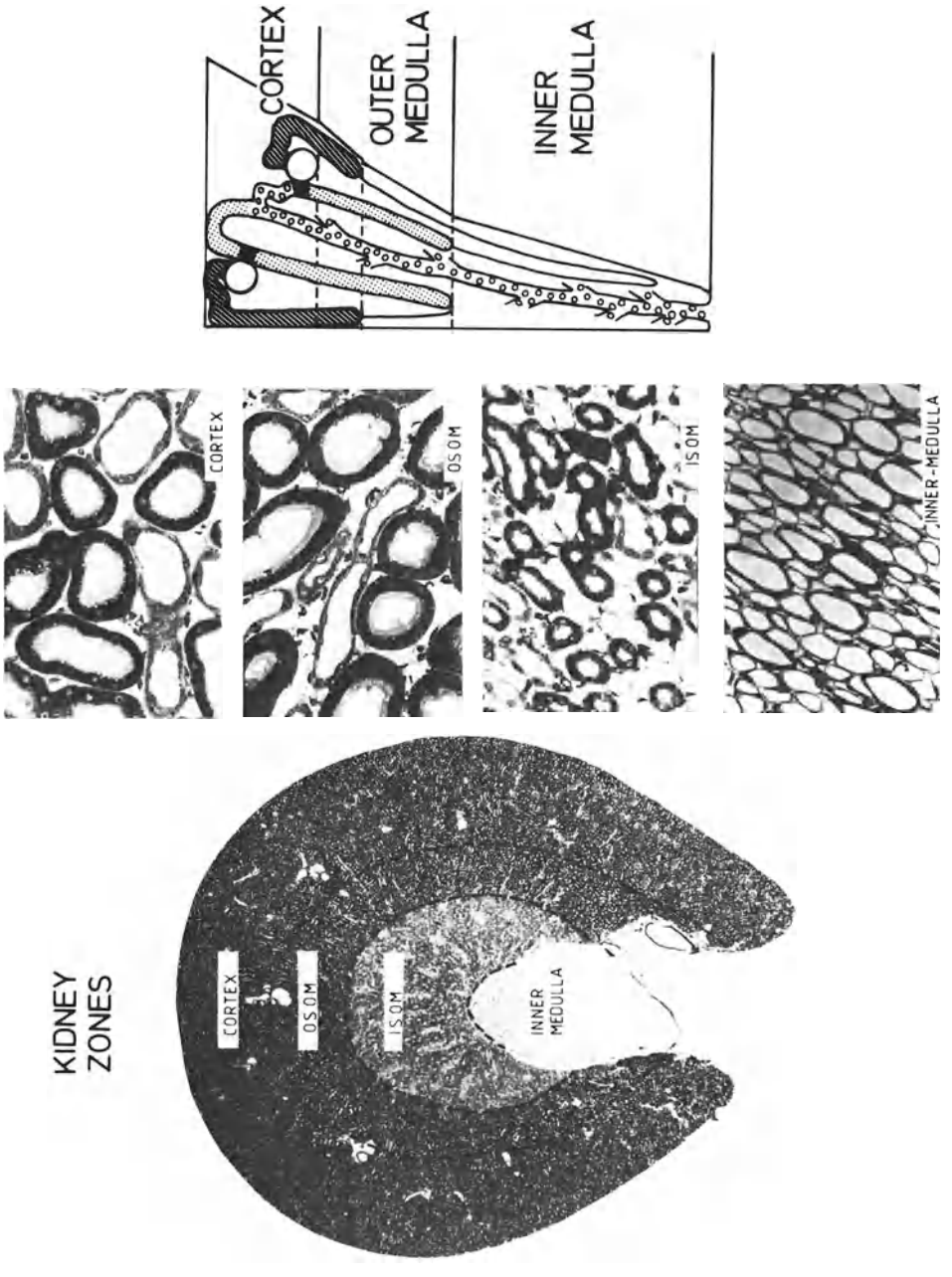

Fig. 1. The kidney zones are displayed first on a paraplast section of a slice obtained by the sampling procedure shown in Fig. 5a. Tissue zone borders are marked by *dashed lines.* In addition typical regions of the four zones, as obtained from 0.5 μm sections after araldite embedding, are shown. Further, a schema of the position of long- and short-looped nephrons is given. Abbreviations used: *OSOM*, outer stripe of outer medulla; *ISOM*, inner stripe of outer medulla. The *proximal nephron* is marked by *parallel lines*, the *thin limb portion* by a *solid line,* the *distal nephron* with *points* (macula densa: *black*), and the *collecting duct* with *small circles*

2.3 Inner Zone of Renal Medulla

This zone contains solely descending and ascending thin limbs belonging to the juxtamedullary or deep nephrons, the descending collecting duct segments and the loops of arterial and venous vasa recta.

2.4 Nephron Structure

2.4.1 Proximal Tubule

The proximal tubule of rat and most other mammalian nephrons extends from the renal corpuscle to the thin limb and can be subdivided in a pars convoluta and a pars recta. The majority of convoluted tubules form as we know the cortical labyrinth and the straight portions (pars recta), together with the collecting ducts and straight ascending distal tubules, the medullary rays. In addition to this first rough subclassification, other morphological features may be used for more detailed description of this nephron segment. Severeal fine structural features detectable by electron microscopy allow a further subclassification into an S_1, S_2, and S_3 segment (Maunsbach 1966; Jacobsen 1975). The characteristics utilized to identify these various segments are extensively described by several authors (Maunsbach 1973; Tisher 1976) and will not be outlined here.

2.4.2 Thin Limb of Henle's Loop

This nephron segment consists of fairly flat epithelial cells and can, similarly to the proximal nephron, be subdivided into at least three subsegments. Each segment is characterized by distinct cell to cell contact features as described in detail by Schwartz and Venkatachalam (1974).

It should be recalled that only the juxtamedullary nephron population displays a "hairpin loop" of the thin limb epithelium whereas the superficial nephron's thin limb epithelium continues into the distal nephron at the bend.

2.4.3 Distal Nephron

In analogy to a subdivision of the nephron segments described so far we may also provide one for the distal nephron. However, the description appears to be more difficult since differences in fine structure between the different portions are less clear cut. Crayen and Thoenes (1975) have tried to give a subsegmentation on the basis of serial sectioning. Despite these difficulties the distal nephron can be roughly subclassified into a medullary ascending straight part penetrating through the inner and outer stripe of outer medulla. This is followed by a cortical straight part which ends at the macula densa where the distal nephron contacts the vascular pole of the renal corpuscle from which it originates. The cortical straight part continues to the distal convoluted part which then shows a gradual transition into the connecting tubule and finally enters a collecting duct. The endportion of the distal convolution and the connecting tubule's epithelium are assembled by different cell types.

2.4.4 Collecting Duct

In analogy to the previous nephron portions this part (although strictly speaking it does not belong to the nephron) may be subdivided into four segments (Ericson and Trump 1969): The connecting portion, the medullary ray segment, the outer medullary ray segment, the outer medullary portion and the inner medullary portion.

3 Basic Principles of Stereology

Stereology is often confused with morphometry, which is the commensuration of structure. The measurement of tissue elements on slides or photomicrographs disregarding their three-dimensional property is a kind of morphometry. A tailor who measures the customer for a suit is a practising morphometrist. Stereology, however, is the rigorous extrapolation from two- to three-dimensional space and a complex body based upon geometrical probability and mathematical methods that derive three-dimensional information from random sections or projections. Every section can be considered as a planar probe utilized to penetrate an aggregate structure. The resolution obtained will depend on section thickness and on the mode of observation. In biologic research the optimum resolution will be achieved by penetrating an aggregate with ultrathin sections and observing them using transmission electron microscopy. Quantitative relationships exist between the dimensions of cells or organelles and their profiles displayed on a section. This means that the aggregate of profiles on the planar probe or a unit area of it is reflecting quantitatively the aggregate of the corresponding structure in space or in a unit volume. This means that measurements obtained on sections can be described in terms of a structural dimension by stereological relationships. Stereological analysis of tissue and cells is based on several presuppositions. The individual tissue or cell component to be investigated must be (a) present in an adequate number; (b) unequivocally identifiable on the section; and (c) of similar size and shape at different locations within the tissue.

The conditions (a) and (b) are fulfilled for most types of organs and cells. The last condition (c) is not necessarily met (Loud 1968). In such situations it must be decided beforehand whether or not this is of biologic significance and if it should be considered accordingly when sampling the tissue. Another condition necessary for stereological analysis can be stated: The structures must be orientated at random with regard to the section plane. Does this situation ever arise in biology? One may argue that this hardly applies to biologic tissue since polarization of structures, one of the most fundamental characteristics in biologic organization, makes a random orientation between section and structure impossible. We know, however, that higher order units like glandular acini, lobes or lobules, which form an organ, permit nearly unlimited variability of axes with respect to a section plane. In a limited number of cases preferential orientation – anisotropy – is not eliminated. The kidney, especially the renal medulla, is assumed to be a highly anisotropic aggregate and will be dealt with in subsequent chapters. A structure in space may be defined by its three-, two-, one- or zero-dimensional features. Putting a planar probe at random through such an aggregate provides us with essentially flat transsection profiles. Volumes, three-dimensional structures (V) will then be seen as areal profiles (A) and their sur-

faces (S) will appear as contour lines of a certain length (B). One-dimensional structures, or more precise linear elements (M), will appear as points on the section. This means that sectioning reduces the original dimension by one. "Point objects" or numbers are zero-dimensional objects (N) and therefore, lost on a section. From this consideration it follows that volumes (V) are related to areas (A) on a planar probe, surfaces (S) are related to length (L), and linear structures (M) related to points (Q). We are also in agreement that aggregate structures are always defined with regard to a given container or a unit of it. The volume of mitochondria or nuclei in a unit of cell or tissue would thus be defined as a concentration or volume density (V_V), their surface per unit volume as surface density (S_V) and so on. If the total volume of the container the kidney, for example, is known, the absolute volume of mitochondria (V) or their surface (S) can be easily calculated.

3.1 Structural Parameters and Profiles on Sections

Suppose a model tissue contains a large number of similar components, e.g., mitochondria. These may be characterized by their volume or surface density, but we would also like to know how they are represented on a random section through the tissue. The answer regarding this relationship was provided by the French petrographer Delesse (1847) who empirically found that the areal density of profiles on a section A_A is equal to their volume density V_V in space:

$$A_A = V_V \tag{1}$$

The exact proof of this relationship has been provided by several authors (Smith and Guttman 1953; Weibel 1963; Underwood 1968). Saltykov (1958) has shown that the surface of structures S_V, displayed by profile contour lines on a section, is directly related to the density of the profile border length on the section area B_A:

$$B_A = \frac{\pi}{4} S_V \tag{2}$$

The length of linear elements curving through the space (M_V), for example, filamentous structures or axes of tubules, is proportional to the density of intersection points of these structures with the unit area of the section plane (Q_A):

$$Q_A = \frac{1}{2} M_V \tag{3}$$

3.2 Methods of Estimating Volume Densities

The estimation of volume densities is based on the "Delesse principle" (see above) which states that the volumes of components in a containing volume are related to their profile areas on a section through it.

$$V_1 : V_2 : V_3 \ldots V_n = A_1 : A_2 : A_3 \ldots A_n \tag{4}$$

Delesse himself approached the measurement of V_V by tracing the profile areas on a sheet of paper cutting and weighing them. The Austrian mineralogist Rosiwal (1898) solved the measurement of profile areas (A) by linear integration. He put random lines

of known length on the section and measured the line length contained within the profiles:

$$V_1 : V_2 : V_3 \ldots V_n = A_1 : A_2 : A_3 \ldots A_n = L_1 : L_2 : L_3 \ldots L_n \quad (5)$$

Both methods are quite cumbersome when applied practically. It was, therefore, a big advance when Glagolev (1933) showed that the profile densities A_A can be easily determined by superimposing a regular point lattice onto the section and determining the point fraction P_P enclosed in profiles. This procedure resulted in a third relationship:

$$V_1 : V_2 : V_3 \ldots V_n = A_1 : A_2 : A_3 \ldots A_n = P_1 : P_2 : P_3 \ldots P_n \quad (6)$$

Chalkley (1943), not aware of Glagolev's work, used an analogous method based upon lattices with random points.

Since we all know that biologic tissues are assembled by more than one component we may label them 1, 2, 3. The sum of partial volume densities, by definition, then reflects the unit volume. If we overlay a test grid to such a 3-phase system and differentially count and classify the points coinciding with phases 1, 2, and 3 we will determine from the primary point counts P_1, P_2, P_3 the corresponding volume densities (Fig. 2):

$$V_{V_1} = \frac{P_1}{P_1 + P_2 + P_3} \quad \ldots \quad (7)$$

3.3 Estimation of Surfaces

As explained above, the surface of a structure in space, or more precisely interphase area between two components, is a two-dimensional feature. Any random cut will provide us therefore with a contour or border line between the profiles of components. It was shown by Smith and Guttman (1953) and Saltykov (1958) that B_A, the density of boundary length per unit area, can be determined by superimposing a test grid made up of parallel lines and counting the intercepts (I) of the test lines with the boundary of the component whose surface should be estimated (Fig. 3). The formulation is:

$$B_A = \frac{\pi}{2} \cdot I_L \quad (8)$$

and derives from the famous Buffon needle problem. Buffon, in 1777, asked for the determination of the true length of a needle by counting its intercepts with parallel lines. Any straight or curved line may, as we know, be divided into n short, straight segments of the length ℓ. If we superimpose a grid with parallel lines, the line distance (d) being larger than the short straight segments ($d > \ell$), a number of segments will be intersected by grid lines ($I < n$). The problem now is to find the probability $P = \frac{\ell}{n}$ that a short, straight segment (ℓ) will intersect a grid line. The solution has been provided by Buffon himself (1777) and later by Crofton (1885). Derivations have also been elaborated independently by Tomkeieff (1945), Smith and Guttman (1953), Duffin et al. (1953), Horrikawa (1954), Hennig (1956) and Saltykov (1958). An arrangement of all short, straight segments perpendicular to the test lines gives a probability $P = \frac{\ell}{d}$ for intercepts to occur, arrangements of segments parallel to the

V_V - DETERMINATION

(three phase system)

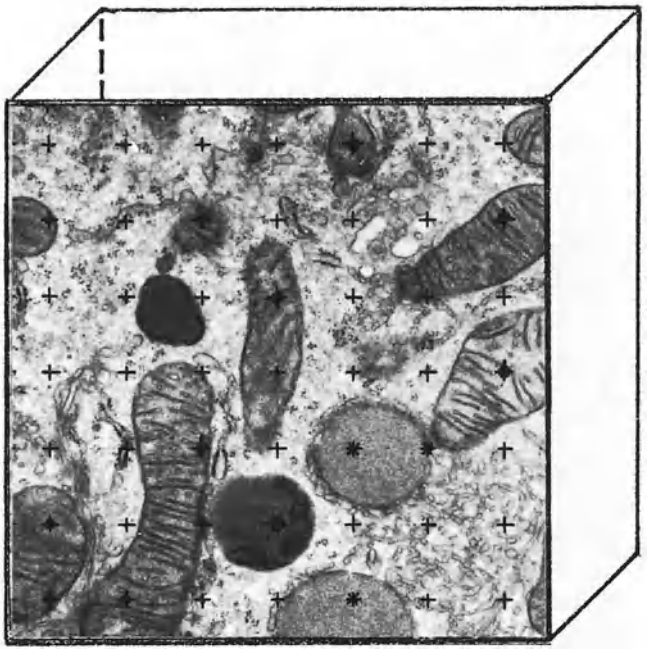

$$V_{V\,mitochondria} = \frac{P(points)_{mitoch.}}{P_{total}}$$

$$V_{V\,lysosomes} = \frac{P_{lysosomes}}{P_{total}}$$

Fig. 2. Illustrates an example for point counting for determination of volume densities. The total point number overlying the test area is 42. The point fraction over mitochondrial transsection profiles (*closed circles*) is 9, the point fraction over lysosomes (*open circles*) is 1 and that over peroxisomes (*asterisks*) is 3. The cube should indicate the containing volume. According to the differential point count V_V mitochondria is 0.21 or 21%, V_V lysosomes 2%, and V_V peroxisomes 7% of the containing or reference volume

S_V - DETERMINATION
sampling level 4

(cristae mitochondriales)

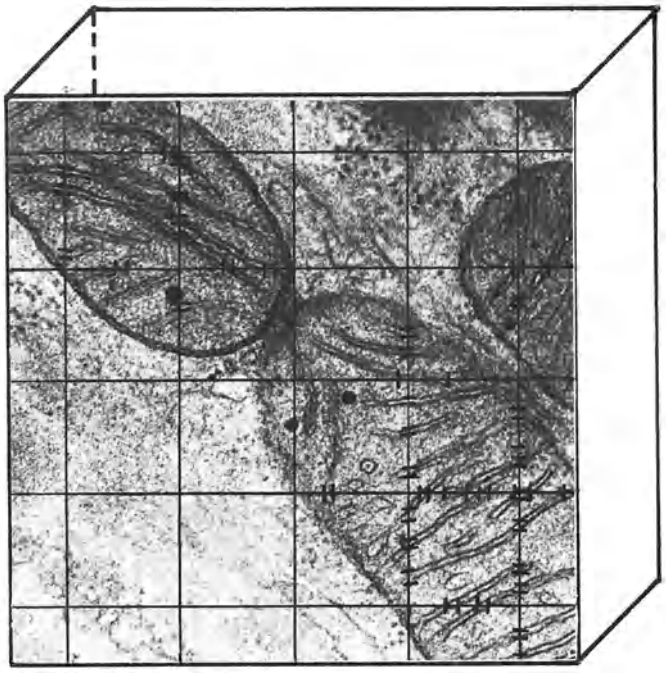

$$S_{V\ cristae} = \frac{I_{cristae}}{P_{total} \times d}$$

(d : lattice spacing)

Fig. 3. Determination of surface density of mitochondrial cristae membranes. The number of intercepts of the two sets of parallel test lines is 72. The total length of test lines is given by the number of lattice corners per test area, which is 25 times the spacing (d) between the lattice corners (d = 0.5 μm). The surface density S_V would then be 5.75 $\mu m^2/\mu m^3$

grid lines will give a probability of P = 0. If we allow all angular positions for ℓ to occur with equal probability from parallel to perpendicular, then the true number of intercepts and therefore the true boundary length density (B_A) will be achieved, since

A is defined by the length of the parallel test lines or lattice points respectively (Fig. 3). Remembering that the boundary length density is proportional to the surface density

$$S_V = \frac{4}{\pi} B_A \tag{9}$$

and having measured B_A as described, where

$$B_A = \frac{\pi}{2} I_L$$

we can substitute for B_A in formula (9) and obtain

$$S_V = 2I_L \tag{10}$$

The components to be analyzed by this approach may have any shape but they must be random. This means that the structures should not exhibit any preferential orientation because they are measured with an anisotropic arrangement of test lines. It is quite evident that in numerous situations, especially using micrographs, preferential orientations may be present. In this case the use of lattices with two sets of parallel lines perpendicular to each other will easily overcome over- or underestimation of intercepts (Fig. 3).

3.4 Estimation of Length

Test lines which pass and therefore intersect an interface between component profiles are in a strict sense penetrating through the surface. Therefore, it is easy to imagine that the lenght of lines or curves (linear elements like filaments or tubular axes) in space, in a unit tissue volume (M_V), is directly related to the number of times they cut a random section plane or a unit of it. It is basically the reverse situation to that described in formula (10). The length density per unit volume can therefore be expressed as

$$M_V = 2 Q_A \tag{11}$$

where Q denotes the number of penetration points (Fig. 4).

4 Material and Methods

4.1 Stereological Analysis

4.1.1 Animal Preparation

In order to obtain estimates of volume, surface and length densities of structures, at various levels of magnification, which as closely as possible resemble the kidney's intravital architecture, several facts have to be kept in mind. Firstly the kidney must be denaturated by chemical fixatives as quickly as possible to prevent cellular damage. Secondly the fixative administered must not induce volume changes in any one of the four basic tissue components outlined in the preceding chapter. This means that the fixative composition has to be carefully adjusted to conditions which correspond to that of the cell's natural environment. Thirdly the quantitative interrelationship between tissue components is highly dependent on the blood pressure and filtration performance. Therefore physiologic conditions must be maintained until denaturation by the fixative starts. The influence of fixative concentration and buffer composition, especially with respect to the osmotic concen-

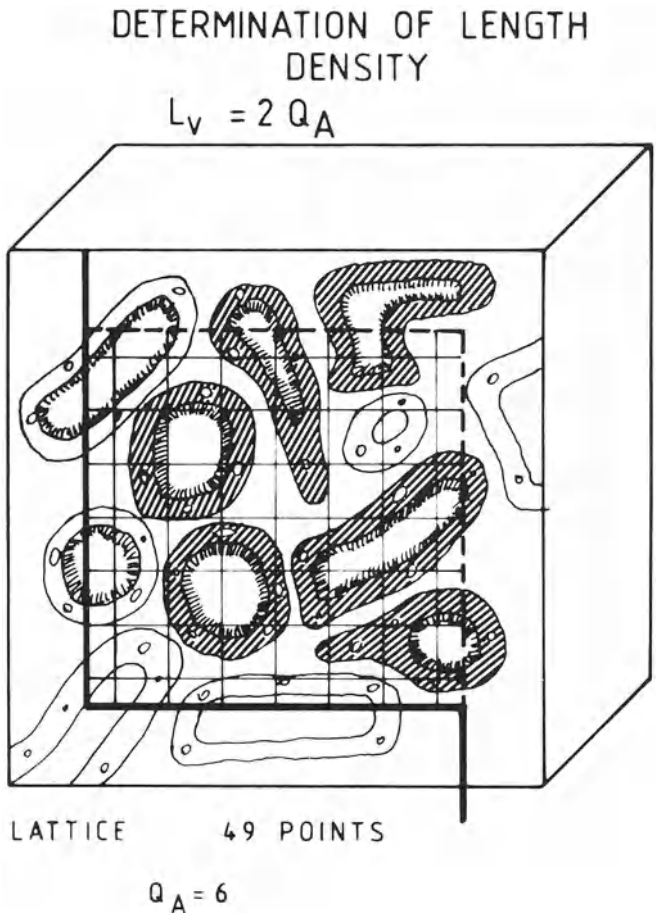

Fig. 4. Illustrates the procedure for determination of the number of intersections of a planar probe with the axes of tubular structures (in the present case proximal tubules). There is no need to define exactly the position of the axis with regard to the tubular transsection profile, only the number of profiles per test area (defined by the number of points) have to be counted. In order to obtain an unbiased estimate of the number of profiles or axes respectively, a specific counting rule has to be considered. All profiles being intersected by the *thick black line* will not be considered while all profiles which intercept only the *broken line* will enter the determination of Q_A; for details see Gundersen (1977)

tration of buffer substances upon the preservation of nephron ultrastructure, has been carefully exploited by Maunsbach (1966) for the renal cortex, and by Bohman (1974) for the interstitial cells of the medulla. For the present investigation, different fixation protocols have been applied for the cortex plus the outer stripe of the outer medulla, the inner stripe of outer medulla and the inner medulla (Table 1). All animals used were Wistar rats (Ivanovas/Bad Kisslegg, FRG) with a body weight (BW) of 280 ± 25 g (SD). The animals were anesthezised with 120 mg/kg BW INACTIN (Byk-Gulden) and kept at 37,5 °C on a heated operation table (Pfaller et al. 1974). A tracheal catheter was inserted to maintain unobstructed respiration and a Ringer solution was infused at a constant rate of 75 µl/min into the jugular vein to counterbalance volume loss induced by the surgical procedure. The blood pressure was permanently monitored via a femoral artery catheter. The abdominal cavity was then opened and the abdominal aorta exposed. A canula was inserted from the bifurcation and tightened, the caudal vena cava cut, and the kidney then perfused retro-

Table 1. Fixation protocol for the electron microscopic investigation

Kidney zone	Osmolarity mOsmol/liter Fixative		Buffersystem
Cortex	1%	60	300[a]
Outer stripe of outer medulla	1%	60	300[a]
Inner stripe of outer medulla	3%	180	750[b]
Inner medulla, outer position	3%	180	1000[b]
Inner medulla, midposition	3%	180	1400[b]
Inner medulla, papillary position	3%	180	1800[b]

Fixative: Glutaraldehyde
Buffersystem [a] Tyrode solution and Dextrane 40
[b] Sodium cacodylate and Dextrane 40

grade with warm (37 °C) Tyrode solution (Maunsbach 1966; Pfaller et al. 1974) containing 2% procaine. This buffer rinse (10–12 s) was followed by perfusion of 1% glutaraldehyde buffered with Tyrode solution (containing only 75% of the regular NaCl amount and no procaine). The left kidney was then removed and tissue sampled for the stereological analysis as described in Chap. 4.1.3. The rinsing buffer and fixative composition was adapted for the deeper zones according to the changed tissue osmolalities due to urine concentration (Table 1). $HgCl_2$ intoxication: To produce tubular injury a group of rats (same weight as controls) were treated with a single subcutaneous injection of 4 mg $HgCl_2$/kg body weight (BW). Kidneys were fixed by vascular perfusion 30 min, 6 h and 24 h after toxin administration. $HgCl_2$ intoxication and counterheating: Additionally the effects of $HgCl_2$ were investigated on a group of rats, which were kept at constant body temperature. These animals received the toxin after they had been anesthezised. In the case of this experimental protocol only the 6-h interval was studied. Maleic acid intoxication: A second type of injury was produced by intraperitoneal administration of maleic acid, 300 mg/kg BW. The acute tubular damage produced by maleic acid was studied 2 h after administration. Ischemia: In a third experiment, renal injury and tubular lesions respectively were elicitated by clamping the renal artery for 45 min duration. The kidney cortex was analysed stereologically immediately after release of the clamp and after allowing a blood reflow of 45 min. Hypothermia: In the last type of experiment hypothermia (30 °C over 2 h) was used to produce acute tubular damage. The animals used were of the same weight and genus as the controls. The surgical treatment was identical to that described above except that the operation table was adjusted, so that 30 °C body temperature could be maintained over an extended period of time.

4.1.2 Sampling of the Normal Rat Kidney for Stereology

The basic stereological relationships as outlined in the previous chapter are well established. However, one has to be careful with their practical application in biology, since all of the principles are based upon the assumption that the objects investigated have a random composition. This criterion certainly is not fulfilled for quite a number of biologic objects and of course not for the object to be discussed here – the rat kidney. We must, therefore, develop a specific sampling procedure which overcomes this problem. Such a sampling protocol must be designed so that all the marginal conditions under which the basic formulations of stereology are valid are considered, that no bias is introduced and that optimum efficiency in terms of time and work input invested is achieved. In the investigation presented here the sampling procedure was designed in order to obtain volume, surface and length densities which are related to various reference volumes, and to obtain absolute volumes with regard to a standard size kidney. The rat kidney is characterized by a zonal construction (v. Möllendorf 1930), which implicates differences in the structural composition. In addition, "structure gradients" within the zones are known to exist (e.g., the renal corpuscles in the cortical tissue). These features must be considered before the decision is made as to where the

blocks and the sections have to be sampled in order to obtain representative estimates. This is the only condition to be fulfilled when the "Delesse principle" for estimating V_V is applied. Another important characteristic of the kidney's construction is the radial arrangement of nephron segments penetrating from the corticomedullary border toward the papillary tip. A preferential arrangement in space for these structures must be assumed. The latter feature is of particular importance since the stereological principle for estimation of S_V needs to have surfaces randomly orientated in space. This raises another problem for sampling, namely how to orientate the planar probes or the test areas respectively in space. Last, but not least, a decision about the sample size for each level of investigation has to be made. Since both volume and surface density are to be considered as concentrations they must be referred to a containing volume. In the case of the kidney various volumes can be utilized as reference values, for example, the cytoplasmic volume, the zonal volume, or the whole sample volume. Considering the question of where to take the samples, the demand for representativity will be fulfilled if the test areas are distributed at random over the whole organ. To proceed in that manner is correct but not efficient, because a number of structures are contained in a few zones of the organ while they are missing in others. Since the borders of the concentrically arranged zones can be distinguished fairly easily, it seems reasonable to treat each of the zones as a separate entity and to carry out sampling separately for each zone. Since this sample can be random we end up with "zonal random sampling", which corresponds to what we know as stratified sampling in statistics. Sampling need not necessarily be random, it may also be systematic. The latter technique has some advantage since the error is usually much smaller than in random sampling. However, sample independence must be ensured. "Zonal random" or even better "zonal systematic sampling" bears an additional advantage. Inner stripe of outer medulla and inner medulla have to be fixed in a different manner due to urine concentration. This means that every kidney can be fixed adequately only with respect to one or at maximum two zones (cortex and outer stripe of outer medulla). Zonal sampling therefore, is in good congruence with the fixation protocol (Table 1). The marginal condition under which the surface density estimations are valid is the random or isotropic orientation of the surfaces to be determined. Apart from structural gradients, differences in structure orientation might be given. This is an additional aspect in favor of stratified systematic sampling. By visual judgement only of sections through the cortex, an orientation of mitochondria, especially of their membranes and of plasma membrane domains, seems to be inherent. Whether or not mitochondria and mitochondria membranes are arranged homogeneously throughout the whole cortex has been determined recently (Pfaller and Fischer 1980), and it could be demonstrated that the cortex, at least with respect to these structures, behaves as an isotropic object. Remembering the cortical labyrinth, made up by the convolution of proximal tubules, isotrophy is not difficult to imagine. As we penetrate into the depth of the kidney preferential orientation of structures is obvious. Since the position of the test area always had to be in a particular zone, the preferential orientation, if given, must be uncovered by two perpendicular sectional directions through the zonal tissue (Pfaller et al. 1979). The following procedure representing a stratified systematic sampling was chosen:

4.1.3 Specimen Preparation

From the perfusion-fixed left kidneys of 5 animals seven slices (0.7 mm thick) equidistantly spaced and independently placed with regard to the organ's long axis, were cut out. The cut surface of the slabs was perpendicular to the long axis. Six cake piece shaped tissue blocks (Fig. 5) were cut out systematically from the three slices which penetrated the central wedge and therefore contained all zones. These pieces were postfixed in the appropriate fixation solutions (Table 1) for 2 h at room temperature, then rinsed in buffer for 30 min, postfixed in 1% osmium tetroxide, buffered with 0.1 mol/liter Na Cacodylate and dehydrated in graded series of acetone (Table 1). Thereafter tissue pieces were embedded in Durcupan ACM (Fluka) using flat embedding molds. For each kidney seven positions were selected to take sections (Fig. 5) in both a tangential and a radial direcion.

4.1.4 Stereological Analysis

The stereological analysis was then performed at four levels of magnification (Fig. 6).

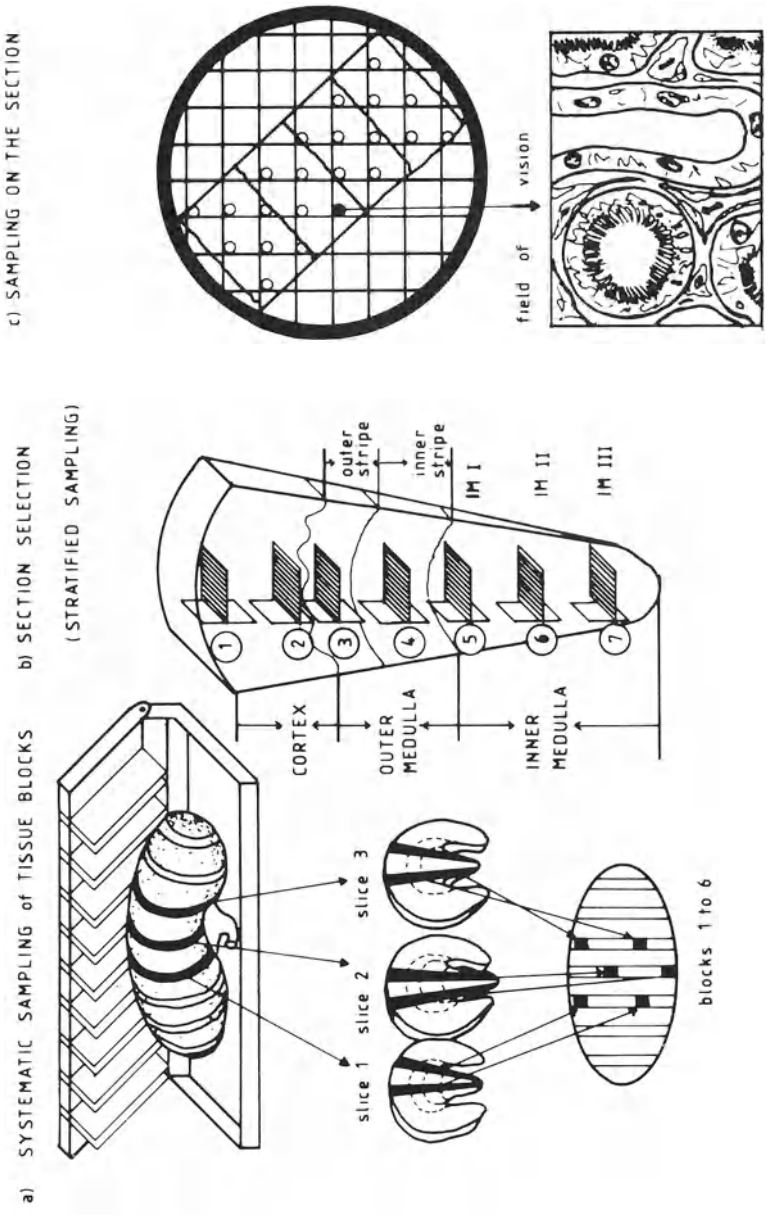

Fig. 5a–c. Using a "tissue slicing" machine equipped with equidistantly spaced pairs of razor blades, the perfusion-fixed organs are divided in to eight thick and seven thin slices. The three thin slices coincident with the organ's central wedge are processed for electron microscopy (*lower portion of a; b*). Starting with the second left slice all the remaining thick slices are processed for light microscopy. One section is taken from every thick slice and evaluated by point counting in order to assess the zonal volume fraction (Fig. 15). *c* illustrates the mode of sampling the micrographs from a section to determine the stereological parameters via point counting

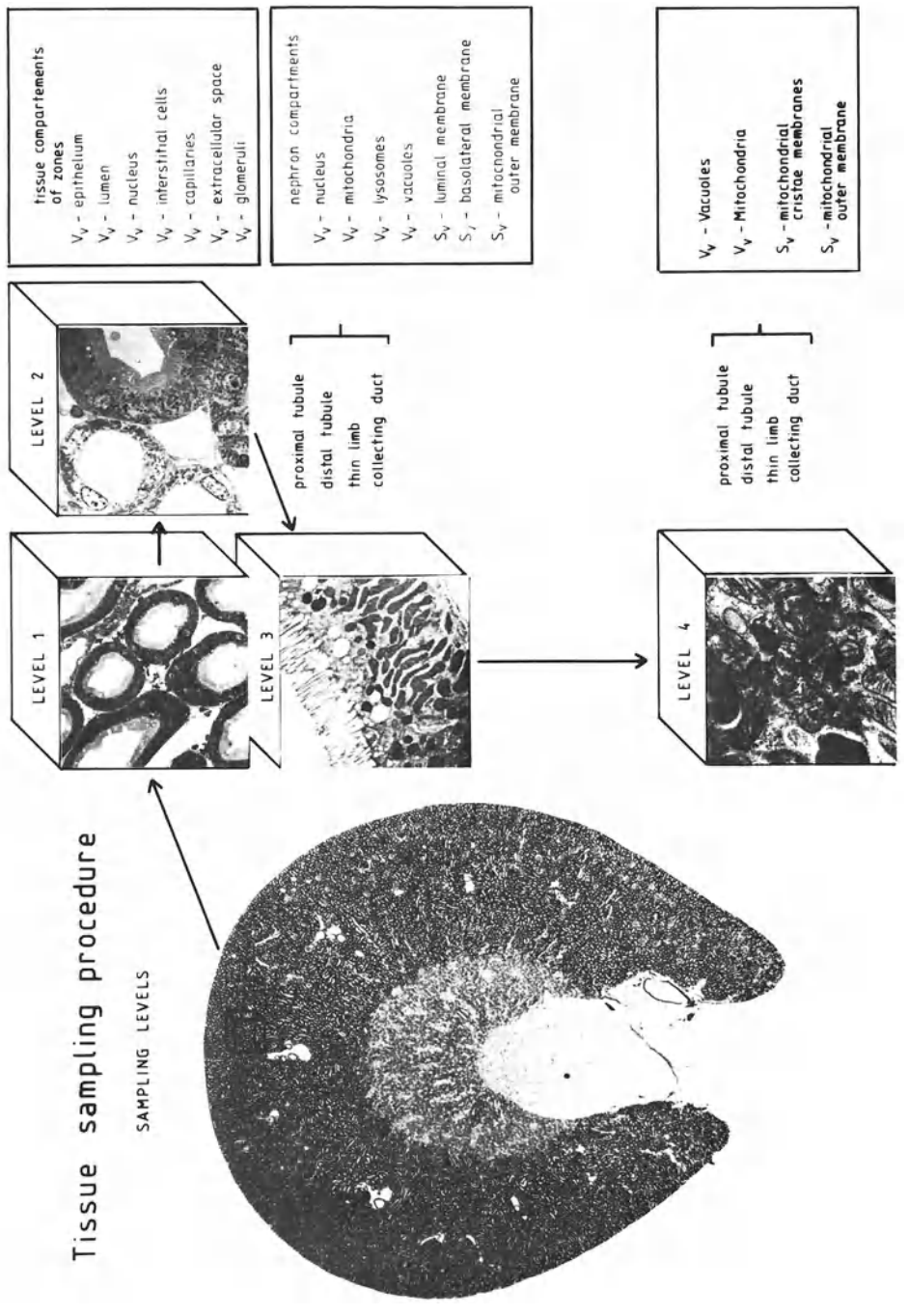

Fig. 6. This figure demonstrates the various sampling levels from light to electron microscopy in the form of tissue probes or containing volumes from one sampling stratum – the kidney cortex. On the *right side* of the figure the various stereological parameters determined within the probes are displayed

4.1.4.1 Light Optical Level (Cortex and Outer Stripe of Outer Medulla)

Sampling Level 1: Per block and sectional orientation six micrographs were taken at 200 times magnification, controlled by a micrometer. The micrographs were then enlarged 5x and printed on Ilfospeed paper. The following parameters were estimated by point counting using a 10 mm-square grid (Fig. 6).

Volume densities (V_V):
- Proximal $S_1 + S_2$ segment epithelium. These two segments were not further subdifferentiated since an unambiguous identification is not always possible.
- Proximal S_3 segment epithelium
- Lumen of $S_1 + S_2$ segment
- Lumen of S_3 segment
- Distal tubular epithelium
- Distal tubular lumen
- Cortical collecting duct epithelium
- Cortical collecting duct lumen
- Capillaries and vessels
- Extracellular space
- Interstitial cells
- Glomeruli (including capillary tuft and urine space)
- Nuclei $S_1 + S_2$ and S_3 segment
- Nuclei of distal tubule and collecting duct

Surface densities (S_V):
- Basal lamina
- Luminal border at the basis of microvilli
- Capillary luminal surface
- Interstitial cell surface

4.1.4.2 Low Electron Microscopic Magnification

Sampling Level 2: This type of sampling was necessary for inner stripe of outer medulla and inner medulla to distinguish between thin limbs of Henle's loop and vasa recta and replaced sampling level 1. In order to obtain representative estimates the number of micrographs taken at 2000 times was increased to ten per block. The parameters estimated were the same as outlined for sampling level 1 except proximal $S_1 + S_2$, S_3, and glomerular values. These structures are not present in inner stripe and inner medulla. In addition, volume and surface densities of the thin limb epithelium of Henle's loop were determined.

Sampling Level 3: At a magnification of 15 000 times, six micrographs from each proximal $S_1 + S_2$, S_3, distal, and collecting duct segment were taken per block, in order to determine volume and surface density parameters of the following structures:

Volume densities (V_V):
- Mitochondria
- Lysosomes (primary and secondary, including hetero and auto phagosomes)
- Nuclei

Surface densities (S_V):
- Luminal membrane
- Basolateral membrane
- Mitochondrial outer membrane

Sampling Level 4: The final level of evaluation was performed at a magnification of 60 000 times in order to assess the following parameters. This step included all nephron segments contained on sections obtained from the seven sampling positions. The parameters estimated were:

Volume densities (V_V):
- Mitochondria
- Lyosomes
- Vacuoles

Surface densities (S_V):
- Mitochondrial outer membrane
- Mitochondrial cristae membrane

4.1.5 Stereological Analysis of the Injured Rat Kidney

(For modes of injury used see Sect., 4.1.1). For all types of injury the identical sampling procedure was applied. Since only the cortex was investigated, a slightly different sampling procedure was selected. The perfusion-fixed left kidneys of six animals were treated as described in 4.1.3 and Fig. 5 and six blocks were taken in a systematic manner from the cortex without differentiating between a subcapsular and a deep sampling position (Fig. 7). For this reason the cortex was cut off the rest of the slabs six blocks were punched out systematically utilizing a biopsy needle 0.7 mm in diameter (Fig. 7). Sampling level 2 (low EM magnification) was omitted.

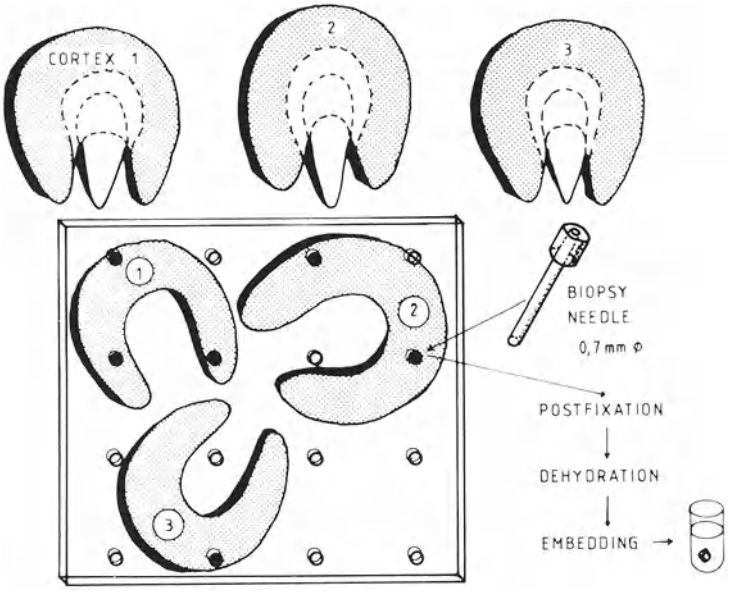

Fig. 7. For systematic sampling of kidney cortex (only applied for studies of injured kidneys) the systematic sampling was carried out by separating cortical tissue of the three thin midpart slices (Fig. 5) from the other zones and placing them in a Petri dish filled with fixative. Then a Plexiglas plate with holes punched through in a systematic manner is overlayed and cylindrical tissue blocks are produced with a dermatologic biopsy needle. The blocks are then processed for electron microscopy in the usual manner

4.2 Determination of Size of Reference Volumes

The methodology and sampling described before only reveals relative estimates, volume densities and surface densities per unit volume of a reference space. The values obtained may be difficult to interpret in the event of changes induced by injuries which may very well affect the reference space. In order to overcome this problem, the average kidney volume was determined after clamp-

ing the renal artery, vein, and ureter at a defined position, and submersing them in a graded cylinder. The same procedure was carried out on kidneys perfused with fixative and the thick slices obtained according to Fig. 5 before and after dehydration with ethanol prior to embedding in paraplast. From each paraplast-embedded slice one section (section thickness: 10 μm) was cut perpendicular to the long organ axis. This technique was carried out for controls as well as for the experimental animals. The paraplast section profile areas of the different kidney zones were estimated by point counting utilizing a light microscope.

4.3 Biochemical Investigations

4.3.1 Marker Enzymes

In order to correlate between the measured membrane surface ar 1 the function of enzymes bound to them, the following seven marker enzyme activities have been assayed.

Plasma membrane (luminal and basolateral): 5′-nucleotidase [E.C. 3.1.3.5 (Aronson and Touster 1974)].

Luminal plasma membrane domain: alkaline phosphatase [E.C. 3.1.3.1 (Bessey et al. 1946)].

Basolateral membrane domain: ouabain-sensitive Na-K-ATPase [E.C. 3.6.1.3 (Silva et al. 1976)].

Mitochondrial cristae membrane: succinate dehydrogenase (SDH), [E.C. 1.3.9.9.1 (Singer 1974)]; cytochrome c-oxidase (CCO), [E.C. 1.9.3.1 (Wharton and Tzagoloff 1967)]; α-glycerophosphate dehydrogenase (α-GPDH), [E.C. 1.1.1.8 (Singer 1974)].

In addition glutathione reductase (E.C. 1.6.4.2) evenly distributed in the cytosol and the mitochondrial matrix was measured according to the method of Carlberg and Mannervik (1975).

4.3.2 Metabolites

In order to be able to judge gross metabolic disturbances due to kidney injury incited by $HgCl_2$, maleic acid, ischemia, or hypothermia, several metabolites have been analyzed. Extreme care was taken to freeze kidneys as quickly as possible. For this purpose the kidney was mobilized surgically, the renal pedicle clamped cut, and the organ immediately transferred to isopentane cooled by liquid nitrogen. The transfer time was less than 1 s on average and at maximum 1 s.

ATP analysis was carried out according to the assay described by Javorek et al. (1974) using 3-phosphoglyceratekinase.

ADP and AMP were determined simultaneously according to the method of Javorek et al. (1974) utilizing myokinase and pyruvate kinase.

Glucose was assayed by the commonly used hexokinase method (Bergmeyer et al. 1974).

Lactate accumulated in tissue was measured according to Noll (1974) via lactate dehydrogenase. Also, in addition to adenine nucleotides, the tripeptide glutathione, reduced and oxidized (GSH, GSSG), was assayed from kidney cortex homogenate, isolated mitochondria, and the microsomal fraction.

Glutathione was determined as total glutathione which means as the sum of both the reduced and oxidized form of the tripeptide. The method used was that reported by Brehe and Burch (1976) with some minor modifications. Instead of perchloric acid, m-phosphoric acid was used for deproteinization and the 0.1 mol/liter Na_2HPO_4 buffer was replaced by a 0.1 mol/liter KH_2PO_4 buffer system.

4.3.3 Mercury and Calcium Accumulation

In the experiments where acute renal failure was induced by $HgCl_2$ the mercury accumulation within the cortical tissue was monitored at 30 min, 1 h, 6 h, and 24 h after toxin administration. For this purpose the kidneys were removed and $HgCl_2$ extracted by concentrated nitric acid at high temperatures. After reducing the Hg^{2+} by $ZnCl_2$, the elemental Hg was measured in the gas

phase with an atomic absorption spectrophotometer. From the same nitric acid extract Ca was determined, also by atomic absorption spectrometry.

4.4 Physiologic Parameters

Some physiologic parameters characterizing renal function have been analyzed.

4.4.1 Glomerular Filtration Rate (GFR)

GFR was determined from the clearance of inulin. Constant plasma levels were produced by infusion via the jugular vein. For this purpose inulin was dissolved in Tris ringer buffer (10% solution) and administered at a rate of 75 µl/min. Urine was collected via a catheter inserted into the bladder. Before and after the urine collection blood samples were taken from the femoral artery by a polyethylene catheter. A polyethylene tube was also utilized to monitor the arterial blood pressure. The blood samples taken, were deproteinized with 5% trichloroacetic acid, centrifuged and analysed for inulin. Urine samples were also analysed for sodium. In addition, urine osmolality was measured cryoscopically using a Knauer semimicroosmometer. The inulin analysis was carried out according to the method of Vurek and Pegram (1966). GFR was calculated in the usual manner as

$$GFR = \dot{V} \frac{U_{in}}{P_{in}}$$

and referred to a unit weight of kidney. In the case of acutely injured kidneys GFR has been determined at various intervals after toxin administration or production of ischemia: 6 and 24 h after mercuric chloride administration, 2 h after maleic acid, 45 min after releasing the artery clamp, and blood reflow in the case of the ischemic injury model.

In animals submitted to hypothermia GFR was determined 1 h after reaching a body temperature of 30 °C. In another set of experiments using the same intervals at which GFR has been determined, animals subjected to the appropriate type of experimental protocol were anesthezised, the kidneys removed, mitochondria isolated (Pfaller et al. 1981), and mitochondrial respiratory activity and ADP/O ratios determined.

4.4.2 Measurement of Mitochondrial Respiration

Mitochondrial respiration was selected as another parameter since it provides information on aerobic metabolism and energy production of renal cortical epithelium. Mitochondrial respiration was measured in a thermostatically controlled chamber (Gilson Inst.), equipped with a clark-type pO_2 electrode. The chamber medium was made up of 225 mmol/liter sucrose, 10 mmol/liter KH_2PO_4, 20 mmol/liter KCl, 10 mmol/liter TRIS and 10 mmol/liter $MgCl_2.6H_2O$ at pH 7.4. One minute after addition of mitochondria and equilibration, a substrate (30 mmol/liter sodium succinate, sodium glutamate, or sodium pyruvate) was injected into the chamber and the changes in O_2 consumption recorded. Respiratory control and ADP/O ratios were obtained by repeated injection of 5 µl of a 0.3 mmol/liter ADP solution. The ADP/O ratio was calculated considering the O_2 dissolution coefficient published by Chappell (1964), Sendroy et al. (1934) and Van Slyke et al. (1928). Respiratory control rates or acceptor control rates respectively, have been calculated in the usual way as the ratios of the registration curve slopes of state 4 and state 3.

The statistical analysis of all data, stereological as well as biochemical has been performed with a one way classification after homogeneity of data has been proven by Bartlett's test. Significant differences between the different groups of treatment have been determined with Scheffe's test of linear contrasts (Sachs 1969).

5 Results

5.1 Quantitative Morphology of the Normal Rat*

As outlined in the chapter: "Material and Methods" two sets of stereological estimates have been elaborated: *Relative values:* volume or surface densities referred to a specific space and; *Absolute values:* volumes and surfaces contained in an average single kidney or in the total reference space and not in a unit volume of it.

5.1.1 Relative Values

Sampling Level 1 and 2:

It can clearly be recognized that the volume fraction of the vascular compartment, is increasing from the cortex down to the medullary region (Fig. 8), whereas the nephron epithelium and the nephron's lumen exhibits the reverse behavior. Only within the inner stripe of the outer medulla does the sum of the nephron's luminal volume per unit volume of zonal tissue occupy a larger fraction than in all other kidney zones or sampling stratas respectively. The interstitial cell's volume fraction displays a continuous increase toward the papillary region. The volume densities for the various epithelial and cellular components relative to a unit of the respective kidney zone are listed in detail in Tables 2 and 3.

Table 4 gives the estimates on volume density of nuclei utilizing the same reference system. Table 5 displays surface density measures on some specific parameters per unit of tissue which may be of especial importance for electro- or transport physiologic considerations: The interface area between proximal tubular cells and the brush border region; the interface area between nephron epithelium and the basal lamina; the capillary wall-blood interface area and the interstitial cell surface.

Sampling Level 3 and 4:

Tables 6 to 9 summarize the volume and surface densities for subcellular organelles relative to a unit volume of zonal tissue. The M_V value or the length densities of tubular axes per unit of zonal tissue is shown in Table 10. The raw data have been determined at sampling level 1 for all zones in order to obtain representative estimates at a reasonable work input. No M_V value is given for the thin limb segments since at this level of sampling no unambiguous differentiation from the vasa recta is possible. The subsequent Tables 11–16 again provide us with mean values and spread measures on volume and surface densities of the nephron segment's subcellular organelles, but instead of a unit volume of zonal tissue a unit of cellular protoplasm is taken as a reference. Finally, a last mode of data presentation is displayed in Table 17, where the mitochondrial membrane surface densities are given as surface per unit volume of the organelle itself. This might be useful when, for example, information on the packing density of cristae membranes is needed.

---

* Part of the quantitative morphological data has been elaborated by Rittinger (1980).

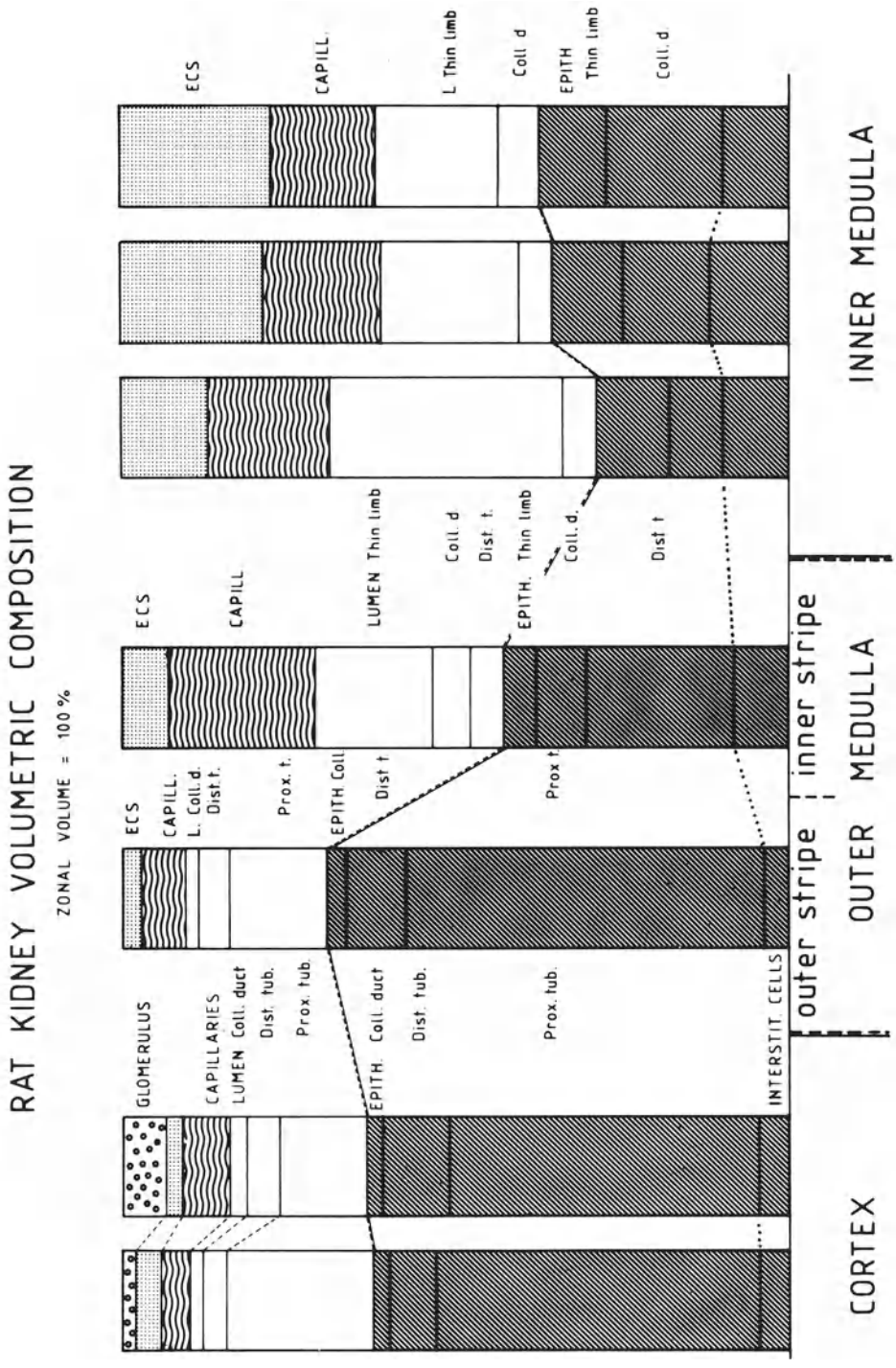

Fig. 8. Graphic representation of the tissue composition within the seven sampling stratas or renal tissue zones. Each column resembles the containing or reference volume and is to be considered as 100%

Table 2. Volume densities of nephron epithelium relative to total kidney tissue (%)

Sampling position	Cortex 1	Cortex 2	OSOM 3	ISOM 4	IM I 5	IM II 6	IM III 7
Epithelium proximal ($S_1 + S_2$) including brush border	47.82 ± 0.11	46.64 ± 3.30					
Epithelium proximal (S_3) including brush border			53.67 ± 2.34				
Brush border region ($S_1 + S_2$)	15.96 ± 1.54	14.40 ± 0.73					
Brush border region (S_3)			21.16 ± 0.98				
Epithelium distal	7.04 ± 0.90	10.01 ± 0.88	9.03 ± 1.37	22.09 ± 2.39			
Epithelium thin limb				4.95 ± 1.70	11.12 ± 0.98	10.34 ± 0.93	9.76 ± 1.47
Epithelium collecting duct	2.39 ± 0.24	2.56 ± 0.44	3.16 ± 0.16	7.41 ± 1.60	7.76 ± 0.52	13.19 ± 1.15	17.62 ± 2.08
Glomerula including capillary tuft and urine space	1.65 ± 0.92	6.45 ± 2.58					

Values are mean ± standard error (SEM)

5.1.1.1 Proximal Tubule: $S_1 + S_2$ Segments

The proximal tubular segments S_1 and S_2 (as a combined parameter) show a high luminal and basolateral membrane surface density (Table 8). However, there appears to be a small insignificant difference between the subcapsular and the juxtamedullary layers of the cortex. In the case of the basolateral membrane (Table 8) this effect is statistically significant ($P < 0.05$). A similar gradient can be observed for the mitochondrial lysosomal and vacuole volume (Tables 6, 7) and the mitochondrial outer and inner membrane system (Table 9). This pattern is revealed when a unit volume of tissue (zone) is taken as a reference. The situation is similar using a unit volume of protoplasm as a reference value. No change in surface density of the luminal membrane but a change in basolateral surface becomes apparent. A slight decrease is also given for the apical vacuoles, indicating pinocytotic activity, and the lysosomal compartment within the juxtamedullary cortex.

5.1.1.2 Proximal Straight Tubule: S_3 Segment

Following the proximal tubule's path further into the outer stripe the quantitative subcellular organization changes even further. There is an additional decrease in mitochondrial, lysosomal and vacuole density (Tables 6, 7), and luminal and basolateral membrane surface per unit volume of zone (Table 8). Surprisingly, the baso-

Table 3. Volume densities relative to total kidney tissue (%)

Sampling position	Cortex 1	Cortex 2	OSOM 3	ISOM 4	IM I 5	IM II 6	IM III 7
Lumen proximal $S_1 + S_2$	21.81 ± 3.10	12.79 ± 1.10					
Lumen proximal S_3			14.40 ± 2.78				
Lumen distal	3.32 ± 0.19	5.12 ± 0.57	4.39 ± 1.17	5.15 ± 1.99			
Lumen thin limb				17.76 ± 1.79	34.92 ± 2.77	20.70 ± 1.57	18.09 ± 1.16
Lumen collecting duct	2.05 ± 0.10	2.52 ± 0.43	2.01 ± 0.54	5.41 ± 0.90	4.92 ± 1.70	4.77 ± 0.84	6.23 ± 1.40
Capillary lumen	4.67 ± 0.65	4.78 ± 1.10	4.62 ± 1.07	19.12 ± 2.30	14.62 ± 1.88	14.32 ± 1.42	12.55 ± 2.04
Capillary wall	0.97 ± 0.12	0.65 ± 0.12	0.93 ± 0.06	2.79 ± 0.20	3.52 ± 0.58	3.33 ± 0.41	3.08 ± 0.45
Vascular space including wall	0.19 ± 0.07	1.55 ± 0.14	0.81 ± 0.12				
Interstitial cells	4.34 ± 0.07	4.34 ± 0.85	3.71 ± 0.24	8.27 ± 0.60	10.31 ± 0.54	11.79 ± 1.09	9.96 ± 0.57
Interstitial space	3.77 ± 0.30	2.61 ± 0.44	1.96 ± 0.13	7.06 ± 0.75	11.83 ± 1.22	21.57 ± 1.89	22.72 ± 1.00

Values are mean ± standard error (SEM)

Table 4. Volume densities of nuclei relative to total kidney tissue (%)

Sampling position	Cortex 1	Cortex 2	OSOM 3	ISOM 4	IM I 5	IM II 6	IM III 6
Proximal tubule $S_1 + S_2$	2.17 ± 0.18	2.47 ± 0.28					
Proximal tubule S_3			3.02 ± 0.39				
Distal tubule	0.96 ± 0.15	2.07 ± 0.53	0.53 ± 0.22	2.29 ± 0.37			
Thin limb				0.78 ± 0.07	2.27 ± 0.31	2.05 ± 0.26	2.00 ± 0.25
Collecting duct	0.23 ± 0.06	0.33 ± 0.08	0.44 ± 0.07	1.11 ± 0.15	1.05 ± 0.16	1.83 ± 0.48	2.52 ± 0.46
Capillary endothelial cells	0.45 ± 0.14	0.46 ± 0.08	0.43 ± 0.09	0.42 ± 0.06	0.70 ± 0.13	0.65 ± 0.06	0.70 ± 0.16
Interstitial cells	0.77 ± 0.07	0.73 ± 0.11	1.06 ± 0.24	1.68 ± 0.13	2.06 ± 0.23	2.27 ± 0.40	1.55 ± 0.17

Values are mean ± standard error (SEM)

Table 5. Surface densities relative to total kidney tissue ($\mu m^2/\mu m^3$)

Sampling position	Cortex 1	Cortex 2	OSOM 3	ISOM 4	IM I 5	IM II 5	IM III 7
Basal lamina	0.067 ± 0.003	0.061 ± 0.006	0.052 ± 0.003	0.066 ± 0.009	0.146 ± 0.015	0.110 ± 0.010	0.087 ± 0.008
Luminal border (at the basis of microvilli) $S_1 + S_2$	0.027 ± 0.004	0.033 ± 0.003					
Luminal border (at the basis of microvilli) S_3			0.027 ± 0.004				
Capillary luminal surface	0.044 ± 0.001	0.039 ± 0.005	0.056 ± 0.004	0.068 ± 0.006	0.071 ± 0.001	0.062 ± 0.006	0.050 ± 0.006
Arteriolar surface	0.0021 ± 0.0015	0.0021 ± 0.0011	0.0019 ± 0.0006				
Interstitial cell surface	0.143 ± 0.013	0.132 ± 0.009	0.126 ± 0.012	0.225 ± 0.007	0.277 ± 0.013	0.306 ± 0.022	0.294 ± 0.018

Values are mean ± standard error (SEM)

Table 6. Volume density of mitochondria relative to total kidney tissue (%)

Sampling position	Cortex 1	Cortex 2	OSOM 3	ISOM 4	IM I 5	IM II 6	IM III 7
Proximal tubule $S_1 + S_2$	13.74 ± 0.54	13.23 ± 0.80					
Proximal tubule S_3			11.58 ± 0.02				
Distal tubule	2.27 ± 0.08	3.25 ± 0.07	3.02 ± 0.02	9.91 ± 0.03			
Thin limb				0.41 ± 0.02	0.87 ± 0.01	0.58 ± 0.02	0.76 ± 0.02
Collecting duct	0.53 ± 0.05	0.41 ± 0.01	0.36 ± 0.01	0.76 ± 0.02	0.68 ± 0.01	0.56 ± 0.01	0.73 ± 0.02

Values are mean ± standard error (SEM)

lateral cell membrane decrease is much smaller than one would expect from visual judgement of this segment (Table 8). When referring the parameters to a unit volume of cytoplasm the microvilli surface displays about the same surface as in the $S_1 + S_2$ segment contained in the cortical sampling regions (Table 15) whereas the basolateral membrane surface is significantly ($P < 0.05$) smaller as compared to the juxtamedullary located $S_1 + S_2$ segment (Table 15).

Table 7. Volume density of lysosomes relative to total kidney tissue (%)

Sampling position	Cortex 1	Cortex 2	OSOM 3	ISOM 4	IM I 5	IM II 6	IM III 7
Proximal tubule $S_1 + S_2$	3.45 ± 0.37	3.11 ± 0.18					
Proximal tubule S_3			1.55 ± 0.23				
Distal tubule	0.10 ± 0.01	0.12 ± 0.03	0.05 ± 0.01	0.10 ± 0.03			
Thin limb				0.02 ± 0.01	0.09 ± 0.01	0.11 ± 0.01	0.17 ± 0.06
Collecting duct	0.05 ± 0.01	0.03 ± 0.01	0.02 ± 0.005	0.09 ± 0.02	0.12 ± 0.02	0.12 ± 0.02	0.11 ± 0.03
Volume density of vacuoles per unit of zonal tissue (%)							
Proximal tubule $S_1 + S_2$	1.76 ± 0.08	1.58 ± 0.32					
Proximal tubule S_3			0.72 ± 0.10				
Distal tubule	0.06 ± 0.02	0.09 ± 0.01	0.13 ± 0.02	0.05 ± 0.01			
Thin limb				0.02 ± 0.005	0.06 ± 0.01	0.08 ± 0.02	0.13 ± 0.04
Collecting duct	0.06 ± 0.02	0.02 ± 0.005	0.02 ± 0.005	0.07 ± 0.01	0.06 ± 0.01	0.17 ± 0.05	0.17 ± 0.05

Values are mean ± standard error (SEM)

5.1.1.3 Thin Limb of Henle's Loop

The quantitative assembly of the thin limb of Henle's loop contained in the inner stripe of outer medulla represents a mixture of descending limbs of the short- and long-looped nephrons made up of cells with different shape characteristics. There is, however, no way of discriminating these two populations unambiguously. If we penetrate further down into the inner medulla our data resemble characteristics of descending and ascending segments of only the long-looped or juxtamedullary nephrons. Since these segments also contain cells with various shape features, the data at the first glance seem to be somwhat scattered. If one recalls the morphological differences described (Schwartz and Venkatachalam 1974) we may understand the variation of data, especially those of the basolateral surface density. From these qualitative observations it can be seen that the inner stripe of outer medulla contains predominantly type 1 cells, due to the larger number of short nephrons, which is illustrated by the fairly low basolateral membrane surface (Table 8) per unit of tissue.

Table 8. Surface density of luminal membranes relative to total kidney tissue ($\mu m^2/\mu m^3$)

Sampling position	Cortex 1	Cortex 2	OSOM 3	ISOM 4	IM I 5	IM II 6	IM III 7
Proximal tubule $S_1 + S_2$	2.25 ± 0.09	2.05 ± 0.12					
Proximal tubule S_3			1.95 ± 0.08				
Distal tubule	0.032 ± 0.006	0.033 ± 0.007	0.028 ± 0.001	0.036 ± 0.005			
Thin limb				0.109 ± 0.008	0.230 ± 0.020	0.167 ± 0.018	0.139 ± 0.005
Collecting duct	0.015 ± 0.009	0.009 ± 0.001	0.010 ± 0.001	0.050 ± 0.004	0.048 ± 0.005	0.093 ± 0.010	0.087 ± 0.015

Surface density of basolateral membranes relative to total kidney tissue ($\mu m^2/\mu m^3$)

Proximal tubule $S_1 + S_2$	1.334 ± 0.237	0.878 ± 0.142					
Proximal tubule S_3			0.630 ± 0.055				
Distal tubule	0.371 ± 0.048	0.526 ± 0.059	0.291 ± 0.019	0.859 ± 0.073			
Thin limb				0.123 ± 0.015	0.205 ± 0.024	0.166 ± 0.018	0.171 ± 0.016
Collecting duct	0.146 ± 0.017	0.053 ± 0.006	0.055 ± 0.006	0.128 ± 0.012	0.220 ± 0.022	0.250 ± 0.025	0.267 ± 0.023

Values are mean ± standard error (SEM)

The outer part of the medulla contains type 3 and type 2 segments composed of cells with dense basolateral infoldings as substantiated by a higher surface density per unit of zonal tissue (Table 8). The midpart and papillary region, on the other hand, contains type 3 segments, having less infoldings and therefore a lower basolateral membrane density per unit of zonal tissue (Table 8). The high surface densities obtained per unit volume of protoplasm result from the very thin-walled epithelium which leads to an increase in mean curvature and thus to a high surface density per unit volume.

5.1.1.4 Distal Tubule

If we follow the nephron further, the early distal tubule – also known as the thick ascending limb of Henle's loop or medullary ascending limb – must be described. Within the inner stripe we find the highest density of mitochondrial volume, mitochondrial cristae membrane and the second highest density of basolateral mem-

Table 9. Surface density of mitochondrial outer membrane relative to total kidney tissue ($\mu m^2/\mu m^3$)

Sampling position	Cortex 1	Cortex 2	OSOM 3	ISOM 4	IM I 5	IM II 6	IM III 7
Proximal tubule $S_1 + S_2$	1.04 ± 0.07	0.98 ± 0.05					
Proximal tubule S_3			0.81 ± 0.02				
Distal tubule	0.22 ± 0.01	0.33 ± 0.03	0.21 ± 0.006				
Thin limb				0.039 ± 0.005	0.091 ± 0.005	0.066 ± 0.008	0.069 ± 0.005
Collecting duct	0.087 ± 0.009	0.033 ± 0.002	0.024 ± 0.001	0.072 ± 0.007	0.072 ± 0.009	0.066 ± 0.004	0.094 ± 0.009

Surface density of mitochondrial cristae membrane relative to total kidney tissue ($\mu m^2/\mu m^3$)

Proximal tubule $S_1 + S_2$	2.86 ± 0.40	2.00 ± 0.10					
Proximal tubule S_3			1.62 ± 0.11				
Distal tubule	0.67 ± 0.08	0.68 ± 0.05	0.62 ± 0.06	1.86 ± 0.15			
Thin limb				0.079 ± 0.010	0.17 ± 0.02	0.11 ± 0.01	0.12 ± 0.02
Collecting duct	0.20 ± 0.03	0.058 ± 0.004	0.052 ± 0.002	0.15 ± 0.02	0.14 ± 0.02	0.12 ± 0.01	0.14 ± 0.01

Values are mean ± standard error

branes, when the unit volume of protoplasm is taken as a reference (Tables 12, 15). Using a unit volume of zone as a reference space the basolateral membrane surface displays the highest value within the inner stripe, whereas the mitochondrial inner membrane is of about the size found for the proximal tubule of the juxtamedullary cortex. In the distal tubules path toward the cortex, all of the parameters described show a decrease and exhibit their lowest values in the subcapsular region, when referred to a unit of zonal tissue (Tables 6, 8). Per unit volume of protoplasm the change in geometry of the nephron increases the mean curvature and thus we find the highest luminal and basolateral surface density in the cortex (Table 15).

Table 10. Length density per unit volume of zonal tissue ($\mu m/\mu m^3$)

Sampling pos.	Cortex 1	Cortex 2	OSOM 3	ISOM 4	IM I 5	IM II 6	IM III 7
Proximal tubule $S_1 + S_2$	0.000362 ± 0.000037	0.00039 ± 0.00004					
Proximal tubule S_3			0.00039 ± 0.000032				
Distal tubule	0.0000821 ± 0.0000100	0.00012 ± 0.00002	0.00013 ± 0.00002	0.00077 ± 0.00001			
Thin limb	Not determined						
Collecting duct	0.000042 ± 0.000001	0.000052 ± 0.000008	0.00012 ± 0.00004	0.00026 ± 0.00004	0.00064 ± 0.00004	0.00059 ± 0.00004	0.00048 ± 0.00002

Values are mean ± standard error (SEM)

Table 11. Volume densities of nucleus relative to protoplasm (%)

Sampling position	Cortex 1	Cortex 2	OSOM 3	ISOM 4	IM I 5	IM II 6	IM II 7
Proximal tubule $S_1 + S_2$	4.58 ± 0.29	5.19 ± 0.14					
Proximal tubule S_3			6.44 ± 0.81				
Distal tubule	11.20 ± 0.88	14.63 ± 1.42	11.21 ± 1.87	10.21 ± 0.82			
Thin limb				15.84 ± 1.37	19.75 ± 1.20	20.76 ± 1.16	20.72 ± 1.31
Collecting duct	11.58 ± 1.99	12.18 ± 3.52	16.80 ± 2.49	14.44 ± 1.30	13.80 ± 0.35	13.25 ± 0.55	13.95 ± 1.07
Capillaries	22.43 ± 6.65	25.19 ± 3.02	22.91 ± 2.19	28.36 ± 4.68	31.97 ± 3.80	31.68 ± 1.79	30.90 ± 2.05
Interstitial cells	16.65 ± 0.74	18.40 ± 3.23	20.09 ± 1.86	19.75 ± 1.05	19.74 ± 1.47	19.26 ± 1.32	15.67 ± 1.22

Values are mean ± standard error (SEM)

Table 12. Volume densities of mitochondria relative to protoplasm (%)

Sampling position	Cortex 1	Cortex 2	OSOM 3	ISOM 4	IMI I 5	IMI II 6	IMI III 7
Proximal tubule $S_1 + S_2$	27.42 ± 1.08	26.89 ± 1.62					
Proximal tubule S_3			20.20 ± 0.88				
Distal tubule	28.59 ± 1.02	27.71 ± 2.00	29.66 ± 1.26	40.26 ± 0.98			
Thin limb				7.04 ± 1.17	6.26 ± 0.78	4.48 ± 0.79	6.19 ± 0.89
Collecting duct	19.49 ± 1.71	13.98 ± 1.05	9.40 ± 0.36	8.83 ± 0.92	7.51 ± 1.05	3.65 ± 0.23	3.59 ± 0.33

Values are mean ± standard error (SEM)

Table 13. Volume density of lysosomes relative to protoplasm (%)

Sampling position	Cortex 1	Cortex 2	OSOM 3	ISOM 4	IM I 5	IM II 6	IM III 7
Proximal tubule $S_1 + S_2$	7.28 ± 0.78	6.61 ± 0.39					
Proximal tubule S_3			3.33 ± 0.49				
Distal tubule	1.10 ± 0.13	0.61 ± 0.22	0.49 ± 0.09	0.44 ± 0.13			
Thin limb				0.47 ± 0.35	0.79 ± 0.13	1.02 ± 0.14	1.77 ± 0.60
Collecting duct	1.06 ± 0.40	1.26 ± 0.37	0.92 ± 0.21	1.23 ± 0.28	1.55 ± 0.26	0.95 ± 0.17	0.64 ± 0.19

Values are mean ± standard error (SEM)

5.1.1.5 Collecting Duct

In this evaluation the connecting tubule was considered part of the collecting duct. This means that all segments showing simultaneously intercalated cells [type 4 cells according to Crayen and Thoenes (1975)] and light-collecting duct cells have been denoted as collecting ducts. No subclassification for the cell types contained in the connecting tubule (type 1, 2, 3, and 4) was made. The most important feature to be recognized is an increase in basolateral membrane area occurring as the collecting duct approaches the inner medullary region, which may be explained by the steadily

Table 14. Volume density of vacuoles relative to protoplasm (%)

Sampling position	Cortex 1	Cortex 2	OSOM 3	ISOM 4	IM I 5	IM II 6	IM III 7
Proximal tubule $S_1 + S_2$	1.76 ± 0.08	1.58 ± 0.32					
Proximal tubule S_3			0.72 ± 0.10				
Distal tubule	0.06 ± 0.02	0.09 ± 0.03	0.13 ± 0.03	0.05 ± 0.02			
Thin limb				0.02 ± 0.01	0.06 ± 0.03	0.08 ± 0.04	0.13 ± 0.04
Collecting duct	0.06 ± 0.02	0.02 ± 0.005	0.02 ± 0.005	0.07 ± 0.01	0.06 ± 0.01	0.17 ± 0.05	0.17 ± 0.05

Values are mean ± standard error (SEM)

Table 15. Surface density of luminal membranes relative to protoplasm ($\mu m^2/\mu m^3$)

Sampling position	Cortex 1	Cortex 2	OSOM 3	ISOM 4	IM I 5	IM II 6	IM III 7
Proximal tubule $S_1 + S_2$	4.78 ± 0.46	4.45 ± 0.38					
Proximal tubule S_3			4.48 ± 0.27				
Distal tubule	0.368 ± 0.072	0.228 ± 0.046	0.280 ± 0.013	0.283 ± 0.013			
Thin limb				2.261 ± 0.165	2.087 ± 0.183	1.592 ± 0.176	1.421 ± 0.046
Collecting duct	0.314 ± 0.056	0.361 ± 0.038	0.396 ± 0.031	0.694 ± 0.055	0.614 ± 0.061	0.713 ± 0.078	0.494 ± 0.086

Surface density of basolateral membranes relative to protoplasm ($\mu m^2/\mu m^3$)

Proximal tubule $S_1 + S_2$	2.857 ± 0.511	1.093 ± 0.309					
Proximal tubule S_3			1.406 ± 0.119				
Distal tubule	4.384 ± 0.561	3.798 ± 0.397	3.123 ± 0.194	4.085 ± 0.341			
Thin limb				3.798 ± 0.217	3.366 ± 0.193	2.904 ± 0.217	2.299 ± 0.090
Collecting duct	3.324 ± 0.416	2.363 ± 0.255	2.531 ± 0.243	2.081 ± 0.178	3.165 ± 0.307	2.143 ± 0.221	1.686 ± 0.142

Values are mean ± standard error (SEM)

Table 16. Surface density of mitochondrial outer membranes relative to protoplasm ($\mu m^2/\mu m^3$)

Sampling position	Cortex 1	Cortex 2	OSOM 3	ISOM 4	IM I 5	IM II 6	IM III 7
Proximal tubule $S_1 + S_2$	2.20 ± 0.15	2.08 ± 0.10					
Proximal tubule S_3			1.74 ± 0.04				
Distal tubule	2.50 ± 0.14	2.31 ± 0.18	2.15 ± 0.06	3.11 ± 0.20			
Thin limb				0.81 ± 0.10	0.83 ± 0.05	0.63 ± 0.08	0.71 ± 0.05
Collecting duct	1.85 ± 0.18	1.34 ± 0.07	0.99 ± 0.04	1.00 ± 0.10	0.93 ± 0.12	0.50 ± 0.03	0.54 ± 0.05

Surface density of mitochondrial cristae membranes relative to protoplasm ($\mu m^2/\mu m^3$)

Proximal tubule $S_1 + S_2$	6.04 ± 0.83	4.24 ± 0.21					
Proximal tubule S_3			3.48 ± 0.24				
Distal tubule	7.70 ± 0.91	4.71 ± 0.32	6.32 ± 0.58	8.55 ± 0.69			
Thin limb				1.54 ± 0.21	1.50 ± 0.15	1.03 ± 0.14	1.20 ± 0.16
Collecting duct	4.29 ± 0.61	2.35 ± 0.15	2.11 ± 0.09	2.07 ± 0.26	1.81 ± 0.30	0.90 ± 0.10	0.82 ± 0.06

Values are mean ± standard error (SEM)

increasing collecting duct epithelial volume per zonal reference space (Table 8). Interestingly we find a decrease for both basolateral and mitochondrial cristae membrane surface density (Table 9) from cortex to outer stripe, whereas from the outer stripe to the deep medulla, mitochondrial cristae membrane density increases again. Per unit of protoplasm, about the same distribution pattern along the nephron is present for the basolateral surface. In the case of mitochondria, however, a steady decrease in outer and cristae membrane is shown, due to the decline in volume density along the collecting duct.

5.1.2 Subcellular Parameters per Unit Length of Nephron

This unusual reference system, which is not regularly used in stereology, was chosen in order to gain a more direct comparison to physiologic measurements and to enzyme activity data determined on single microdissected nephron segments. Usually such data

Table 17. Surface density of mitochondrial outer membranes per unit volume of mitochondria ($\mu m^2/\mu m^3$)

Sampling position	Cortex 1	Cortex 2	OSOM 3	ISOM 4	IM I 5	IM II 6	IM III 7
Proximal tubule $S_1 + S_2$	8.00 ± 0.28	7.87 ± 0.43					
Proximal tubule S_3			8.65 ± 0.24				
Distal tubule	8.72 ± 0.44	8.37 ± 0.44	7.31 ± 0.23	7.73 ± 0.44			
Thin limb				10.37 ± 1.51	14.42 ± 2.15	15.60 ± 0.95	12.89 ± 2.41
Collecting duct	9.48 ± 0.40	9.73 ± 0.45	10.57 ± 0.33	11.45 ± 0.23	12.96 ± 0.81	14.04 ± 0.90	15.65 ± 1.72

Surface density of mitochondrial cristae membranes per unit volume of mitochondria ($\mu m^2/\mu m^3$)

Proximal tubule $S_1 + S_2$	21.76 ± 2.24	16.05 ± 0.78					
Proximal tubule S_3			17.04 ± 1.14				
Distal tubule	26.83 ± 2.88	17.07 ± 0.72	21.23 ± 1.23	21.23 ± 1.60			
Thin limb				19.86 ± 2.01	25.84 ± 4.06	24.56 ± 1.60	20.38 ± 2.07
Collecting duct	21.55 ± 1.56	17.20 ± 1.41	22.74 ± 1.61	23.53 ± 1.53	23.78 ± 1.12	24.43 ± 1.05	23.63 ± 2.18

Values are mean ± standard error (SEM)

are expressed per 1 mm of tubule length. Volumes and surfaces have been calculated per mm or per μm of tubule length and are displayed in the Tables 18–23. The calculation is based upon the length density per volume, and results in, utilizing preexisting volume and surface density measures, the V_M or S_M values by two simple relationships:

$$1)\ V_M = \frac{V_V}{M_V} \qquad \text{and} \qquad 2)\ S_M = \frac{S_V}{M_V}$$

The following features can be recognized:

5.1.2.1 Proximal Nephron

There exists a significant fall in the epithelial volume of proximal tubules from the subcapsular sampling position to the juxtamedullary, and a further decrease toward

Table 18. Epithelial volume per unit length of nephron (nl/mm)

Sampling position	Cortex 1	Cortex 2	OSOM 3	ISOM 4	IM I 5	IM II 6	IM III 7
Proximal tubule $S_1 + S_2$	1300 ± 54.2	1179 ± 26					
Proximal tubule S_3			1113 ± 28				
Distal tubule	942 ± 118	843 ± 122	924 ± 235	113 ± 7			
Thin limb	Not determined						
Collecting duct	992 ± 165	413 ± 83	169 ± 24	238 ± 48	105 ± 9	193 ± 16	314 ± 21

Values are mean ± standard error (SEM)

Table 19. Luminal volume per unit length of nephron (nl/mm)

Sampling position	Cortex 1	Cortex 2	OSOM 3	ISOM 4	IM I 5	IM II 6	IM III 7
Proximale tubule $S_1 + S_2$	605.8 ± 86.5	327.9 ± 27.3					
Proximale tubule S_3			369.2 ± 52.7				
Distal tubule	404.8 ± 25.3	426.0 ± 31.6	337.7 ± 67.5	66.9 ± 13.4			
Thin limb	Not determined						
Collecting duct	488.1 ± 24.4	432.7 ± 72.1	167.5 ± 33.5	208.1 ± 34.7	76.9 ± 4.8	80.8 ± 13.5	129.8 ± 21.6

Values are mean ± standard error (SEM)

the outer stripe of outer medulla (Table 18). This change is accompanied by a decrease in luminal volume per unit length (Table 19). In contrast, the nuclear volume per unit length is steadily increasing from subcapsular to outer medullary sampling regions. Mitochondria and lysosomes decrease in volume in a similar way to the epithelial volume (Tables 20, 21). Luminal cell membrane surface is smaller by 15% in the juxtamedullary and 20% in the outer stripe proximal nephron segments (Table 22), as compared to subcapsular segments. Basolateral membrane surface per unit length is highest for subcapsular proximal tubular segments, about 40% smaller in the juxtamedullary sampling region and, as expected, lower for the S_3-segments (−55%) contained in the outer stripe (Table 22). The data in Table 22 also give the luminal to basolateral membrane surface ratio. We find a ratio of 1.6 for the superficial, a ratio of 2.3 for the deep cortical, and a ratio of 3 for the outer stripe proximal nephron

Table 20. Nuclear volume per unit length of nephron segment ($\mu m^3 / \mu m$)

Sampling pos.	Cortex 1	Cortex 2	OSOM 3	ISOM 4	IM I 5	IM II 6	IM III 7
Proximal tubule $S_1 + S_2$	59.94 ± 4.30	63.33 ± 6.33					
Proximal tubule S_3			77.44 ± 8.60				
Distal tubule	116.93 ± 14.61	172.50 ± 21.68	78.46 ± 15.69	37.66 ± 3.76			
Thin limb	Not determined						
Collecting duct	142.85 ± 14.28	63.46 ± 12.70	36.67 ± 6.02	42.69 ± 4.30	16.40 ± 1.42	31.02 ± 6.08	52.20 ± 7.52

Mitochondrial volume per unit length of nephron segment ($\mu m^3 / \mu m$)

Proximal tubule $S_1 + S_2$	358.84 ± 14.32	324.36 ± 13.51					
Proximal tubule S_3			240.26 ± 7.10				
Distal tubule	303.29 ± 11.22	270.83 ± 28.60	225.38 ± 11.69	113.38 ± 2.97			
Thin limb	Not determined						
Collecting duct	219.05 ± 19.00	65.38 ± 5.94	19.17 ± 0.83	24.62 ± 2.74	9.06 ± 1.29	8.13 ± 0.48	13.13 ± 1.31

Values are mean ± standard error (SEM)

Table 21. Lysosomal volume per unit length of nephron ($\mu m^3 / \mu m$)

Sampling position	Cortex 1	Cortex 2	OSOM 3	ISOM 4	IM I 5	IM II 6	IM III 7
Proximal tubule $S_1 + S_2$	95.30 ± 9.50	79.74 ± 4.70					
Proximal tubule S_3			39.74 ± 5.57				
Distal tubule	12.18 ± 1.22	10.00 ± 1.36	3.85 ± 0.77	1.30 ± 0.32			
Thin limb	Not determined						
Collecting duct	9.52 ± 1.90	5.76 ± 1.44	1.67 ± 0.33	3.46 ± 0.69	1.88 ± 0.37	2.03 ± 0.33	2.29 ± 0.57

Values are mean ± standard error (SEM)

Table 22. Luminal membrane surface per unit length of nephron (mm^2/mm)

Sampling position	Cortex 1	Cortex 2	OSOM 3	ISOM 4	IM I 5	IM II 6	IM III 7
Proximal tubule $S_1 + S_2$	6.22 ± 0.41	5.26 ± 0.31					
Proximal tubule S_3			5.00 ± 0.27				
Distal tubule	0.39 ± 0.06	0.28 ± 0.07	0.22 ± 0.01	0.05 ± 0.006			
Thin limb	Not determined						
Collecting duct	0.36 ± 0.02	0.17 ± 0.02	0.08 ± 0.008	0.19 ± 0.02	0.08 ± 0.008	0.16 ± 0.02	0.18 ± 0.07

Basolateral membrane surface per unit length of nephron (mm^2/mm)

Proximal tubule $S_1 + S_2$	3.74 ± 0.62	2.29 ± 0.29					
Proximal tubule S_3			1.67 ± 0.11				
Distal tubule	5.66 ± 0.25	4.38 ± 0.90	2.37 ± 0.37	1.15 ± 0.095			
Thin limb	Not determined						
Collecting duct	3.74 ± 0.42	1.12 ± 0.11	0.52 ± 0.05	0.58 ± 0.06	0.40 ± 0.04	0.48 ± 0.05	0.06 ± 0.004

Values are mean ± standard error (SEM)

segments. As a consequence of the continuous diminution in mitochondrial volume per unit length, the mitochondrial outer and cristae membrane surface decreases (Table 23). The decline of the cristae membrane surface corresponds to that determined for basolateral membranes and is smaller by 35% for the deep cortical and smaller by 47% for the outer medullary sampling position, when compared to the subcapsular position, which is taken as 100%.

5.1.2.2 Thin Limb

For the thin limb, as outlined earlier, no values have been calculated.

5.1.2.3 Distal Nephron

Tracing the distal nephron from its "startpoint" within the inner stripe of outer medulla, the following results are obtained. Inner stripe segments or medullary ascending limbs exhibit the smallest epithelial volume and luminal volume per unit length. Both parameters are increased within the outer stripe sampling stratum by a factor

Table 23. Mitochondrial outer membrane surface per unit length of nephron (mm^2/mm)

Sampling position	Cortex 1	Cortex 2	OSOM 3	ISOM 4	IM I 5	IM II 6	IM III 7
Proximal tubule $S_1 + S_2$	2.87 ± 0.20	2.51 ± 0.13					
Proximal tubule S_3			2.08 ± 0.05				
Distal tubule	2.68 ± 0.13	2.75 ± 0.37	1.62 ± 0.46	0.87 ± 0.06			
Thin limb	Not determined						
Collecting duct	1.67 ± 0.21	0.63	0.20 ± 0.01	0.28 ± 0.03	0.11 ± 0.01	0.11 ± 0.007	0.20 ± 0.02
Mitochondrial cristae membrane surface per unit length of nephron							
Proximal tubule $S_1 + S_2$	7.90 ± 0.99	5.13 ± 0.26					
Proximal tubule S_3			4.15 ± 0.26				
Distal tubule	8.16 ± 0.90	5.60 ± 0.63	4.77 ± 0.48	2.42 ± 0.20			
Thin limb	Not determined						
Collecting duct	4.76 ± 0.68	1.12 ± 0.09	0.433 ± 0.02	0.58 ± 0.07	0.218 ± 0.03	0.20 ± 0.02	0.24 ± 0.02

Values are mean ± standard error (SEM)

of 8 and 5 respectively. The highest values are found within the cortical regions (Tables 18, 19) where the epithelial volume is increased by a factor of 8,3 and that of the lumen by a factor of 6 as compared to the early medullary ascending portion. A quite comparable distribution pattern exists for the nuclear (Table 20), the mitochondrial (Table 20), the lysosomal volume (Table 21), and the surface areas of luminal, basolateral (Table 22), and mitochondrial (Table 23) membrane surfaces.

5.1.2.4 Collecting Duct

The collecting duct segment possesses the largest volume per length for epithelial volume in the subcapsular and juxtamedullary region, whereas the luminal volume is lower in the juxtamedullary sampling position by roughly a factor of 2. In the outer stripe position a decrease in both epithelial and luminal volume is apparent (Tables 18, 19) followed by a slight increase within the inner stripe, a decline in the medullary sampling position I and II, and again an increase in the deep medulla (position III). Identical patterns can be revealed for the other parameters (Tables 20, 21, 22, 23) with the exception of the basolateral membrane surface, which is continuously dimished in area per length from the cortex toward the deep medulla, where the surface amounts to only 2% of that found in subcapsular portions.

5.1.3 Absolute Values

The in situ volume of unfixed kidneys determined from rats with a mean body weight of 339 ± 12 (SE) g is 1450 ± 200 µl (n = 30) and that after perfusion fixation is 1320 ± 180 µl (n = 10). The third volume measurement carried out before infiltrating the tissue with a benzene-paraplast mixture was found to be 810 ± 50 µl (n = 10). This difference is significant at the 0.05 level. After sampling eight sections by the procedure described in Chap. 4.1.3, and correcting for shrinkage, we obtain the volumes shown in Table 24.

Table 24

Total kidney	1320 ± 177 µl	or	100 ± 13%
Cortex	829 ± 124 µl		63.8 ± 9.4%
OSOM	290 ± 26 µl		22.0 ± 2.0%
ISOM	157 ± 21 µl		12.0 ± 1.6%
IM	44 ± 6 µl		3.4 ± 0.5%

No division into cortical and inner medullary sublayers can be given since there is no possibility of defining the limits of these compartments in an unequivocal manner. The total kidney volume calculated from the morphometric evaluation of zones is quite different from that revealed for unfixed or glutaraldehyde-fixed organs. The obvious reason is a shrinkage due to paraplast embedding as outlined above. Therefore the zonal volumes now used as absolute reference spaces must be corrected for concentric shrinkage. On the basis of this absolute reference space absolute values for the kidney's and the nephron's most important structural components can be calculated (Tables 24–31).

5.2 Quantitative Morphology of the Acutely Injured Kidney Cortex

All of the following stereological data (volumes and surfaces) for the various modes of acute renal injury are given only as relative values (per unit of cortex or per unit of tubular cytoplasm), since no significant changes in the absolute volume of the kidney cortex have been detected.

5.2.1 The $HgCl_2$ Model

5.2.1.1 Qualitative Morphology

Thirty min after $HgCl_2$ administration no morphological changes are visible either by light microscopic or by electron microscopic evaluation. After 6 h marked changes in proximal tubular cells become visible which may be summarized as follows (Figs. 9, 10): A loss of microvilli, occurrence of large apical vacuoles, and in addition an enlarged number of small, possibly pinocytotic vacuoles (Fig. 10b). Furthermore there seems to be an increased number of lysosomes in the apex of proximal tubular cells of the S_3 segment (Fig. 10c). Mitochondria exhibit normal appearance. Changes compared to control animals exist for the endoplasmic reticulum and the perinuclear cisternae which become widened. Polysomes tend to disperse. These damages seem to be distributed uniformly over the whole cortical labyrinth. The medullary ray

Table 25. Absolute volumes for standard sized kidney of 1320 µl (µl)

	Cortex 1+2	OSOM 3	ISOM 4	IM 5 6 7
Epithelium proximal ($S_1 + S_2$) including brush border	391.40 ± 4.89			
Epithelium proximal (S_3) including brush border		155.43 ± 2.34		
Epithelium distal	70.69 ± 12.35	26.15 ± 3.97	34.73 ± 3.76	
Epithelium thin limb			7.78 ± 0.57	4.63 ± 0.17
Epithelium collecting duct	20.55 ± 0.75	4.46 ± 0.72	11.65 ± 2.52	5.72 ± 1.27
Glomerula including capillary tuft and urine space	35.56 ± 19.89			

Values are mean ± standard error (SEM)

Table 26. Absolute volumes for a standard sized kidney of 1350 µl (µl)

	Cortex	OSOM	ISOM	IM	Total kidney
Lumen proximal $S_1 + S_2$	143.37 ± 37.37				
Lumen proximal S_3		41.70 ± 8.05			185.07 ± 45.40
Lumen distal	34.97 ± 7.46	12.71 ± 3.39	8.10 ± 3.13		55.87 ± 13.98
Lumen thin limb			27.92 ± 2.81	10.92 ± 2.32	38.84 ± 5.13
Lumen collecting duct	18.98 ± 1.91	5.82 ± 1.56	8.51 ± 1.41	2.36 ± 0.20	35.67 ± 5.08
Glomerula	35.56 ± 19.89				35.56 ± 19.89
Vascular space of big vessels	4.47 ± 1.81	1.19 ± 0.41			5.66 ± 2.22
Interstitial cells	35.97 ± 7.04	10.74 ± 0.70	13.38 ± 1.32	4.75 ± 0.25	64.84 ± 9.31
Interstitial space	26.44 ± 4.81	5.68 ± 0.93	10.72 ± 1.67	8.32 ± 1.54	51.16 ± 8.95
Capillary lumen vasorecta lumen	39.20 ± 0.50	22.07 ± 3.10	30.06 ± 3.62	6.30 ± 0.40	97.63 ± 7.62

Values are mean ± standard error (SEM)

regions, however, appear to be affected more intensively. Twentyfour hours after $HgCl_2$ administration, tubules with signs of early necrosis can be observed, this being indicated by cytoplasmic swelling, condensation, and an initial calcification of mitochondria and disruption of the luminal plasma membrane (Fig. 11a–d). Also, sequestration of cell fragments into the lumen occurs. Besides these effects less severely injured cells with changes comparable to that seen after 6 h, as well as absolutely normal cells, are present. No such signs of injury can be detected for distal tubules and collecting ducts except a collapse of these tubules (Fig. 11e, f) due to obstructive events in the nephrons. The only observable irregularity concerns the distal tubular cells which accumulate remarkable amounts of glycogen (Fig. 11e) within their cytoplasm (Pfaller and Trump 1980).

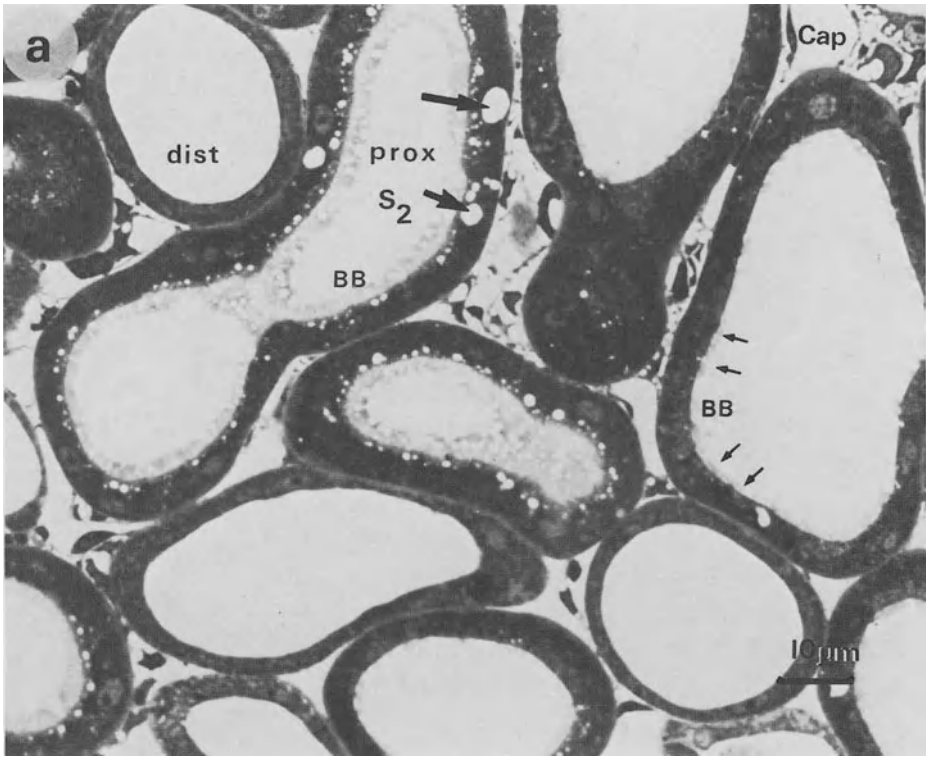

Fig. 9. *a* Cortical tissue (sampling level 1) 6 h after administration of a single dose of $HgCl_2$ (4 mg/kg BW). The changes which can be recognized are a diminuation of the brush border regions (*BB, small arrows*) vacuolization (*thick arrows*) of apical regions of proximal tubular cells and the occurrence of big vacuoles. No changes or alterations are detectable for distal tubules or collecting ducts. *b* Proximal S_2 segment 6 h after $HgCl_2$. Microvilli show a rarefication and shortening. Vacuoles, presumably of endocytotic origin, are accumulating in the apical portion of cells. The basolateral cell membrane system can still be recognized but seems to be less well defined as in controls. No changes in appearance of mitochondria can be seen. *c* Proximal tubular S_3 segment. The luminal surface seems reduced, and the microvilli are shorter and less densely packed than in control animals. An increased number of lysosomal transsection profiles (L_y) can be recognized as well as an enormously increased number of apical endocytotic vacuoles (V). The basal part of the cell exhibits dilated cisternae of smooth endoplasmic reticulum (*SER*). Nuclear chromatin (*NUC*) seems to be condensed and the perinuclear cisternae (*PNC*) widened. Mitochondria (*Mi*) look totally normal

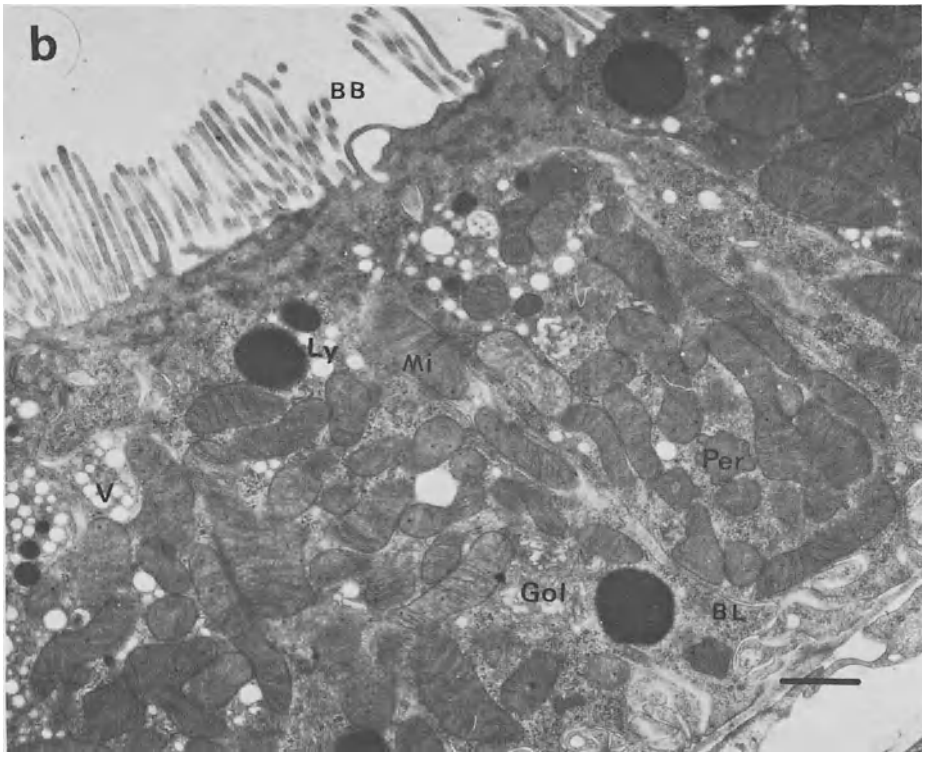
b
BB
Ly
Mi
Per
V
Gol
BL

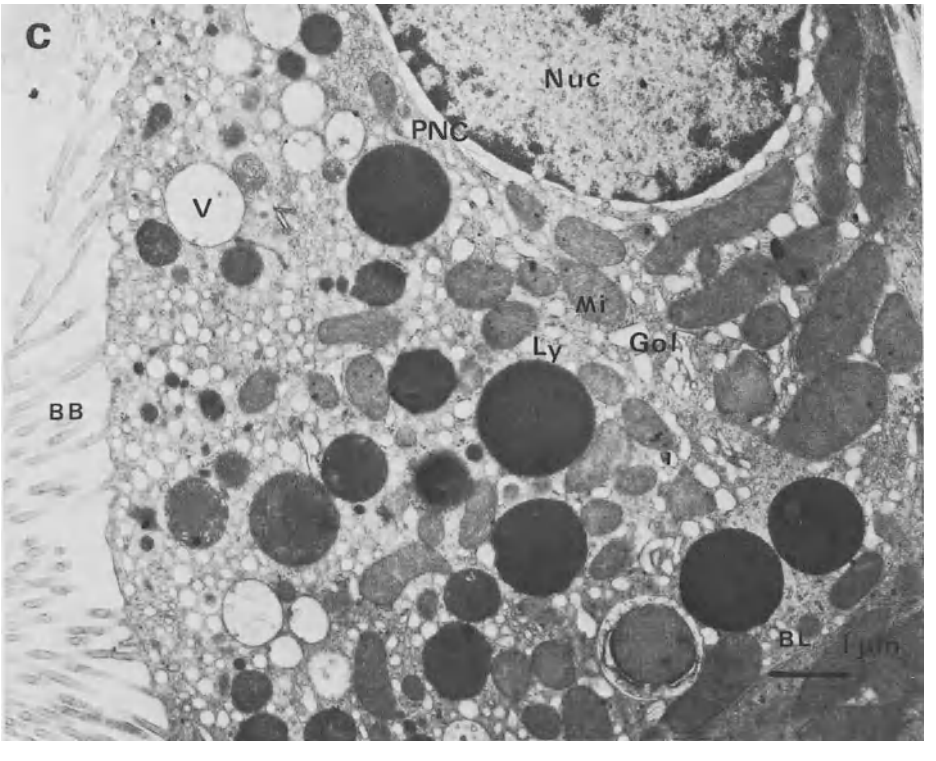
c
Nuc
PNC
V
Mi
Ly
Gol
BB
BL
1 µm

Table 27. Absolute volumes for nuclei for a standard sized kidney of 1320 µl (µl)

	Cortex	OSOM	ISOM	IM
Proximal tubule $S_1 + S_2$	19.06 ± 2.65			
Proximal tubule S_3		8.75 ± 1.13		
Distal tubule	12.60 ± 1.64	2.95 ± 0.64	3.60 ± 0.58	
Thin limb			1.23 ± 0.22	0.94 ± 0.04
Collecting duct	2.89 ± 1.01	1.27 ± 0.20	1.74 ± 0.39	0.80 ± 0.19
Capillary endothelial cells	3.77 ± 0.04	1.25 ± 0.01	0.66 ± 0.09	0.30 ± 0.01
Interstitial cells	6.22 ± 0.17	3.13 ± 0.69	2.56 ± 0.19	0.87 ± 0.09

Values are mean ± standard error (SEM)

5.2.1.2 Quantitative Morphology

Sampling Level 1 (Light Microscopy)

The first change which can be determined 30 min after $HgCl_2$, refers to the cortical interstitial space which increases (+75%) significantly in volume when compared to controls (Table 32). This increase is maintained over the whole experimental period. Six hours after toxin administration we find, in addition, a significant enlargement in volume density of distal (+37%) and collecting duct lumen (+19.1%), whereas in the 24-h interval these values are smaller than those of the controls (Table 32). The distal lumen is decreased by 41%, that of the collecting duct by 78%. At this time a reduction in collecting duct epithelial volume can be determined. The volume density of necrotic epithelium amounts to 14% of the whole proximal tubular epithelium contained in the cortex (Table 32).

Proximal Tubule – Sampling Level 3 and 4

The mitochondrial volume fraction is not altered up to the 6-h interval but is significantly decreased after 24 h (Table 33). The lysosomal compartment stays constant in the S_2 segment but significantly increases by a factor of 2 in the S_3 segment 6 h after $HgCl_2$. In the 24 h interval the S_3 lysosomal volume fraction changes to values identical to that of the control condition (Table 33). A marked increase in volume is detectable for the cell's apical vacuoles. There is a 2.4-fold increase after 6 h and a 13-fold increase after 24 h (Table 33). Surface densities (Table 34) of luminal and basolateral membrane surface are reduced significantly after 6 h and 24 h in both proximal tubular segments. The reduction amounts to 56% at 6 h, to 61% at 24 h

Table 28. Absolute volumes for mitochondria per standard sized kidney of 1320 μl (μl)

	Cortex	OSOM	ISOM	IM
Proximal tubule $S_1 + S_2$	106.69 ± 0.71			
Proximal tubule S_3		31.40 ± 1.37		
Distal tubule	26.86 ± 0.11	7.76 ± 0.22	13.98 ± 0.34	
Thin limb			0.55 ± 0.09	0.27 ± 0.03
Collecting duct	5.03 ± 0.81	0.42 ± 0.02	1.03 ± 0.11	0.28 ± 0.07

Values are mean ± standard error (SEM)

Table 29. Absolute volumes for lysosomes per standard sized kidney of 1320 μl (μl)

	Cortex	OSOM	ISOM	IM
Proximal tubule $S_1 + S_2$	27.28 ± 1.25			
Proximal tubule S_3		5.18 ± 0.76		
Distal tubule	0.81 ± 0.21	0.13 ± 0.02	0.15 ± 0.04	
Thin limb			0.037 ± 0.010	0.057 ± 0.010
Collecting duct				

Absolute volume for vacuoles per standard sized kidney of 1320 μl (μl)

Proximal tubule $S_1 + S_2$	13.90 ± 0.63			
Proximal tubule S_3		2.41 ± 0.32		
Distal tubule	0.72 ± 0.06	0.36 ± 0.05	0.09 ± 0.02	
Thin limb			0.035 ± 0.020	0.043 ± 0.010
Collecting duct	0.34 ± 0.02	0.041 ± 0.010	0.10 ± 0.02	0.06 ± 0.01

Values are mean ± standard error (SEM)

Table 30. Absolute surface of luminal membranes per standard size of kidney of 1320 μl (m^2)

	Cortex	OSOM	ISOM	IM
Proximal tubule $S_1 + S_2$	3.83 ± 0.32			
Proximal tubule S_3		1.10 ± 0.35		
Distal tubule	0.03 ± 0.006	0.007 ± 0.0003	0.006 ± 0.0008	
Thin limb			0.02 ± 0.001	0.008 ± 0.0009
Collecting duct	0.10 ± 0.0007	0.002 ± 0.0001	0.008 ± 0.0006	0.003 ± 0.0004

Absolute surface of basolateral membranes per standard sized kidney of 1320 μl (m^2)

Proximal tubule $S_1 + S_2$	0.93 ± 0.18			
Proximal tubule S_3		0.22 ± 0.02		
Distal tubule	0.38 ± 0.02	0.08 ± 0.005	0.14 ± 0.01	
Thin limb			0.03 ± 0.002	0.01 ± 0.001
Collecting duct	0.08 ± 0.01	0.01 ± 0.001	0.02 ± 0.002	0.01 ± 0.002

Values are mean ± standard error (SEM)

for the luminal surface per unit of cortex and to 27% and 43% respectively for the basolateral membrane. In addition to the changes outlined above we find a significant reduction of mitochondrial cristae membrane surface (Table 34) in both the 6-h (–44%) and 24-h interval (–53%). Changes for the mitochondrial outer membrane and the inner boundary membrane are detectable only in the 24-h interval. The values for the inner boundary membrane are coincident with the outer membrane since they are separated by only a few nanometers.

Distal tubule – Sampling Level 4

There is a slight but significant increase (+10%) in mitochondrial volume fraction at 6 h and a decline to a value slightly below that of controls after 24 h. A similar response can be shown for the lysosomal compartment (Table 35). Luminal and basolateral membrane surfaces are significantly diminished only 24 h after $HgCl_2$ administration (–51% and –50%). No change is found for the mitochondrial cristae membrane, whereas outer membrane and inner boundary membrane are reduced in both the 6 h and the 24 h interval (Table 36).

Table 31. Absolute surface of mitochondrial outer membrane per standard sized kidney of 1320 µl (m^2)

	Cortex	OSOM	ISOM	IM
Proximal tubule $S_1 + S_2$	0.84 ± 0.02			
Proximal tubule S_3		0.270 ± 0.007		
Distal tubule	0.23 ± 0.004	0.06 ± 0.0001	0.11 ± 0.0007	
Thin limb			0.006 ± 0.0007	0.003 ± 0.0003
Collecting duct	0.05 ± 0.0008	0.004 ± 0.0002	0.01 ± 0.001	0.004 ± 0.0008

Absolute surface of mitochondrial cristae membranes per standard sized kidney of 1320 µl (m^2)

Proximal tubule $S_1 + S_2$	2.08 ± 0.36			
Proximal tubule S_3		0.460 ± 0.031		
Distal tubule	0.587 ± 0.131	0.180 ± 0.016	0.292 ± 0.024	
Thin limb			0.012 ± 0.002	0.006 ± 0.0006
Collecting duct	0.099 ± 0.029	0.015 ± 0.0006	0.024 ± 0.003	0.007 ± 0.001

Values are mean ± standard error (SEM)

Collecting Duct – Sampling Level 4

Both volume and surface densities of the structural parameters described above for the proximal and distal tubule remain constant, at least through to the 6 h interval (Tables 34, 36). With regard to the 24-h interval no change in mitochondrial volume can be detected. The lysosomal compartment, however, is significantly increased (+165%). The luminal surface is increased by 82% whereas the basolateral surface is reduced by 48%. Mitochondrial outer membrane, inner boundary membrane, and cristae membrane are unaltered throughout the whole experiment.

5.2.2 The $HgCl_2$ Model; Six Hours After a Single $HgCl_2$ Dose and Counterheating

5.2.2.1 Qualitative Morphology

The changes observed by light microscopic investigation are only subtle. The tubular lumina are wide, a denudation of the brush border, as seen after $HgCl_2$ administration

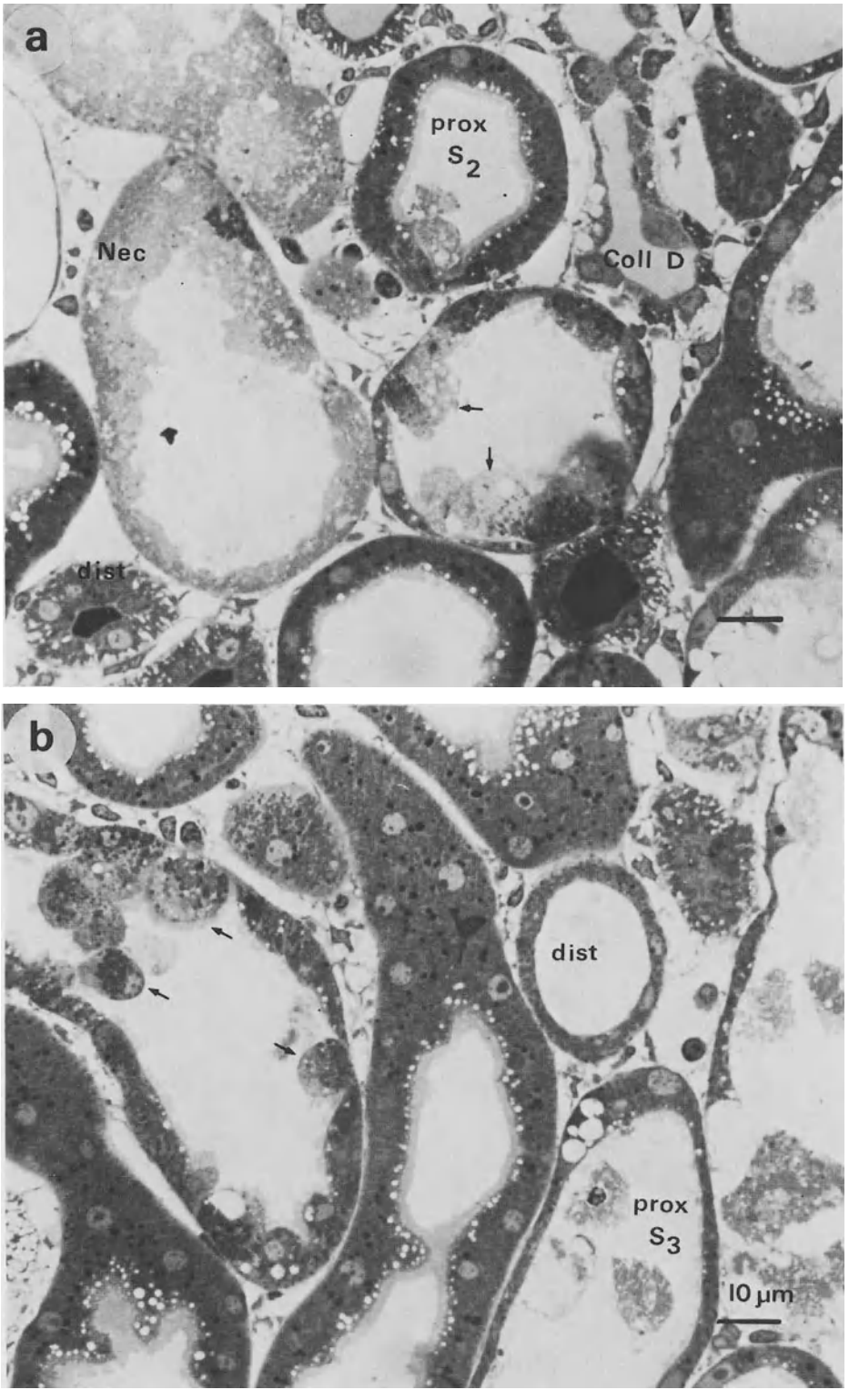
a
prox
S_2
Nec
Coll D
dist
b
dist
prox
S_3
10 µm

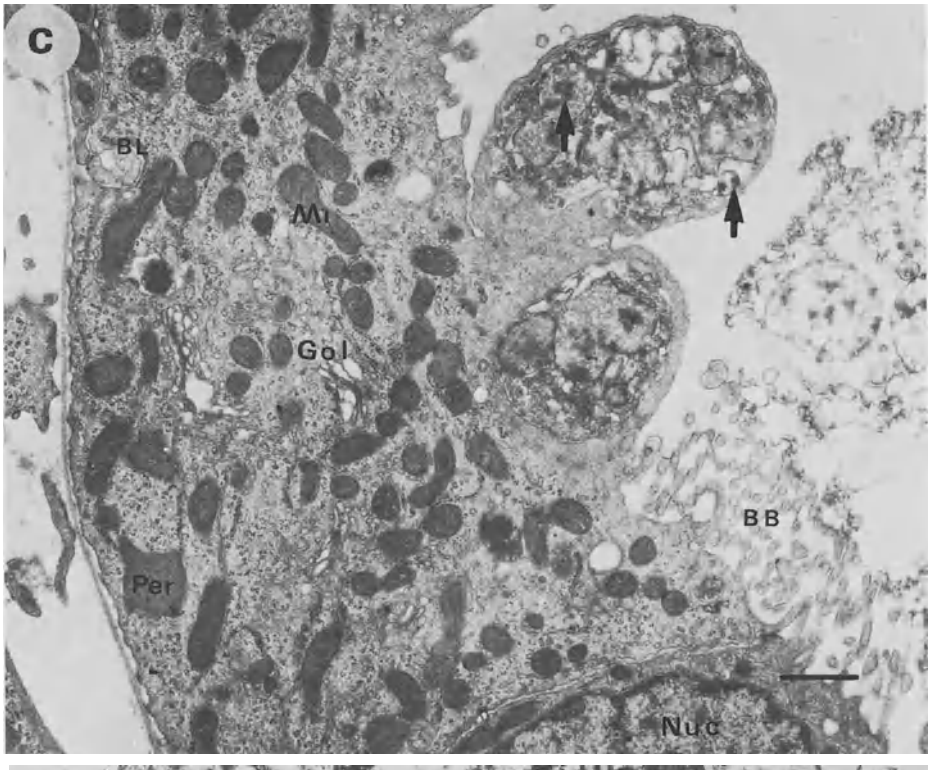
c
BL
Mi
Gol
BB
Per
Nuc

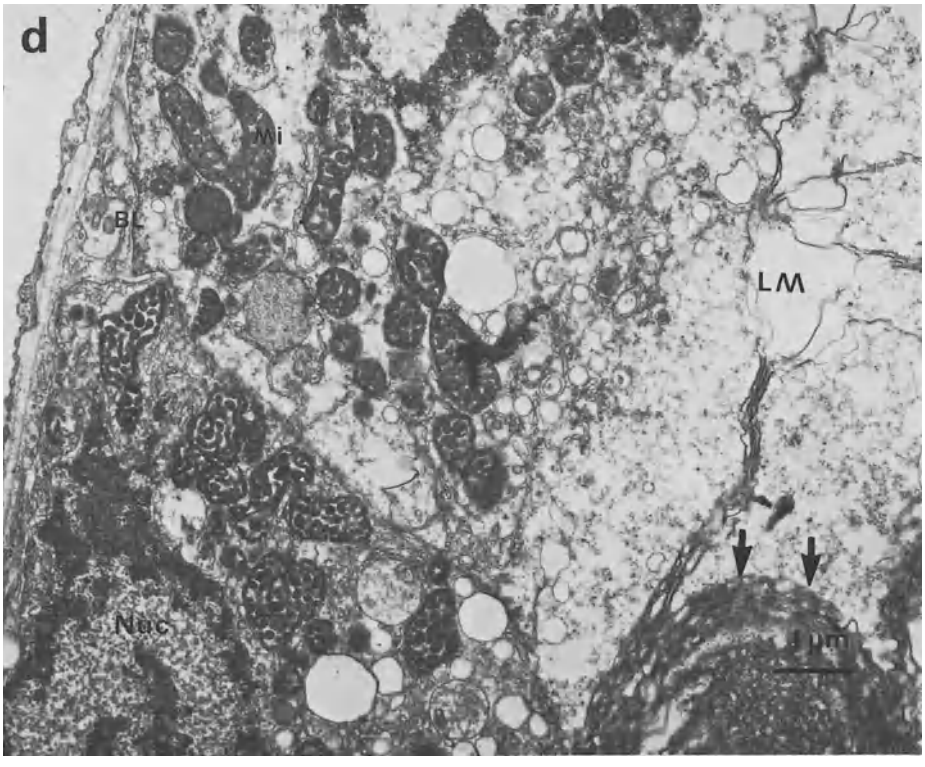
d
Mi
BL
LM
Nuc
1 µm

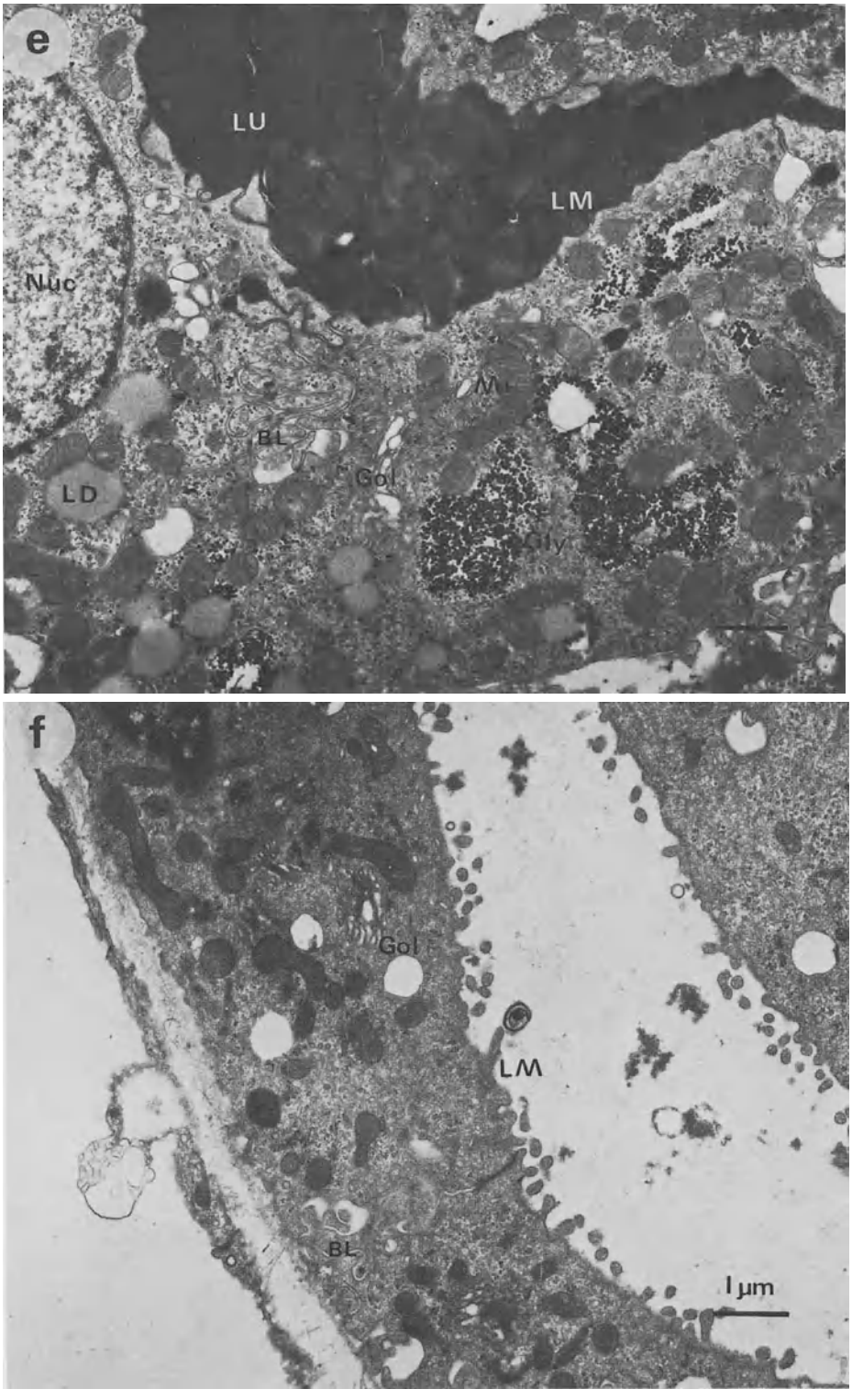
e
LU
LM
Nuc
M
BL
Gol
LD
Gly
f
Gol
LM
BL
1 µm

Table 32. Volumetric composition of acutely injured renal cortex (%)

	Control	$HgCl_2$ 30 min	$HgCl_2$ 6 h	$HgCl_2$ 24 h	$HgCl_2$ 6 h rewarmed	Maleic acid	Ischemia 45 min	Ischemia 45 min + 45 min blood reflow	Hypothermia 2 h at 30 °C
Epithelium proximal $S_1+S_2+S_3$	40.00 ± 8.20	45.80 ± 10.60	40.10 ± 8.50	34.00 ± 5.40	50.78 ± 1.87	43.16 ± 4.30	54.31 ± 4.39	37.76 ± 9.10	47.00 ± 1.20
Necrotic epithelium				14.00 ± 1.80					
Epithelium distal	6.70 ± 0.70	7.50 ± 1.00	6.30 ± 0.10	6.90 ± 0.70	6.04 ± 0.60	5.74 ± 0.60	5.50 ± 0.61	5.15 ± 0.06	4.91 ± 1.20
Epithelium collecting duct	3.70 ± 0.90	2.30 ± 0.40	1.60[a] ± 0.40	1.20[a] ± 0.20	3.27 ± 0.50	4.20 ± 0.84	2.83 ± 0.10	3.00 ± 1.81	4.32 ± 1.00
Interstitial space and cells	8.00 ± 0.70	14.00[a] ± 0.80	10.70[a] ± 0.40	12.60[a] ± 1.10	8.78 ± 0.39	8.43 ± 1.08	9.29 ± 0.67	8.37 ± 0.72	8.30 ± 1.25
Lumen proximal $S_1+S_2+S_3$	21.40 ± 8.30	14.40 ± 3.90	18.30 ± 5.20	17.00 ± 0.20	11.61 ± 2.90	18.21 ± 1.80	13.41 ± 1.38	31.02[a] ± 4.48	14.62 ± 4.79
Lumen distal	4.60 ± 0.10	4.00 ± 0.50	6.30 ± 1.50	2.70 ± 0.30	5.98[a] ± 0.25	4.49 ± 1.25	0.72[a] ± 0.56	3.19 ± 2.72	3.90 ± 0.29
Lumen collecting duct	2.30 ± 0.60	2.70 ± 0.70	6.70 ± 1.10	0.50 ± 0.10	2.45 ± 0.80	2.87 ± 0.70	0.52[a] ± 0.36	0.41[a] ± 0.14	4.48 ± 1.33
Capillary and vasc. lumen incl. glomeruli	13.30 ± 0.90	10.00 ± 1.20	9.60 ± 1.00	11.80 ± 1.90	11.19 ± 0.88	12.50 ± 2.28	14.40 ± 1.20	11.19 ± 0.92	12.50 ± 1.30

Values are mean ± standard error (SEM)
[a]Statistically significant difference from control ($P < 0.05$)

◀ Fig 10. *a* View of cortical tissue (level 1 – light microscopy) 24h after $HgCl_2$. Proximal tubules are partly necrotized (Nec, lethal injury). Others show severe alterations, mainly protrusions of cytoplasmic blebs (*arrows*) into the tubular lumen. Distal tubule and collecting duct lumina are filled with dense casts and display widened intercellular spaces. *b* Another view of kidney cortex which shows a region where less necrotic tubules are present. The changes of sublethally injured proximal tubules seem to be confined preferentially to S_3 segments contained in the medullary rays. *c* Proximal tubule. Changes are severe. No more differentiation between S_2 and S_3 segments is possible. A bleb protruding into the lumen contains mitochondria with small electron dense precipitations (*arrows*). The majority of mitochondria (*Mi*), however, is structurally unaltered. Luminal brush border and basolateral cell surface is reduced. *d* Part of a prenecrotic proximal tubule. Mitochondria are condensed, the endoplasmic reticulum is swollen and in addition forms curls (*arrows*) in some regions of the cells. The number of lysosomes is reduced. *e* Distal tubule. The tubule is collapsed and the lumen filled with an electron dense cast. Within the cells large amounts of glycogen (*asterisks*) and some lipid droplets (*LD*) have accumulated. *f* Collecting duct. Apart from a high number of vacuoles and a collapsed tubular lumen no differences are detectable when compared with the controls

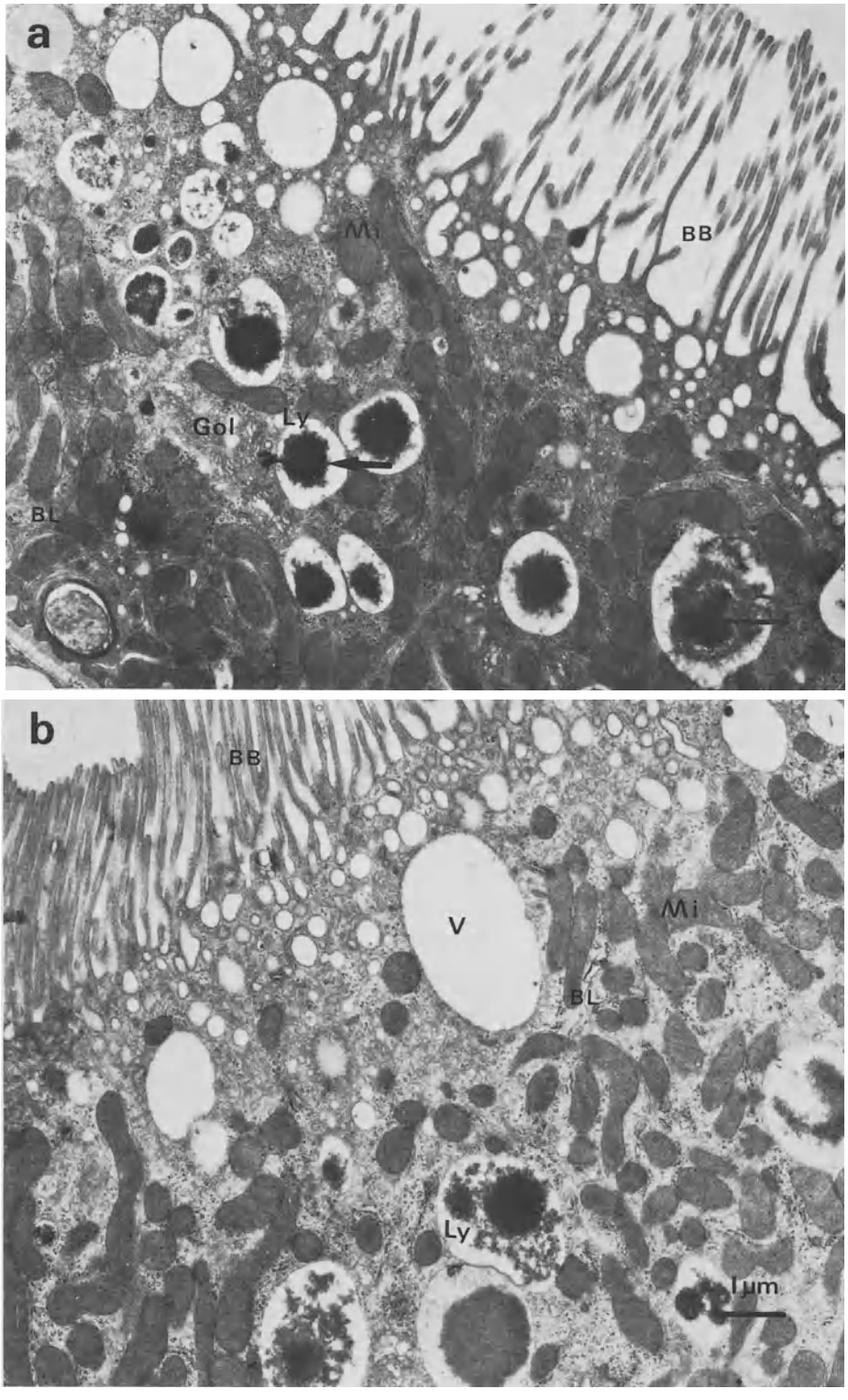
a
Mi
BB
Gol
Ly
BL
b
BB
V
Mi
BL
Ly
1µm

Table 33. Volume densities relative to a unit of cytoplasm (%)

	Control	$HgCl_2$ 30 min	$HgCl_2$ 6 h	$HgCl_2$ 24 h	$HgCl_2$ 6 h rewarmed	Maleic acid 2 h	Ischemia 45 min	Ischmia 45 min + 45 min blood reflow	Hypothermia 2 h at 30 °C
Proximal tubule $S_1 + S_2$									
Mitochondria	31.46 ± 1.9	34.05 ± 1.5	31.26 ± 3.6	24.06[a] ± 2.6	27.32 ± 4.2	27.78 ± 3.05	22.94[a] ± 0.85	22.70[a] ± 2.0	18.56[a] ± 1.26
Lysosomes	6.4 ± 0.9	6.2 ± 1.5	7.2 ± 1.1	9.1 ± 1.3	8.42 ± 1.03	4.99 ± 0.89	4.94 ± 0.46	6.0 ± 1.0	6.03 ± 1.06
Vacuoles	4.3 ± 0.1	3.73 ± 0.6	4.0 ± 0.9	5.8[a] ± 0.6	4.38 ± 1.52	12.65 ± 2.49	3.7 ± 0.5	6.32 ± 1.87	7.02 ± 1.47
Proximal tubule S_3									
Mitochondria	22.58 ± 4.2	28.56 ± 1.4	26.88 ± 3.1	25.19 ± 2.4	23.22 ± 1.81	25.78 ± 2.3			20.26 ± 1.39
Lysosomes	4.32 ± 1.0	5.9 ± 1.1	9.32[a] ± 0.2	3.1 ± 0.2	8.91[a] ± 0.4	2.84 ± 0.73			0.9 ± 0.5
Vacuoles	0.74 ± 0.06	0.72 ± 0.1	1.79[a] ± 0.6	9.62[a] ± 2.6	3.23[a] ± 0.7	5.41[a] ± 1.46			1.14[a] ± 0.22

Values are mean ± standard error (SEM)
[a]Statistically significant difference from control ($P < 0.05$)

without counterheating during this period, being much less pronounced. The same is valid for the apical vacuolization, which is missing under rewarming conditions. The alterations of medullary ray region found in animals not counterheated are extremely seldom (Fig. 12). In a very few cases proximal tubular lumina display cellular debris probably sequestered by sublethally injured cells. At the electron microscopic level an increase in unusually configurated lysosomal structures is evident. They are characterized by a condensation of the electron dense content in the core of the transection profile, whereas the regions adjacent to the organelles, membrane are electron translucent. In addition, some of the apical reabsorptive vacuoles contain electron-dense material. Distal tubular and collecting duct epithelium do not differ from controls in their qualitative morphology.

Fig. 11. *a* Proximal tubular S_2 segment 6 h after $HgCl_2$ and counterheating. The only aberration from normal tubular structures are strange-looking heterophagosomes (*Ly*) with an electron dense core and a halo around it (*arrows*). All other structures like luminal, basolateral membrane, and mitochondria seem unaffected. *b* Proximal tubular S_3 segment. The same or quite similar lysosomal structures (*Ly*) to those present in the S_2 segment can be found. A difference seems to exist for the electron dense core which is more disintegrated. In addition an increased amount of apical vacuoles (*V*) is evident

Table 34. Volume densities relative to a unit of cytoplasm (%)

	Control	$HgCl_2$ 30 min	$HgCl_2$ 6 h	$HgCl_2$ 24 h	$HgCl_2$ 6 h rewarmed	Maleic acid 2 h	Ischemia 45 min	Ischmia 45 min + 45 min blood reflow	Hypothermia 2 h at 30 °C
Distal tubules									
Mitochondria	30.97 ± 2.90	31.41 ± 1.10	40.26[a] ± 3.10	25.34[a] ± 0.30	35.35[a] ± 0.30	32.99 ± 3.40	33.5 ± 5.11	29.47 ± 1.90	28.71 ± 6.06
Lysosomes	1.24 ± 0.3	0.64 ± 0.4	0.7 ± 0.1	2.44[a] ± 0.1	0.38[a] ± 0.08	1.12 ± 0.2	1.73 ± 0.7	0.8 ± 0.2	2.13[a] ± 0.2
Vacuoles	0.75 ± 0.4	0.51 ± 0.3	0.56 ± 0.2	0.18 ± 0.6	3.49[a] ± 1.9	4.9[a] ± 1.2	1.8 ± 1.2	7.35[a] ± 2.1	2.86[a] ± 1.4
Collecting duct									
Mitochondria	18.03 ± 3.7	17.33 ± 3.7	13.82 ± 2.6	14.11 ± 2.6	22.83 ± 3.18	15.72[a] ± 1.4	19.81 ± 2.1	14.90[a] ± 1.68	19,20 ± 0.02
Lysosomes	0.80 ± 0.4	0.60 ± 0.4	0.70 ± 0.3	1.59 ± 0.3	0.72 ± 0.22	1.22 ± 0.4	4.52 ± 3.4	0.80 ± 0.4	0.90 ± 0.5
Vacuoles	0.3 ± 0.1	0.27 ± 0.2	0.80 ± 0.3	0.31 ± 0.1	0.32 ± 0.03	5.27[a] ± 1.4	5.24[a] ± 2.7	3.4[a] ± 1.6	3.60[a] ± 0.5

Values are mean ± standard error (SEM)
[a]Statistically significant difference from control ($P < 0.05$)

Table 35. Surface densities relative to a unit of cytoplasm ($\mu m^2/\mu m^3$)

	Control	$HgCl_2$ 30 min	$HgCl_2$ 6 h	$HgCl_2$ 24 h	$HgCl_2$ 6 h rewarmed	Maleic acid 2 h	Ischemia 45 min	Ischemia 45 min + 45 min blood reflow	Hypothermia 2 h at 30 °C
Proximal tubule $S_1 + S_2$									
Luminal membrane	4.98 ± 0.76	4.54 ± 0.21	2.17[a] ± 0.24	1.93[a] ± 0.38	3.78 ± 0.46	4.48 ± 0.46	0.40 ± 0.21	3.76[a] ± 0.16	3.94 ± 0.27
Basolateral membrane	3.23 ± 0.28	3.88 ± 0.51	2.35[a] ± 0.37	1.82[a] ± 0.52	2.75 ± 0.11	3.37 ± 0.55	2.17[a] ± 0.18	2.87 ± 0.18	2.77 ± 0.28
Mitochondrial outer membrane	2.12 ± 0.12	2.00 ± 0.11	1.82 ± 0.11	1.51[a] ± 0.29	1.23[a] ± 0.12	1.99 ± 0.46	0.91[a] ± 0.02	1.53[a] ± 0.14	1.51[a] ± 0.05
Mitochondrial cristae membrane	5.68 ± 0.10	6.20 ± 0.44	3.20[a] ± 0.26	2.68[a] ± 0.26	3.02[a] ± 0.57	2.28[a] ± 0.40	3.76[a] ± 0.38	3.03[a] ± 0.40	4.06[a] ± 0.33

Proximal Tubule S_3

Luminal membrane	4.60 ± 0.37	4.59 ± 0.40	2.77[a] ± 0.48	1.96[a] ± 0.81	3.38[a] ± 0.26	4.60 ± 0.53			4.37 ± 0.54
Basolateral membrane	1.40 ± 0.11	1.29 ± 0.16	0.86[a] ± 0.10	0.84[a] ± 0.15	1.03[a] ± 0.19	1.61 ± 0.48			1.42 ± 0.32
Mitochondrial outer membrane	1.79 ± 0.22	2.13 ± 0.14	1.88 ± 0.18	1.79 ± 0.73	1.65 ± 0.29	1.38[a] ± 0.17			1.14 ± 0.22
Mitochondrial cristae membrane	3.68 ± 0.34	3.86 ± 0.26	2.70[a] ± 0.32	2.60[a] ± 0.08	2.75[a] ± 0.15	1.55[a] ± 0.15			1.42[a] ± 0.09

Values are mean ± standard error (SEM)
[a]Statistically significant difference from control ($P < 0.05$)

Table 36. Surface densities relative to a unit of cytoplasm ($\mu m^2/\mu m^3$)

	Control	$HgCl_2$ 30 min	$HgCl_2$ 6 h	$HgCl_2$ 24 h	$HgCl_2$ 6 h rewarmed	Maleic acid 2 h	Ischemia 45 min	Ischemia 45 min, 45 min blood reflow	Hypothermia 2 h at 30 °C
Distal tubule									
Luminal membrane	0.37 ± 0.08	0.45 ± 0.15	0.55 ± 0.16	0.18 ± 0.05	0.30 ± 0.06	0.37 ± 0.04	0.02[a] ± 0.01	0.32 ± 0.07	0.37 ± 0.05
Basolateral membrane	4.34 ± 0.68	3.53 ± 0.35	4.32 ± 0.75	2.14[a] ± 0.52	4.05 ± 0.61	3.41[a] ± 0.20	2.34[a] ± 0.46	3.87 ± 0.61	3.11 ± 0.73
Mitochondrial outer membrane	2.25 ± 0.28	2.03 ± 0.18	2.47 ± 0.24	1.64[a] ± 0.05	1.41[a] ± 0.04	1.75[a] ± 0.19	1.47[a] ± 0.35	1.62[a] ± 0.19	1.99[a] ± 0.04
Mitochondrial cristae membrane	6.08 ± 0.72	5.12 ± 0.81	6.82 ± 0.80	6.31 ± 0.30	4.99 ± 0.51	1.51 ± 0.20	3.62 ± 0.73	2.60 ± 0.07	3.45 ± 0.93
Collecting duct									
Luminal membrane	0.28 ± 0.03	0.41 ± 0.08	0.43 ± 0.08	0.51 ± 0.04	0.23 ± 0.03	0.31 ± 0.04	0.95[a] ± 0.29	0.15[a] ± 0.08	0.17 ± 0.09
Basolateral membrane	3.51 ± 0.20	3.52 ± 0.08	2.98 ± 0.58	1.81[a] ± 0.50	2.30 ± 0.84	3.68 ± 0.36	0.99[a] ± 0.02	2.43 ± 0.67	2.22[a] ± 0.18
Mitochondrial outer membrane	1.56 ± 0.06	1.51 ± 0.04	1.52 ± 0.20	1.33 ± 0.08	1.28 ± 0.27	1.09 ± 0.13	0.97[a] ± 0.02	0.68[a] ± 0.31	1.15[a] ± 0.17
Mitochondrial cristae membrane	2.39 ± 0.49	1.58[a] ± 0.36	1.36[a] ± 0.11	2.16 ± 0.33	2.44 ± 0.43	0.58[a] ± 0.29	1.08[a] ± 0.08	1.74 ± 0.30	1.61[a] ± 0.20

Values are mean ± standard error (SEM)
[a]Statistically significant difference from control ($P < 0.05$)

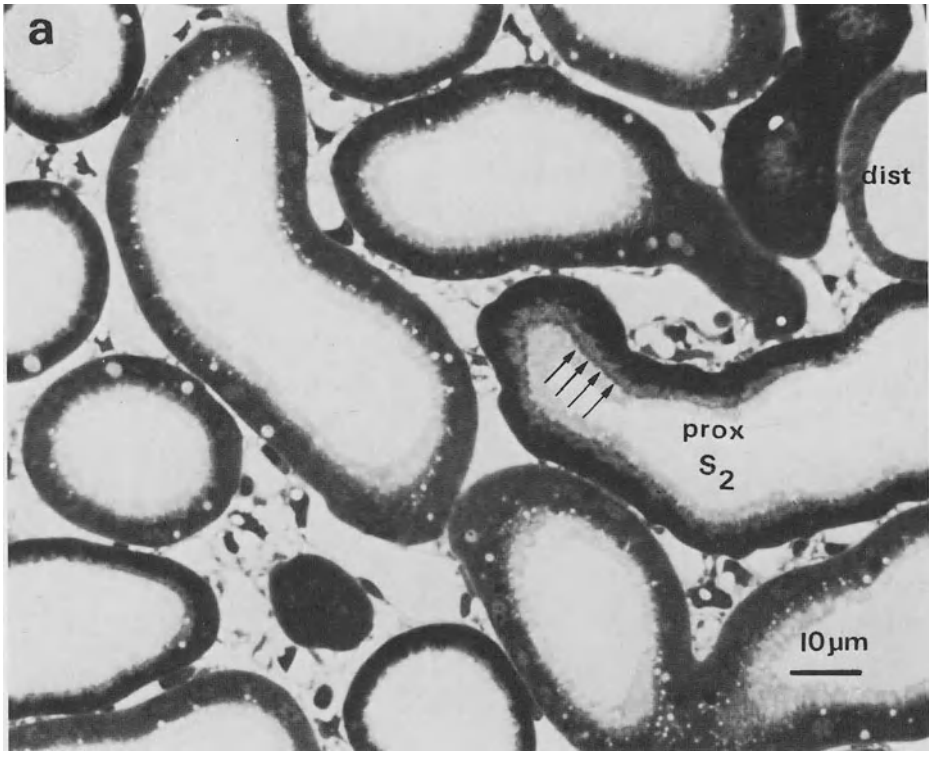
a
dist
prox
S_2
10µm

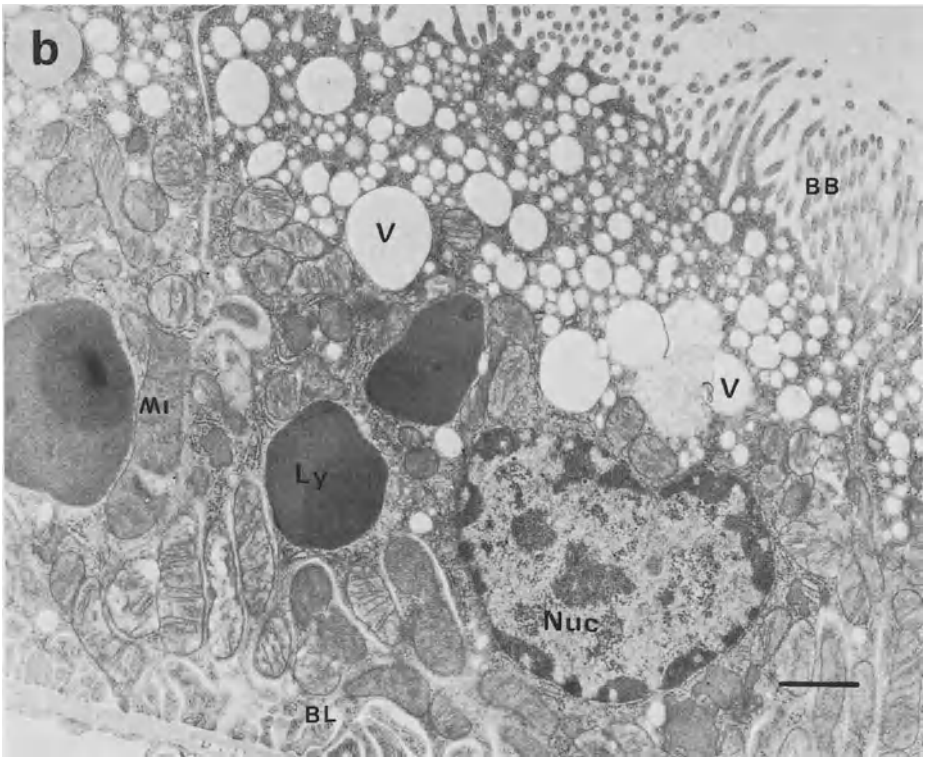
b
BB
V
V
Mi
Ly
Nuc
BL

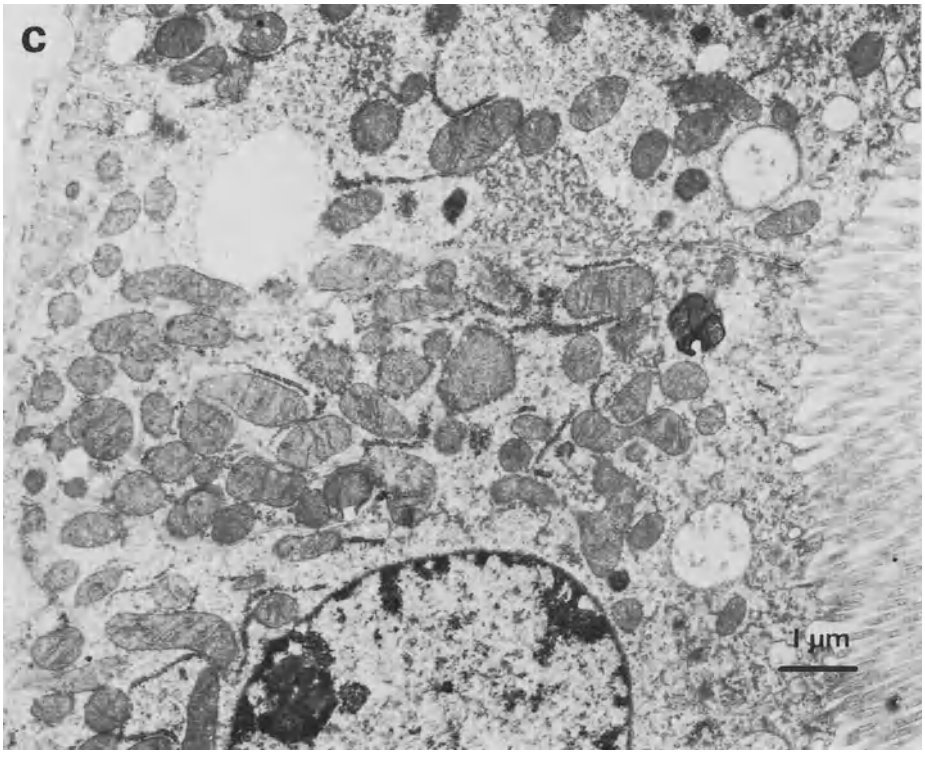
c
1 µm

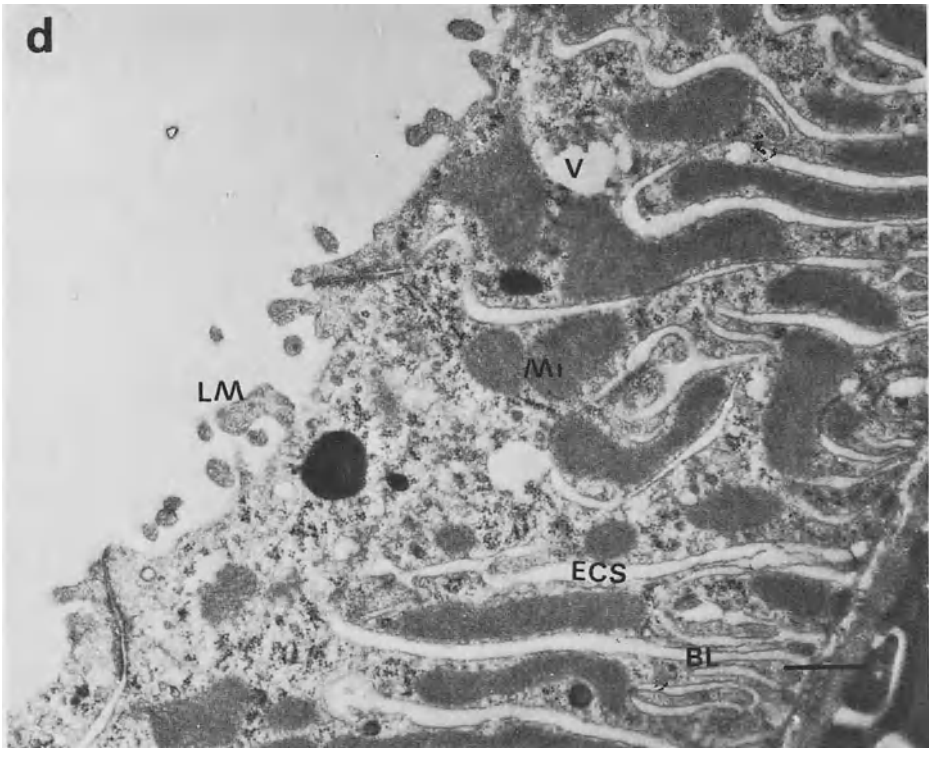
d
V
LM
ECS
BL

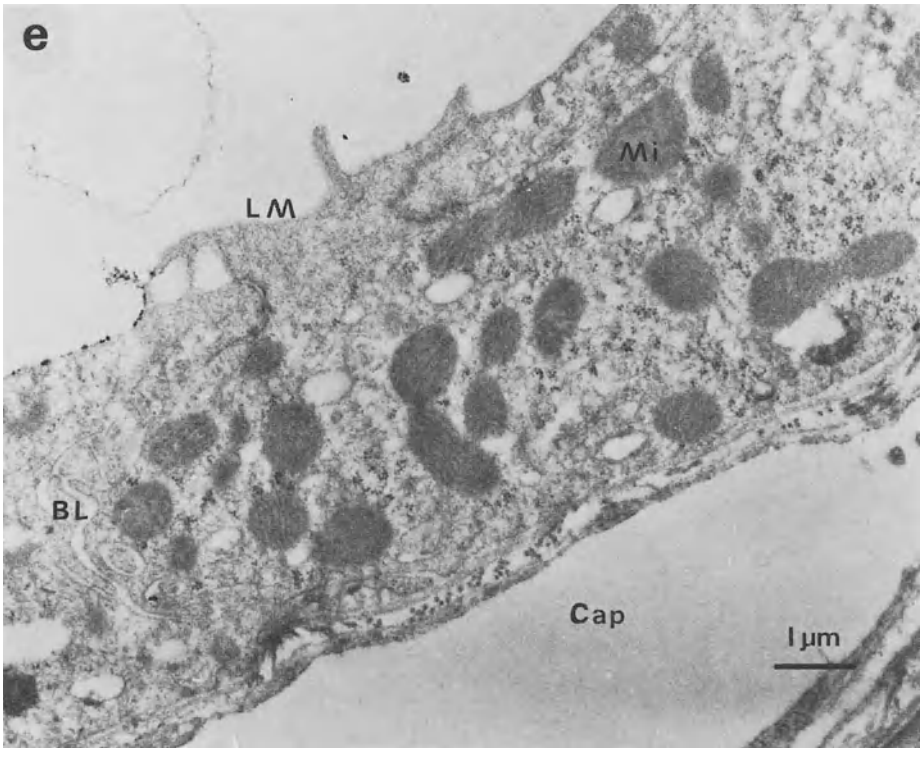

Fig. 12. *a* Cortical tissue 2 h after maleic acid. The change found is an increase in the staining intensity of some tubules which also exhibit a sharply demarcated light region below the brush border (*arrows*). Some of the transsected proximal tubules show large vacuoles. *b* Proximal tubular S_2 segment. The apical cell portion is filled with vacuoles (*V*), which are in close association with lysosomes. The matrix of mitochondria seems slightly less electron dense than in controls. *c* Proximal tubular S_3 segment. Apart from a slightly higher frequency of large vacuoles and apically located multivesicular bodies there exist no striking differences when a comparison is made with the controls. *d* Distal tubular epithelium (distal convolution). The only difference when compared to control conditions is a widening of basolateral intercellular space (*ECS*) and a denser mitochondrial matrix. *e* Cortical collecting duct which does not display an ultrastructural assembly different from the controls, except perhaps a swelling of the endoplasmic reticulum

5.2.2.2 Quantitative Morphology

Sampling Level 1 (Light Microscopy)

The following changes are detected: The volume fraction of proximal tubular S_2 segment epithelium appears slightly increased. The luminal compartment of distal tubules displays a significantly elevated volume density, when compared to controls (+30%, Table 32). All other parameters stay unaltered.

Proximal Tubule – Sampling Level 3 and 4

No changes exist for the lysosomal and the vesicular volume density with regard to the control when referred to a unit of cytoplasm. The luminal membrane surface of

proximal S_2 segment, however, is decreased by 24% and the basolateral surface density by 15%. For the S_3 segment the reduction in luminal surface amounts to 44% and that of the basolateral to 26%. A decrease is also observed in the mitochondrial membrane systems (Table 35) and is especially pronounced for the cristae membrane surface (–64%) of the S_2 segment. In the case of the S_3 segment the decrease is only 25%.

Distal Tubule – Sampling Level 4

For mitochondrial fractional volume a slight but significant increase is found. A similar behavior is found for apical vacuoles but their increase is more pronounced. In contrast to this, we observe a fall in the lysosomal volume fraction (Table 34).

Collecting Duct – Sampling Level 4

The changes in quantitative morphology may be summarized as follows: There exists no change in volume densities for mitochondria, lysosomes and vacuoles (Table 35), no change for the luminal surface and the mitochondrial membrane system, but a significantly reduced (–48%) basolateral membrane surface area per unit of cytoplasm (Table 36).

5.2.3 The Maleic Acid Model

5.2.3.1 Qualitative Morphology

Two hours after intraperitoneal administration of neutralized maleic acid, morphological changes can be observed. Besides normally looking tubular profiles very intensively stained tubular epithelium is found. Their lumina appear to be widened and vacuolization of the apical cytoplasm is apparent; whereas the brush border seems unaltered (Fig. 13).

Proximal Tubule

There is a pronounced accumulation of apical vacuoles which fill nearly the whole apical half of the cell. The lysosomes appear to the enlarged and the frequency of polyribosomes seems to be reduced, single ribosomes instead being scattered all over the cytoplasm (Fig. 13). In comparison to the controls the cytoplasmic ground substance often appears electron dense. The same applies for the nucleus and the mitochondrial matrix. Mitochondria display some swollen transection profiles but no condensed mitochondria can be found. No necrotic or prenecrotic cells are detectable. The height of the epithelial wall of injured proximal tubules appears to be reduced and the apical microvilli display larger interspaces than in control animals. Besides tubules, altered in the described manner, absolutely normal-looking tubular transsection profiles can be observed.

Distal Tubule

No obvious changes in qualitative structural assembly of the cells, as compared to controls, can be recognized. The only alteration which might be noted, and which can sometimes be found, is a lightening of the hyaloplasm and a widening of the basolaterally localized intercellular spaces (Fig. 13d).

Collecting Duct

The structural appearance of epithelial cells assembling this nephron segment is absolutely comparable to that of control animals except for widened basolateral intercellular spaces.

5.2.3.2 Quantitative Morphology

Sampling Level 1 (Light Microscopy)

In general no drastic changes in comparison to the control situation are apparent, except that the lumen volume of the proximal tubule is slightly increased. The data on volumetric composition of the cortex tissue is summarized in Table 33.

Proximal Tubule – Sampling Level 3 and 4

When using a unit volume of cytoplasm as a reference volume the proximal tubular mitochondrial volume density is equal to that of controls, and also the lysosomal compartment is not altered (Table 33). The most prominent change however, is found in the apical pinocytotic vacuoles, which are increased by a factor of 3 in the S_2 segment and by a factor of 7 in the S_3 segment (Table 33). In contrast to the above described $HgCl_2$ model, no reduction in luminal and basolateral membrane surface is detected in both the proximal S_2 and S_3 segment (Table 34). The mitochondrial cristae membrane surface of the proximal S_2 segment is reduced by 60% and that of the S_3 segment by 58%, while the mitochondrial outer membrane remains unaltered.

Distal Tubule – Sampling Level 4

A similar increase in apical vacuoles, as described above for the proximal nephron, can be found in the distal convoluted portion. The factor is 6.5 (Table 35). Mitochondrial and lysosomal volume fractions do not change upon administration of maleic acid. Decreased surface areas are found for the basolateral membrane (–21%) and the mitochondrial cristae (–75%).

Collecting Duct – Sampling Level 4

The only alterations found for this segment are an increase in volume density of vacuoles by a factor of 17 and a decrease in cristae membrane surface by 76% relative to a unit of cytoplasm.

5.2.4 The Ischemic Model – No Blood Reflow

5.2.4.1 Qualitative Morphology

At the light microscopic level tubular lumina which are hardly open are apparent. The cells seem to be swollen and show a light cytoplasmic matrix (Fig. 14a).

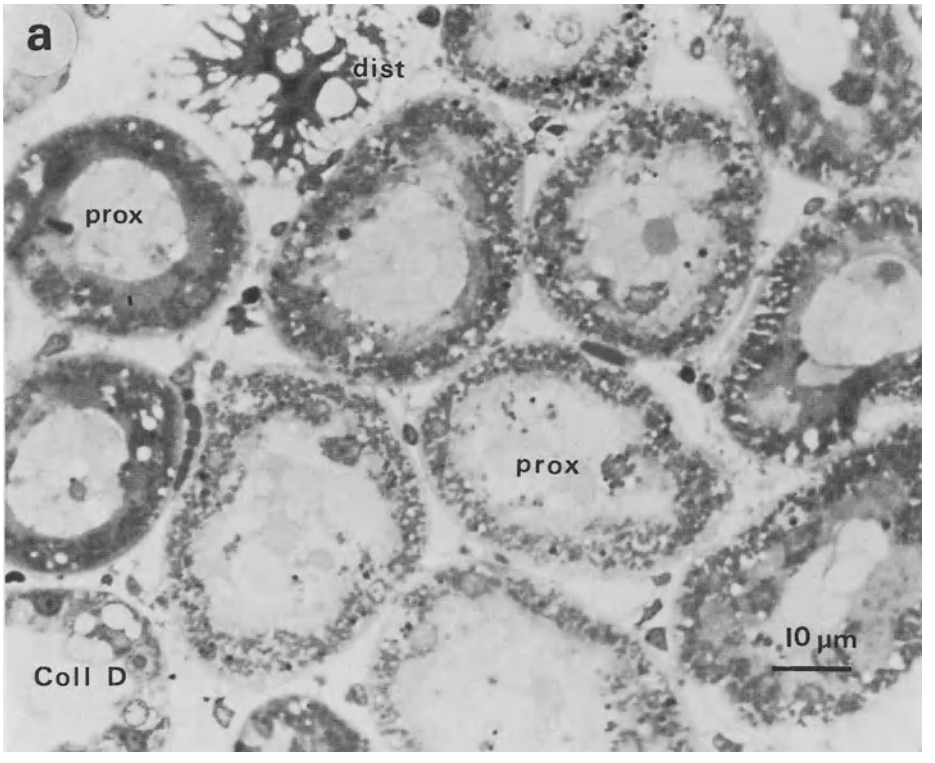
a
dist
prox
prox
10 µm
Coll D

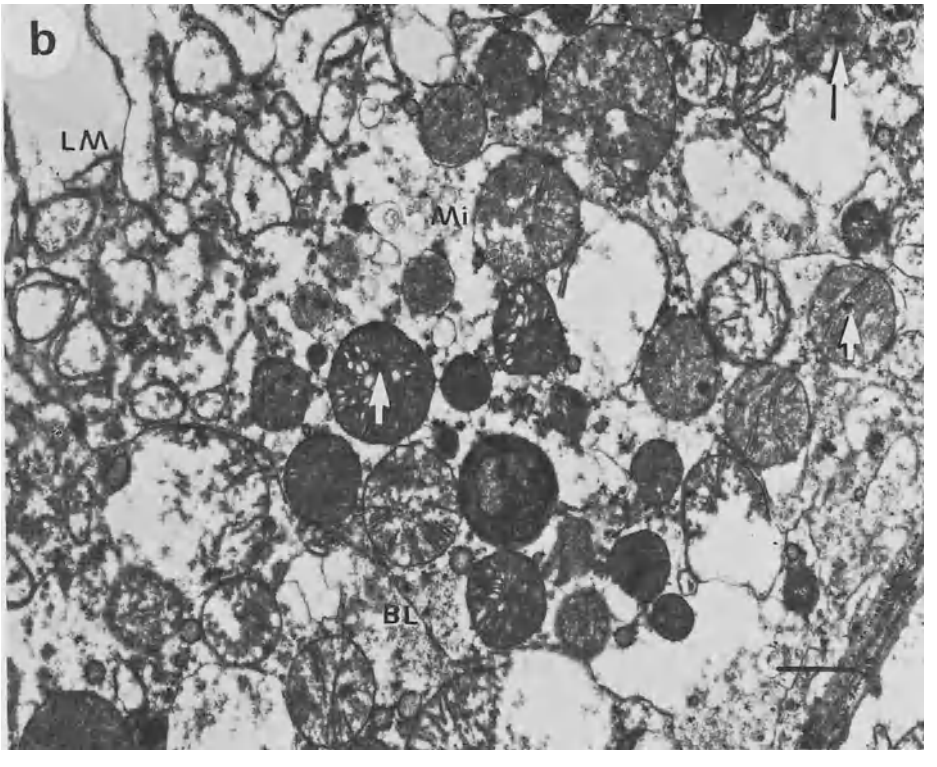
b
LM
Mi
BL

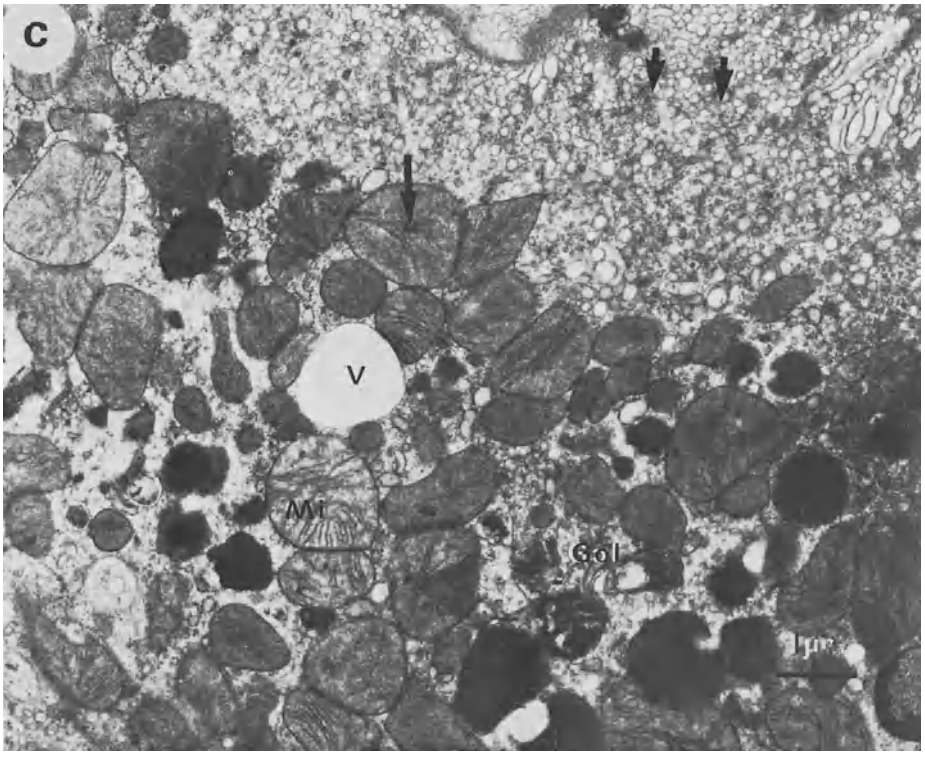
c
V
Mi
Gol
1µm

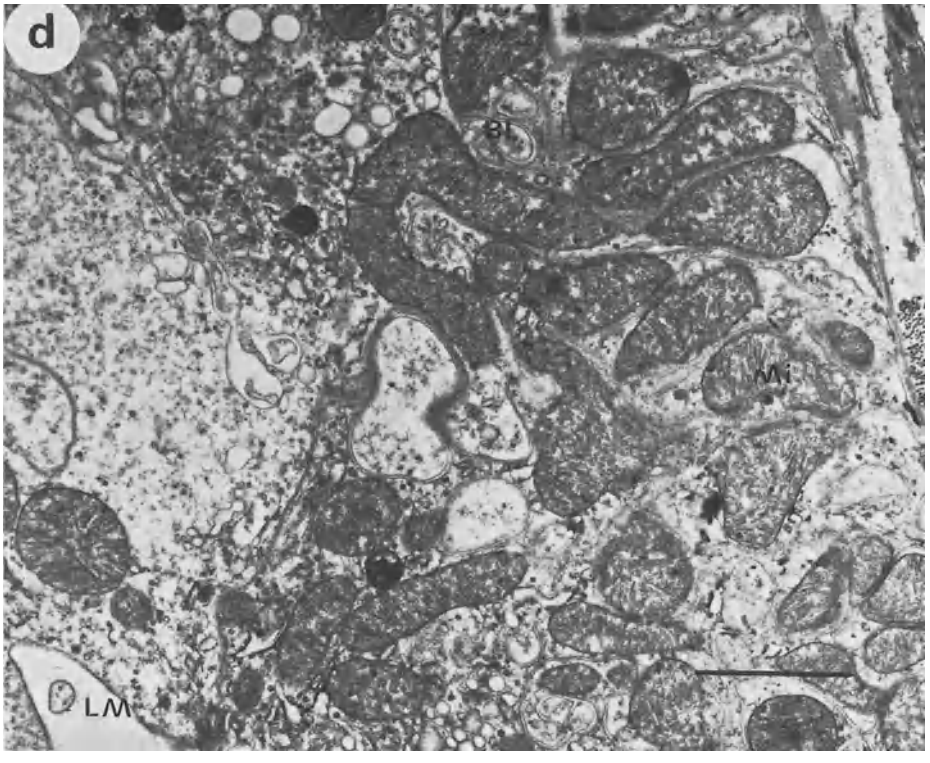
d
Mi
LM

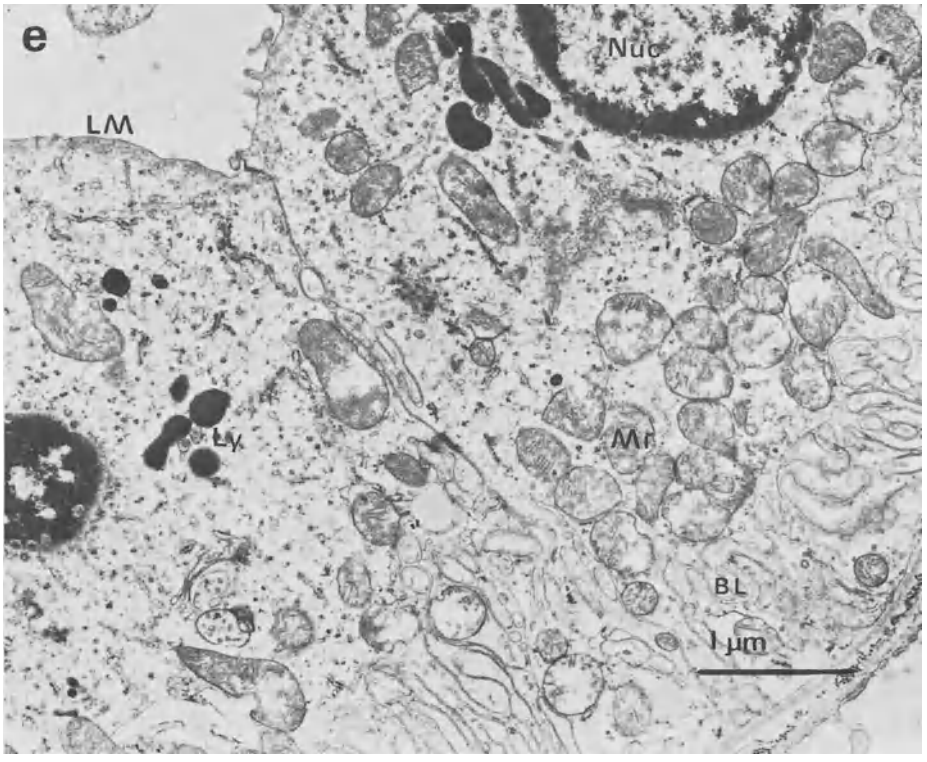

Fig. 13. *a* Kidney cortex (sampling level 1) after 45 min warm ischemia. The proximal tubular lumen is filled with cellular debris and the epithelial wall appears swollen. Distal tubules are collapsed, no lumen can be recognized, and the lateral intercellular spaces are extremely enlarged (*arrows*). *b* and *c* Proximal tubule (sampling level 3). The brush border region is *b* totally disintegrated or *c* internalized into the apical cell pole (*arrows*). Mitochondria seem swollen and sometimes exhibit disrupted outer and inner membranes and flocculent densities within the matrix (*arrows*). *d* Distal tubule (sampling level 4). The cytoplasmic matrix appears less electron dense than normal and mitochondria seem to be swollen. In addition the cisternae of the endoplasmic reticulum are vesiculated and enlarged. *e* Collecting duct (sampling level 4). As in distal tubules the cytoplasmic ground substance is light and the mitochondria swollen. Sometimes within mitochondria fragmentation of cristae occurs. In the perinuclear region clusters of lysosomes may be recognized. In contrast to distal tubules the endoplasmic reticulum seems unaffected

Proximal Tubule

The cells of the S_1 and S_2 segments of proximal nephrons are swollen and display an electron translucent cytoplasm, grossly distorted microvilli, and bleb formations protruding into the tubular lumen. The nuclear chromatin is clumped and the endoplasmic reticulum is vesiculated. The swollen mitochondria sometimes exhibit small flocculent densities (600 nm). Their boundary membranes and their outer membranes are often disrupted (Fig. 14b, c).

Distal Tubule

In general, the same features as just described for proximal tubular cells are valid, with the exception that no chromatin condensation can be found and intramitochondrial flocculent densities are much smaller in number (Fig. 14d).

Collecting Duct

Mitochondrial transsection profiles appear to be swollen and show sometimes a fragmentation of the matrix or in a few cases fragmentation of the inner boundary membrane (Fig. 14e).

5.2.4.2 Quantitative Morphology

Sampling Level 1

At sampling level 1 the volume fraction of proximal tubular epithelium is significantly increased. This swelling of the epithelium is counterbalanced by a decrease in the luminal volume fraction of proximal, distal, and collecting duct segments. All other cortical tissues occupy about the same volume fraction as in control animals (Table 32).

Proximal Tubule – Sampling Level 3 and 4

The swelling of cells and their cytoplasm respectively precedes or does not effect, the mitochondria this being shown by a significantly reduced volume fraction (Table 33). This is substantiated in addition by a reduction in mitochondrial outer membrane surface per unit volume of cytoplasm (Table 35) of roughly 60%. The cristae surface area is reduced by a factor of 1.5, regardless of whether or not a unit of cytoplasm or a unit of mitochondria itself represents the reference space. The two plasma membrane domains and the total cellular surface are also reduced, the most drastic reduction being confined to the luminal membrane (–91%, Table 35).

Distal Tubule – Sampling Level 4

No changes exist for the volume densities of the various subcellular parameters evaluated. The surface densities of all membranes are decreased, the luminal by 94%, the basolateral by 46%, the mitochondrial outer membrane by 35%, and the cristae membrane area by 40%, when referred to a unit of epithelial cytoplasm (Table 36).

Collecting Duct – Sampling Level 4

In case of this segment an increased volume of membrane coated vacuoles by a factor of 17 has to be recognized as well as an increased lysosomal volume density (Table 35). The measures on membrane surface density are all smaller than those of the control animals except that of the luminal membrane surface (Table 36).

5.2.5 The Ischemic Model – Blood Reflow for Forty-five Minutes

5.2.5.1 Qualitative Morphology

Light microscopically the tubular lumina are patent and sometimes appear to be even dilated (Fig. 15a). The characteristic picture of the "brushborder" found in controls is missing. The apical pole of the epithelial cells often displays regions with densely packed fairly large vacuoles or regions containing no, or only a few, cytoplasmic or-

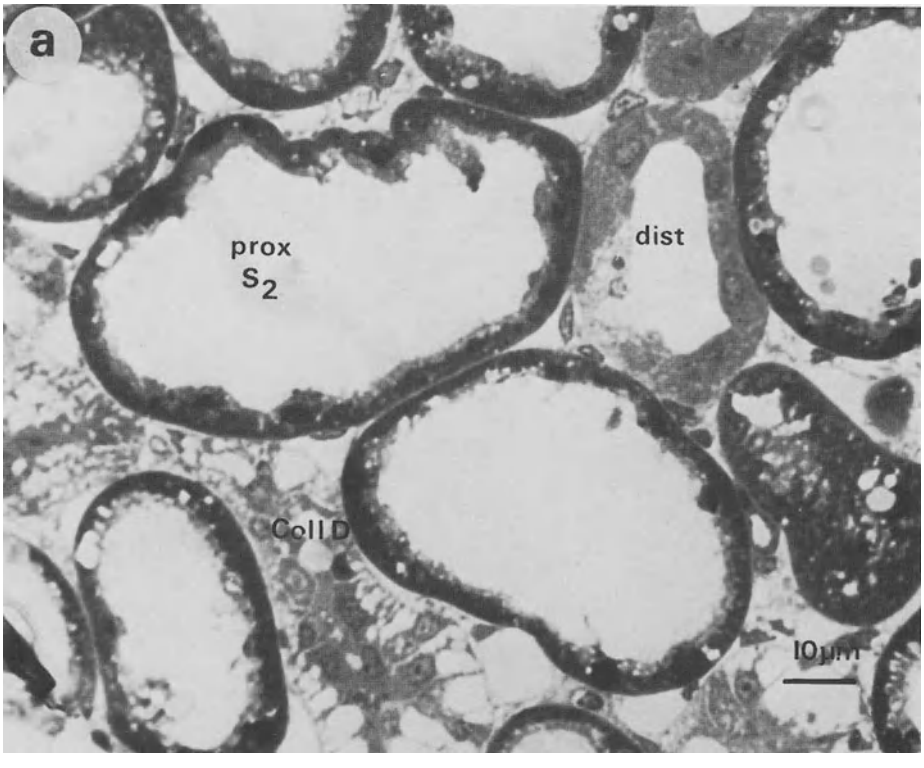
a
prox
S_2
dist
CollD
10µm

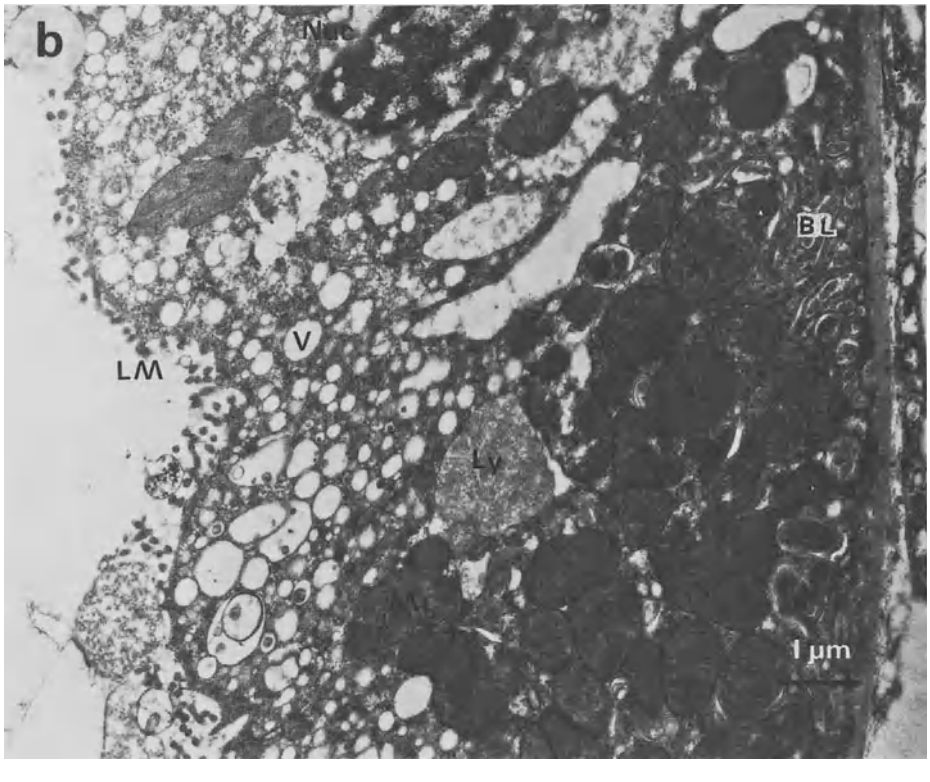
b
Nuc
BL
V
LM
LY
1 µm

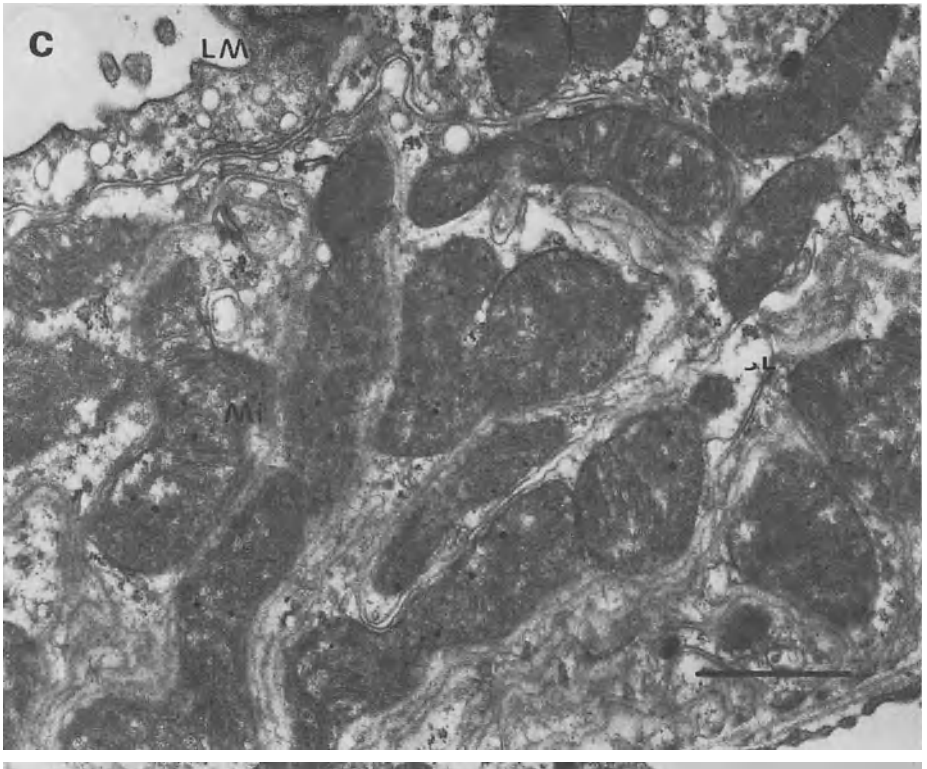
c
LM
Mi

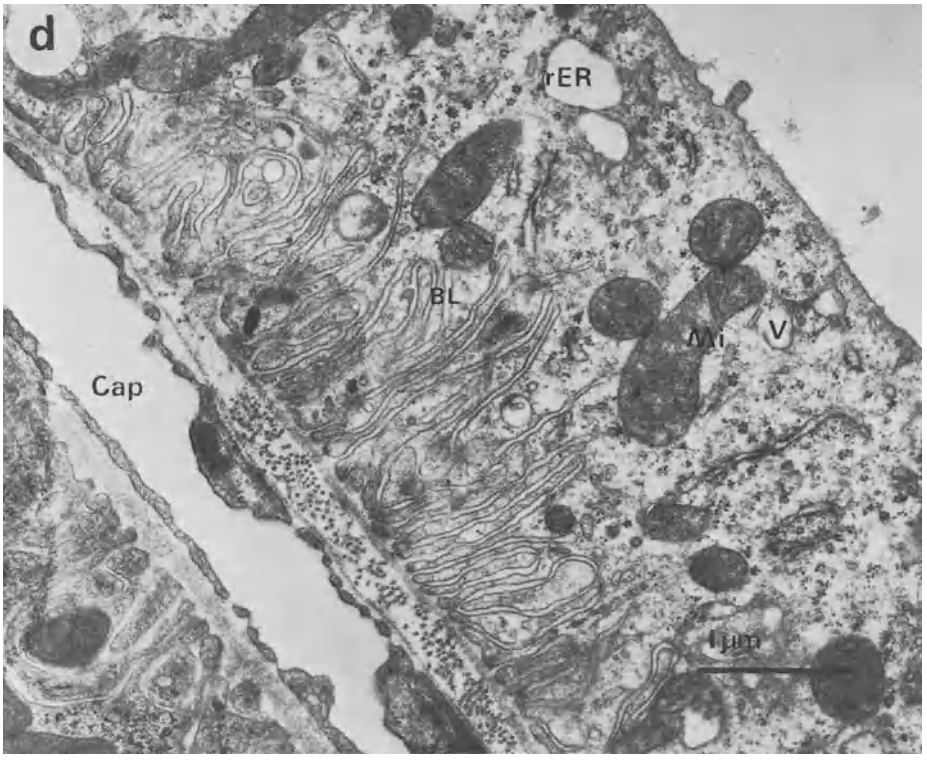
d
rER
BL
Mi
V
Cap
1 µm

ganelles (Fig. 15b, c). A numer of tubular lumina contain debris, mostly in the form of round structures. The transection profiles of distal tubules and collecting ducts seem to have enlarged cisternae of the endoplasmic reticulum and intercellular spaces (Fig. 15c, d).

5.2.5.2 Quantitative Morphology

Sampling Level 1 (Light Microscopy)

At sampling level 1 there is an increase in the volume fraction of proximal tubular lumen, at the expense of the collecting duct luminal volume and the capillary space which decrease.

Proximal Tubule – Sampling Level 3 and 4

In proximal tubular cells recovering from acute ischemia, the mitochondrial volume density is reduced significantly by a factor of 1.4. In addition, luminal (–24%), mitochondrial outer (–28%), and cristae membranes (–47%) are significantly diminished (Table 34).

When referring mitochondrial outer and cristae membrane density to a unit volume of the compartment itself, the decrease is even more pronounced for the latter two parameters.

Distal Tubule – Sampling Level 3 and 4

The most prominent change is confined to the volume of the vacuolar compartment, which increases by a factor of 10, while mitochondria and lysosomes are in the range of the controls (Table 34). Changes in surface density are given for mitochondrial outer membranes (–28%), and the cristae membranes (–57%; Table 36). No alterations are detectable for the various plasma membrane domains.

Collecting Duct – Sampling Level 4

Significant changes detected in the collecting duct epithelium are an increase in volume fraction of vacuoles by a factor of 10 (Table 34), and a significant reduction in basolateral (–30%), mitochondrial outer (–56%) membrane per unit of cytoplasm (Table 36).

Fig. 14. *a* Kidney cortex after 45 min warm ischemia and 45 min blood reflow. Proximal tubules show enlarged lumina, brush border regions are absent, the tubular wall is vacuolized and sometimes cytoplasmic blebs are seen protruding into the tubular lumen. Cellular debris is found within the lumina. Besides distal tubular and collecting duct profiles with completely normal appearance and open lumina, collapsed segments with widened basolateral intercellular spaces are also present. *b* Proximal tubule. The luminal cell surface is characterized by small and very short microvilli: a large number of vacuoles (*V*) fill the apical half of the cells. Nuclear (*Nuc*) chromatin is condensed and the perinuclear cisternae extremely enlarged. Mitochondrial transsection profiles show no alterations but they appear rounded. Polysomes are dispersed and scattered all over the cytoplasm. *c* Distal tubule and *d* Collecting duct. Enlarged vesicle-like cisternae of the endoplasmic reticulum can be found. The intercellular spaces appear slightly enlarged

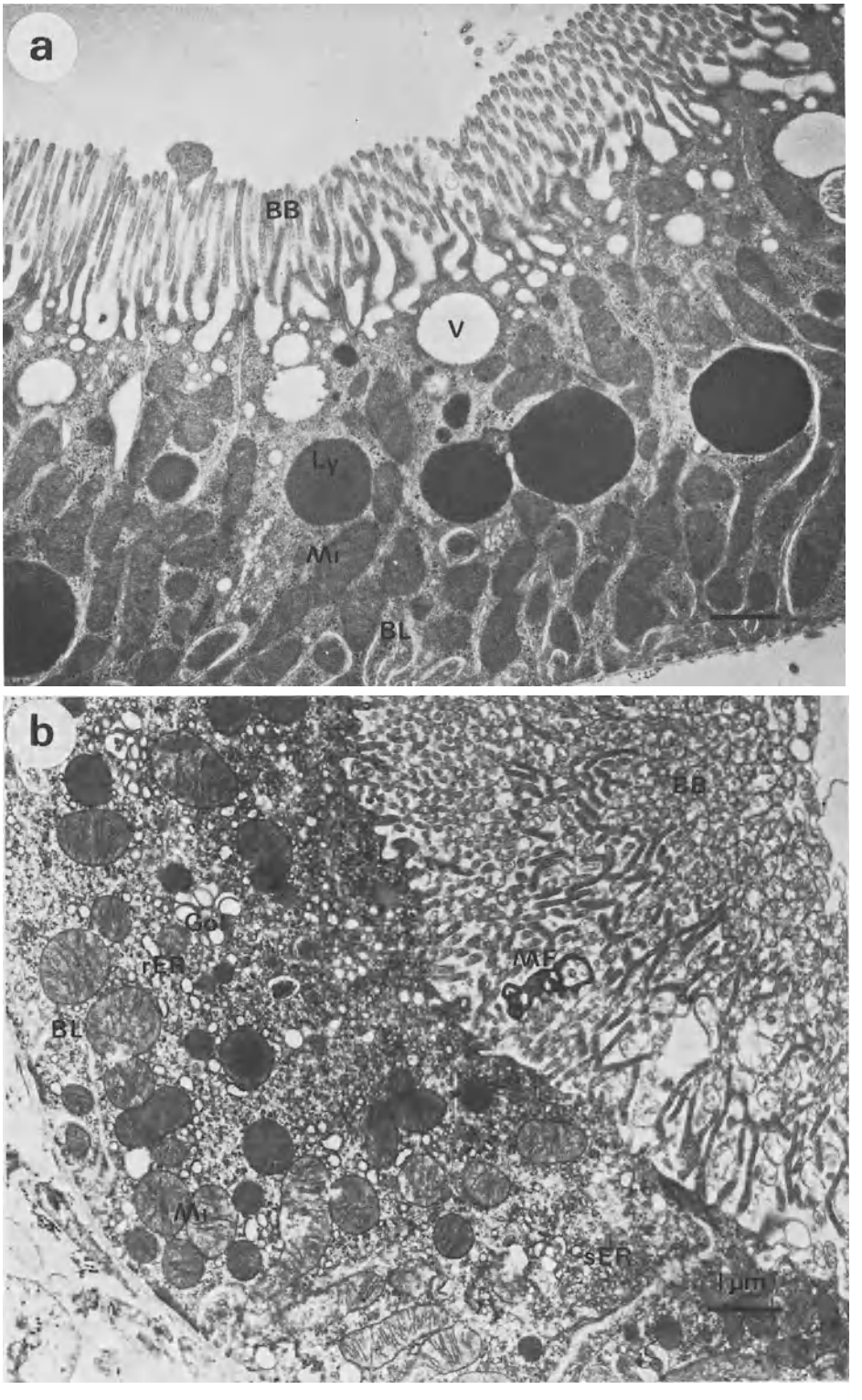
a
BB
V
Ly
Mi
BL
b
BB
Gol
rER
MF
BL
Mi
sER
1 µm

5.2.6 The Hypothermia Model

5.2.6.1 Qualitative Morphology

At the light microscopic level no gross alteration in cortical tissue architecture is visible. The only effect which might be described is a slightly increased vacuolization within the apical pole of proximal S_2 segment. Sometimes also, an enlargement of intercellular spaces seems to be present in this segment (Fig. 16a). In proximal S_3 segment, cytoplasmic ground substance with low electron density is found (Fig. 16b). Distal and collecting duct cells appear to be absolutely normal except for a slightly higher number of lysosomal transection profiles.

5.2.6.2 Quantitative Morphology

No significant difference concerning the volumetric composition can be revealed in comparison to control rat kidney cortex (Table 32).

Proximal Tubule – Sampling Level 3 and 4

Proximal tubular S_2 segments show a striking decrease in mitochondrial volume fraction (–41%) while this parameter is comparable to controls in the S_3 segments. A significantly smaller membrane surface per unit of cytoplasm in comparison to controls exists for the mitochondrial outer (–29%) and the cristae membrane surface (–29%; Table 35) of the S_2 segment. The same applies for the S_3 segment, although the amount in membrane reduction is less in quantity.

Distal Tubule – Sampling Level 4

No statistically significant changes in volume density of lysosomes and mitochondria are present (Table 34). The only surface density value significantly different refers to the mitochondrial cristae per unit of cytoplasm which is lower by 43%.

Collecting Duct – Sampling Level 4

For this nephron segment two parameters are found to be statistically different from the control, the vacuolar volume fraction, which is increased by roughly a factor of 10, and the mitochondrial cristae membrane, which is smaller by 33%.

Fig. 15. *a* Proximal tubular S_2 segment after hypothermia (30 °C for 2 h). Besides a slight tendency for dispersion of polysomes no difference to ultrastructure of controls is found. *b* Proximal tubular S_3 segment. In addition to absolutely normal tubules sometimes changes of the kind displayed here can be detected. These alterations are characterized by swelling and disintegration of microvilli, a vesiculation of smooth and rough endoplasmic reticulum, and Golgi apparatus. Furthermore, mitochondria seem to be swollen. Sometimes myelination figures (*MF*) can be found within the brush border region

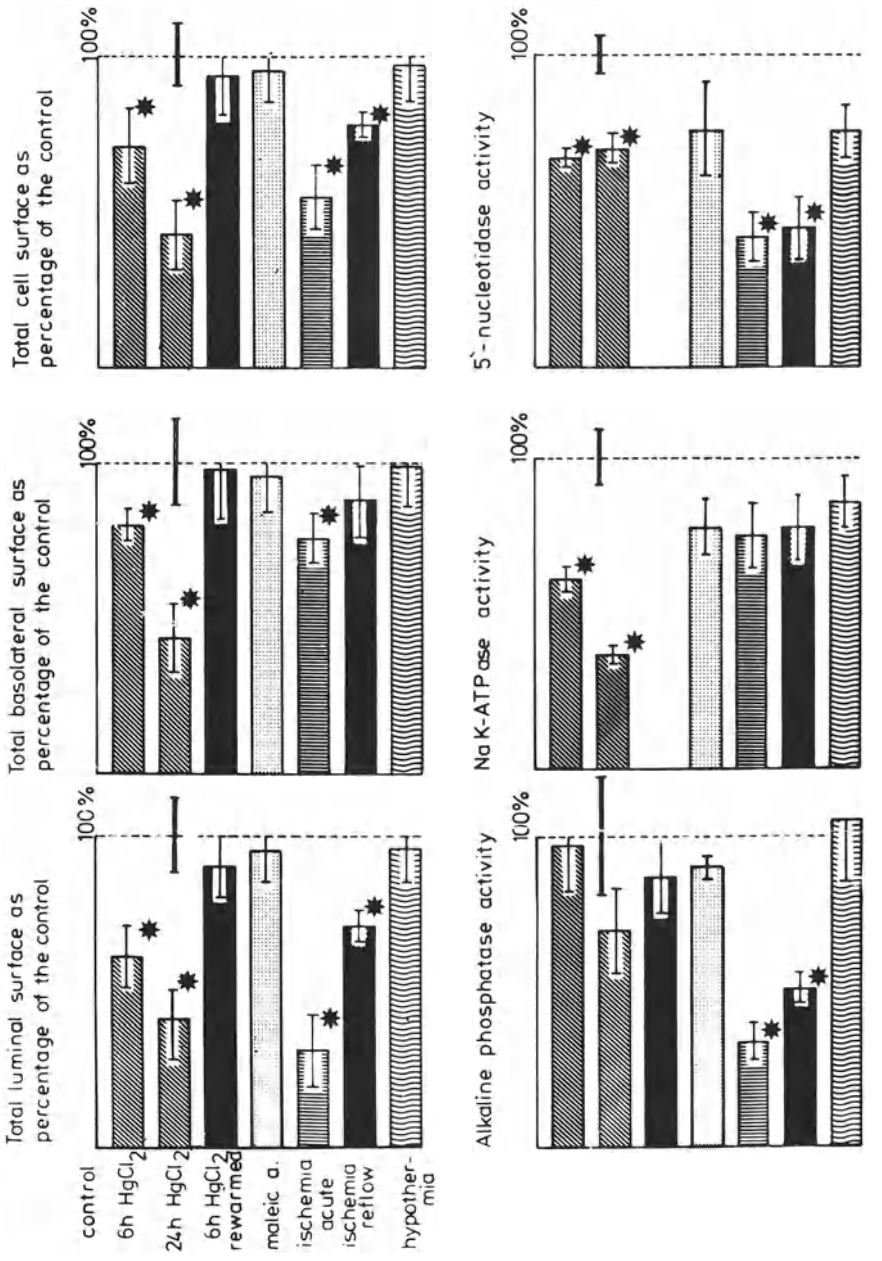

Fig. 16. Changes in cell membrane surfaces and the respective marker enzyme activities. Membrane surface changes are expressed as percentages of the control value, which is 100%. The membrane surfaces given include all nephron segments (proximal $S_1 + S_2$ and S_3 segments, distal segments, and collecting ducts) in order to be directly comparable to the enzyme activities obtained from kidney cortex homogenates. Asterisks indicate statistically significant difference ($P < 0.05$) from the control value

5.3 Functional Changes of the Acutely Injured Kidney Cortex

5.3.1 Enzyme Activities

5.3.1.1 The Plasma Membrane

The $HgCl_2$ Model

The activity of alkaline phosphatase is significantly decreased only after 24 h (Fig. 16). No difference in activity was found for the 5′-nucleotidase assumed to be evenly distributed over the whole membrane of proximal cells. Na-K-ATPase, the representative marker for basolateral membranes has already decreased significantly in specific activity at the 6-h experimental interval. This effect is even more pronounced after 24 h (Fig. 16).

The $HgCl_2$ Model – Six Hours After Toxin Administration and Counterheating

In the case of this experimental extension only alkaline phosphatase activity has been determined, and was found not to be significantly lower than in control animals. No other plasma membrane marker enzyme activities have been determined.

The Maleic Acid Model

Two hours after intraperitoneally administered maleic acid no change in activity for the alkaline phosphatase and 5′-nucleotidase is detectable. The same applies for the basolaterally localized Na-K-ATPase (Fig. 16).

The Ischemic Model

Forty-five minutes after complete renal ischemia induced by renal artery clamping, the alkaline phosphatase activity is diminished by 50%, and that of 5′-nucleotidase by about the same degree. A decrease in Na-K-ATPase activity can be found but it is not statistically significant (Fig. 16). Allowing a 45-min period of blood reflow after releasing the renal artery clamp, the situation is somewhat different. The reduction in alkaline phosphatase activity is less pronounced, while that of 5'-nucleotidase is the same as in acute ischemia; Na-K-ATPase activity, is still depressed (Fig. 16) but no statistically significant difference can be found.

The Hypothermia Model

No statistically significant alterations for plasma membrane marker activities of the above enzymes can be observed after the 2-h hypothermia interval at 30 °C when the enzymes are assayed at 37 °C.

5.3.1.2 The Mitochondrial Cristae Membrane System

The $HgCl_2$ Model

Six hours after $HgCl_2$ administration the cytochrome c-oxidase shows only 80% and after 24 h 60% of its regular activity. For this specific model α-glycerophosphate dehydrogenase (α-GPDH) as a marker for inner boundary membrane was also

determined. A change in activity is given only for the 24-h interval. A reduced activity is also found for SDH after 24 h (Fig. 17).

The $HgCl_2$ Model – Six Hours After Toxin Administration and Counterheating

During this type of treatment a 19% lower CCO activity in mitochondria isolated is measured (Fig. 17). α-GPDH and SDH have not been determined.

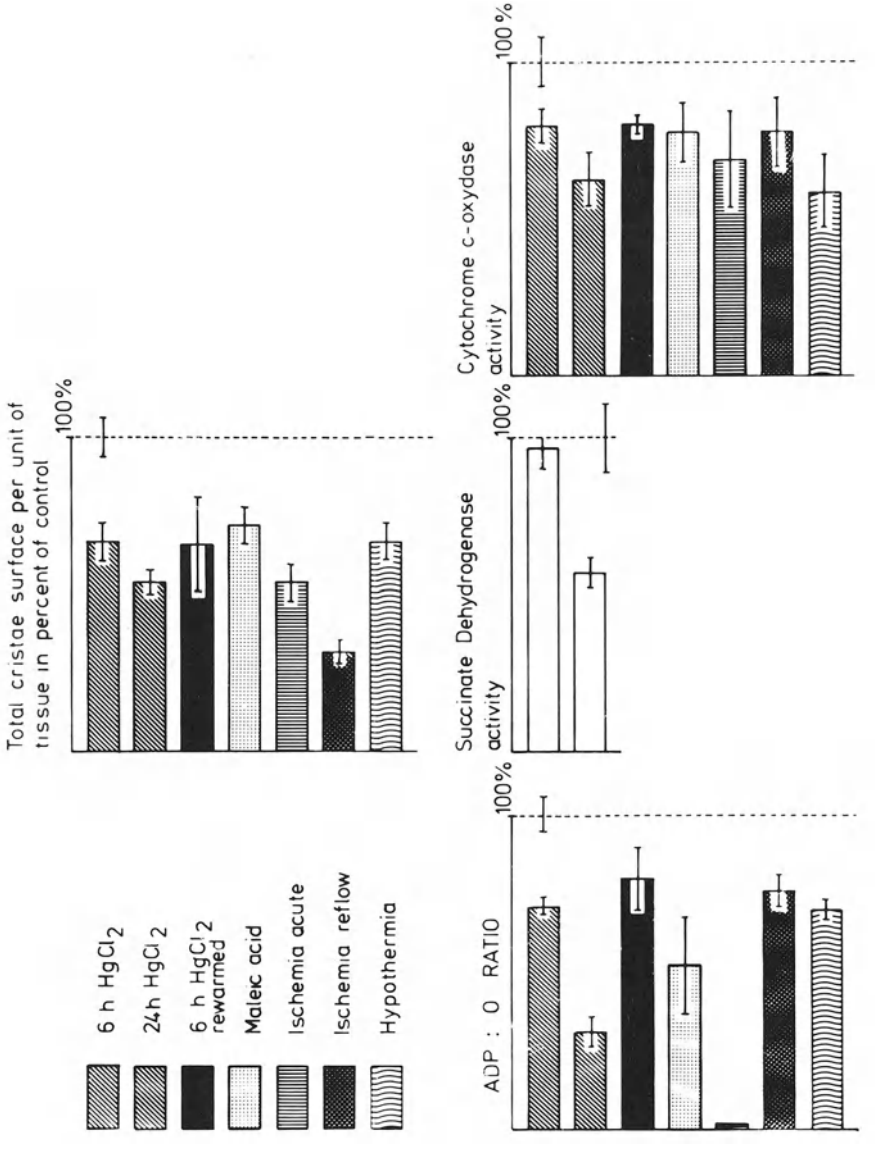

Fig. 17. Mitochondrial cristae membrane surfaces as a combined value of all cortical nephron segments (proximal $S_1 + S_2$ and S_3 segments, distal segments, and collecting ducts). The control value is represented as 100%. All values of the experimental groups are significantly different from control ($P < 0.05$) except the succinate dehydrogenase activity 6 hours after $HgCl_2$

The Maleic Acid Model

In the case of this model, cytochrome c-oxidase activity is reduced by 22% as compared to the controls.

The Ischemic Model

In ischemia, without allowing a blood reflow, a 30% depression in CCO activity is detected, which slightly recovers following the 45-min blood reflow period where the depression in activity amounts to 20% (Fig. 17).

The Hypothermia Model

In prolonged hypothermia we also find a significant fall in CCO. The activity measured is 40% lower than that of controls. No values have been determined for α-GPDH and SDH.

5.3.2 Mitochondrial Respiration

In the $HgCl_2$ model of cortical injury, the respiratory control (RCI) and the ADP/O ratios, using, succinate, glutamate or α-Keto-glutarate, are identical to control values when mitochondria are taken 30 min after toxin administration. However, respiratory control was diminished by 37% in mitochondria isolated 6 h after $HgCl_2$ administration and RCI values close to 1 are reached in the 24-h experimental interval. Oxygen consumption becomes reduced by 20% 6 h and by 60% 24 h after $HgCl_2$. ADP/O ratios declined by about the same amount, namely by 20% at 6 h and by 67% at 24 h (Fig. 18). In addition, the isolated mitochondria show a very differentiated type of behavior to Ca^{2+}-induced high amplitude swelling. While mitochondria isolated from animals of the 30-min $HgCl_2$ interval perfectly retract upon addition of ATP and Mg^{2+}, mitochondria of the 6-h interval stay slightly swollen when the retraction medium is added. Organelles isolated after 24 h are already swollen, increase their volume following CA^{2+} administration, and do not react upon the addition of ATP and Mg^{2+} (Pfaller et al., to be published).

5.3.3 Metabolite Concentrations

Of equal importance to enzyme activities are of course the metabolites fueling these enzymes systems or being produced by them. Common to all injury models used are changes in adenine nucleotides (ATP, ADP and AMP; Fig. 18), lactate (Fig. 19), glucose (Fig. 20), and glutathione (GSH and GSSG; Fig. 21). In the course of $HgCl_2$ intoxication we find steadily decreasing concentrations of ATP (Fig. 18). Following maleic acid intoxication the same pattern can be recognized (Fig. 18).

5.3.4 Renal Functional Parameters During Acute Injury

5.3.4.1 The $HgCl_2$ Model

Glomerular filtration rate (GFR) is significantly reduced in all injury models (Fig. 22). It is only one-tenth of that from controls in animals of the 24 h $HgCl_2$ experimental interval. Blood urea nitrogen (BUN) level remained unchanged 6 h after mercury, as compared to the control value of 26 mg/100 ml, but increased by 330% within 24 h, clearly indicating renal insufficiency (Pfaller et al., to be published). The body temperature, which was monitored in an additional set of 12 conscious experimental animals, decreased after subcutaneous injection of 4 mg $HgCl_2$/kg body weight. A value of 36 °C was recorded 2 h, and a value of 32 °C 24 h, after mercury administration. The fractional excretion of Na^+ increased during the experimental treatment and was found to be higher after 24 h (Fig. 23). When anesthetized animals kept on a heated table at a constant temperature of 37.5 °C are treated with a single $HgCl_2$ dose, the decrease in GFR was significantly smaller than in animals having been exposed to the $HgCl_2$ dose in a conscious state and being anesthetized exactly 6 h after mercury exposure in order to determine changes in GFR and sodium excretion. The reabsorption of sodium was much better under rewarming conditions.

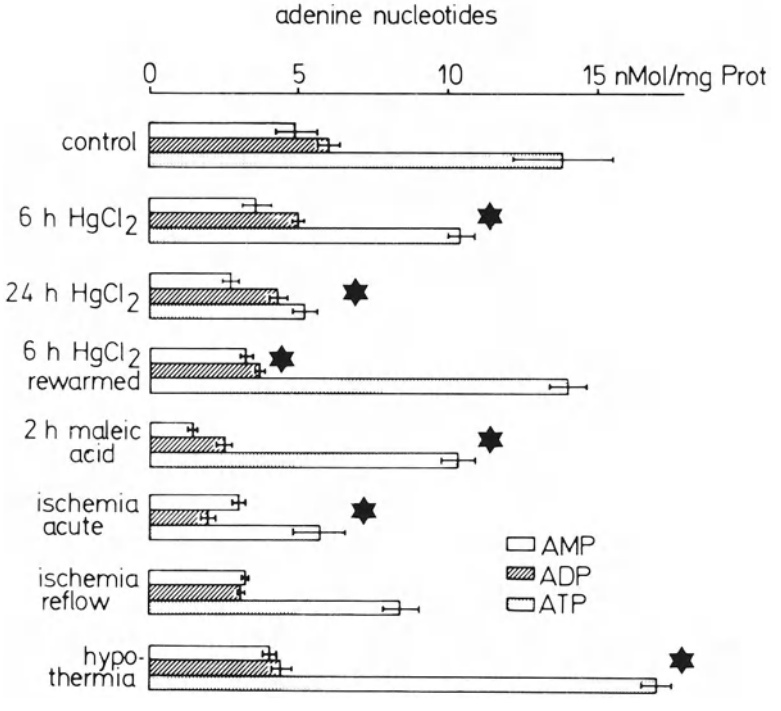

Fig. 18. Adenine nucleotide concentrations in rat kidney cortex after the various types of acute renal injury. All values are means ± SEM of 40 rat kidneys. Significant differences ($P < 0.05$) from control values are marked with *asterisks*

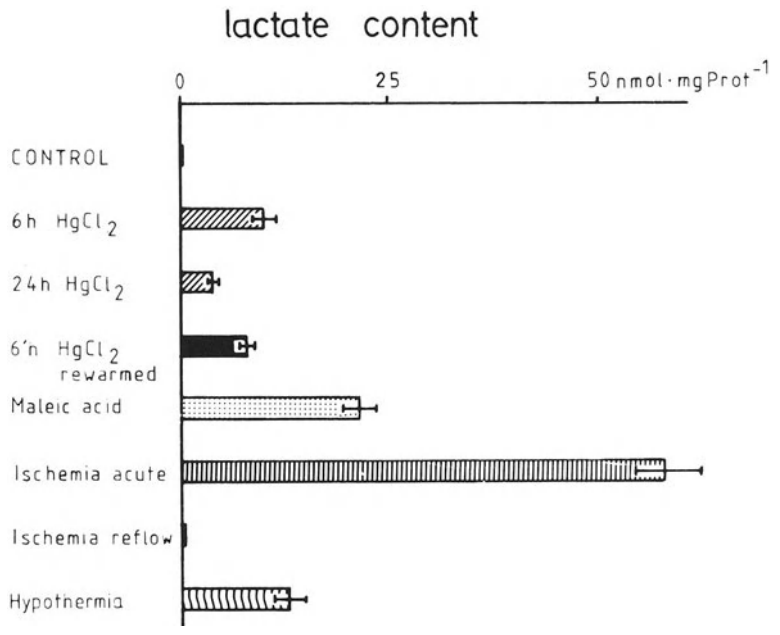

Fig. 19. Lactate contents of kidney cortex: After all types of treatment except 45-min ischemia with a 45-min blood reflow period a significant increase ($P < 0.05$) far exceeding control concentrations can be recognized

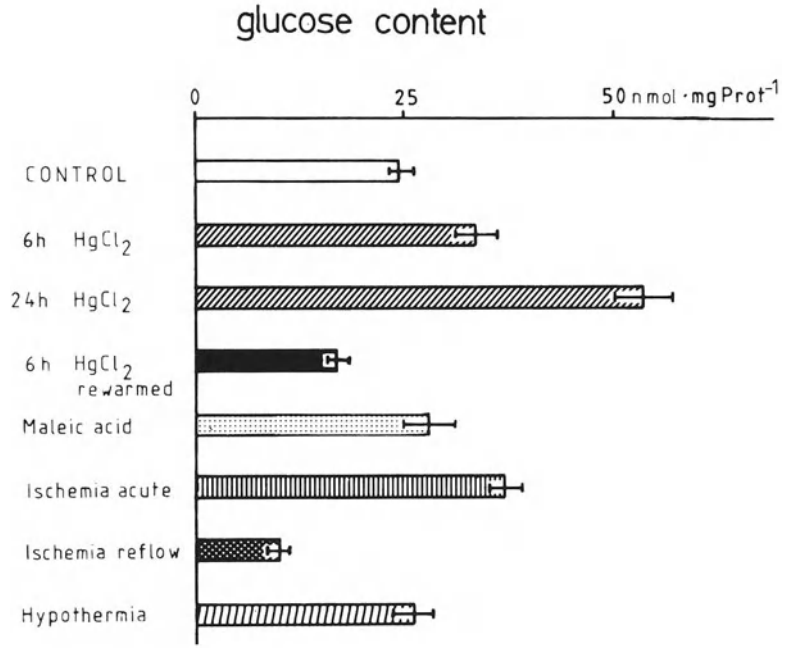

Fig. 20. Glucose content of kidney cortex: Except for maleic acid treatment and hypothermia all other procedures inducing acute injury of the rat kidney deliver tissue glucose contents significantly ($P < 0.05$) different from controls

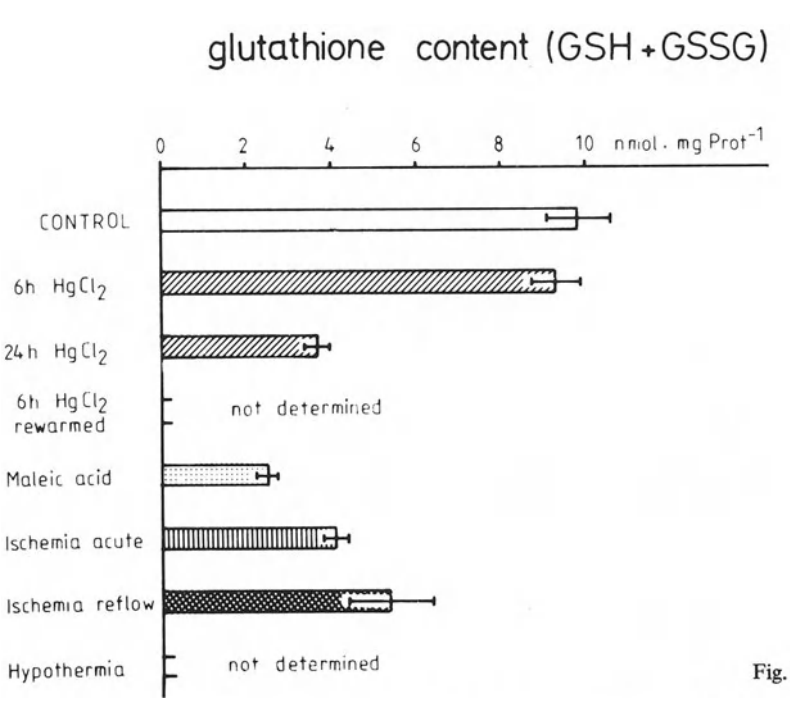
glutathione content (GSH + GSSG)
0
2
4
6
8
10
nmol . mg Prot^{-1}
CONTROL
6h $HgCl_2$
24h $HgCl_2$
6h $HgCl_2$ rewarmed
not determined
Maleic acid
Ischemia acute
Ischemia reflow
Hypothermia
not determined

Fig. 21.

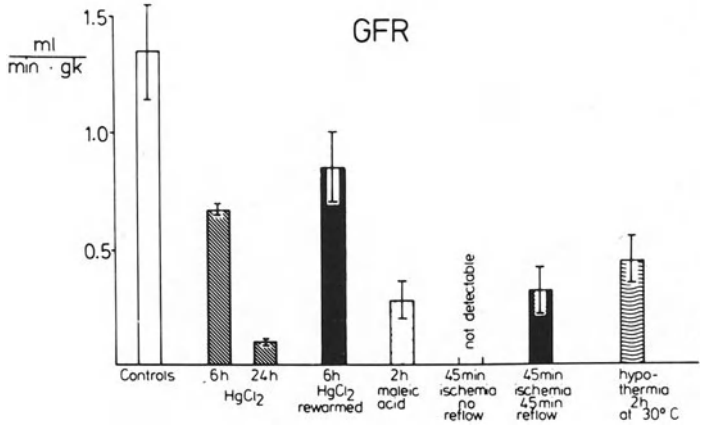
GFR
ml / min · gk
1.5
1.0
0.5
Controls
6h $HgCl_2$
24h $HgCl_2$
6h $HgCl_2$ rewarmed
2h maleic acid
not detectable
45min ischemia no reflow
45min ischemia 45min reflow
hypothermia 2h at 30° C

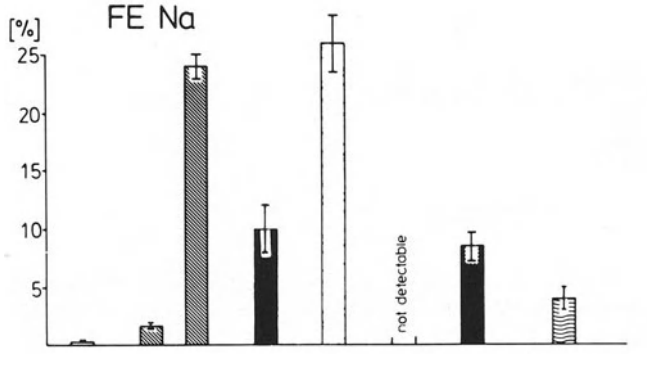
FE Na
[%]
25
20
15
10
5
not detectable

Fig. 22.

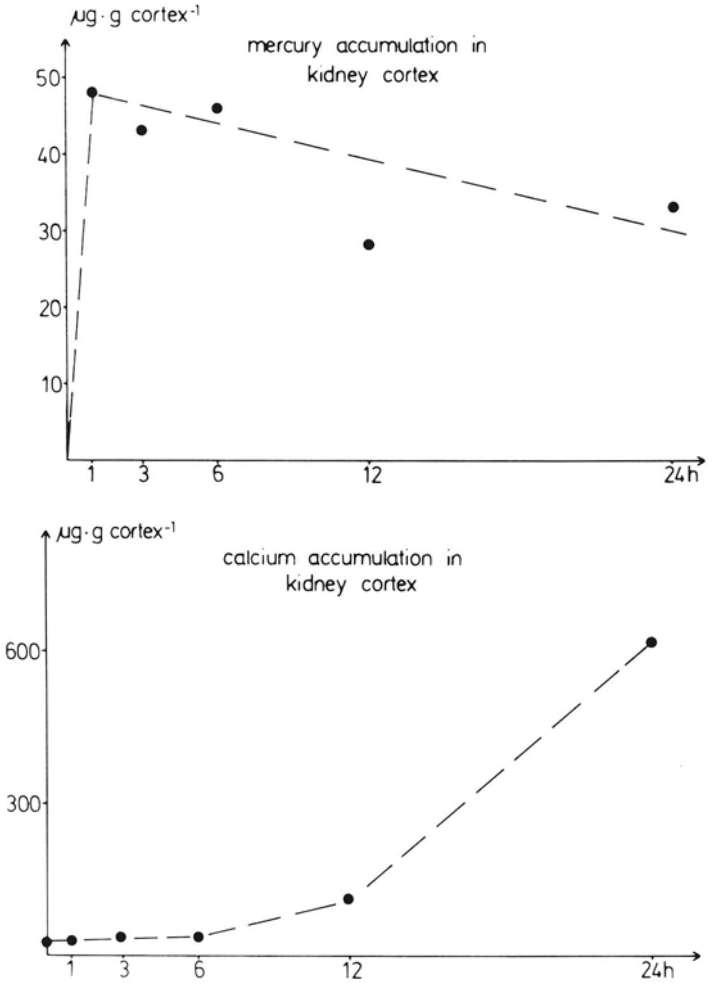

Fig. 23. Renal cortical tissue Hg and Ca concentrations at various intervals after administration of a single dose of $HgCl_2$ (4 mg/kg body weight)

5.3.4.2 The Maleic Acid Model

In comparison to controls, following this type of treatment GFR was found to be reduced by roughly 70% and fractional excretion of sodium is significantly increased (Fig. 22). The body temperature, again monitored on conscious rats, showed an enormous decrease. Within the treatment time of 2 h the rectally measured temperature was 30 °C.

5.3.4.3 The Ischemic Model

Unilateral renal ischemia (left kidney) leads to a reduction in glomerular filtration rate to some 20% of its original value. This value has been determined allowing a 45-min blood reflow interval after releasing the clamp. At this time reabsorption of sodium is also significantly decreased (Fig. 22).

5.3.4.4 The Hypothermia Model

Rats cooled down under anesthesia to 30 °C and kept at this temperature over a period of 2 h slow a glomerular filtration rate which amounts to 33% of the controls. Sodium reabsorption decreased and amounted to only 96% of the filtered load (Fig. 22).

6 Discussion

6.1 The Normal Kidney

It is the purpose of this work to give a detailed analysis of those kidney structures involved in the major task of this organ, namely in transportation of solutes between the four components: urine space, nephron epithelium, interstitium, and vascular space. The first question which arises in this context is: Does a quantification of tissue components as outlined above provide us with new information? Considering the data on volume densities of tissue compartments with regard to the different sampling positions, the first unexpected result is the significant decrease in volume density of proximal tubular lumen, when proximal $S_1 + S_2$ and cortical S_3 segments are represented as a combined value. Since the number of deep, juxtamedullary, nephrons is much greater than the number of subcapsular ones, which may easily be recognized by the differences in glomerular volume density (Table 2) implications for renal function may be questioned. Free flow micropuncture investigations suggest that juxtamedullary nephrons contribute to solute composition of final urine in a different way from the cortical (Stein et al. 1976; Osgood et al. 1978; Higashimara et al. 1978). This evidence is based upon micropuncture studies in which volume expansion was induced by 10% body weight Ringer loading, and measurement of the fractional delivery of Na^+ to the base of the papillary collecting ducts, the late distal segment of cortical nephrons, and into the final urine. The same has been performed for fractional phosphate (Knox et al. 1977) and potassium delivery (Wright and Giebisch 1978). A decreased luminal diameter in connection with an identical tubule length per unit volume (Table 10) of deep nephrons, as compared to superficial nephrons revealed in the present study in combination with a higher GFR of deep nephrons (Baines and De Rouffiniac 1969), must result in high tubular flow rates which potentially may result in higher fractional Cl delivery, for example, to the loop of Henle. The lower density in the basolateral membrane surface or the location area of outward-orientated pumping sites may additionally contribute to this effect (Table 22). The volumetric data obtained show another somewhat surprising result, which concerns the vascular compartment of the inner stripe of outer medulla and the inner medulla. Usually this part of the kidney is regarded as being relatively avascular. The presented data, however, clearly show that the volume density of the vascular compartment is twice as high as in the cortex, when a unit volume of kidney zone is taken as a reference. A similar observation can be made for the volume density of interstitial cells, utilizing the same reference system. The volume density of the various lumina contributing to the urine-space component is at its highest within the outermost part of the inner

medulla. The epithelial component therefore, steadily decreases in its zonal volume fraction toward the midpart of inner medulla, but again increases at the expense of the urinary, and to some extent the vascular space, in the region of the papillary tip. This latter result might correspond to the phenomenon of permanent squeezing of the papilla by smooth muscle bundles encircling the papilla, which was described recently by Schmidt-Nielsen and Reinking (1980). When the total kidney volume, or the real volume of the different zones from wich samples have been taken, is utilized as a reference system, we obtain the absolute value of the measured parameters. Two restrictions, however, should be outlined clearly at this point. There is no possibility of distinguishing superficial from juxtamedullary cortex, or outer mid- or deep part of the inner medulla in a reproducible manner. Therefore, the stereological estimates determined for subcapsular and juxtamedullary cortex, as well as the measures revealed for the three inner medullary sampling positions, must be combined and referred to the total zonal volume. The stereological estimate on vascular volume can at least be compared to an estimate obtained by tracer techniques (Rasmussen 1973). The stereologically determined value for total renal vascular space differs only by a few microliters from that determined radiologically. Estimations of the interstitial space performed by Bell et al. (1970) for the cortex, also utilizing tracer techniques, are consistent with the stereological data reported here. The conclusion that can be drawn from the consistency which exists between these data, is that the preparational procedure selected did not significantly influence the volume of these two compartments assumed to be sensitive to changes in solute osmolality (Bohman 1974). Without adjusting the perfusion fixation solution to the correct oncotic pressure, even for those tissue regions with isotonic extracellular tubular and vascular fluid, the vascular volume will be overestimated (W. Pfaller, unpublished results). If we now turn to the quantitative evaluation of nephron structures, especially those interferring with transepithelial solute transport, again the question for new aspects arises.

6.1.1 Proximal Nephron

6.1.1.1 Cortex

Following the proximal nephron's path through the cortex, the stereological data revealed correspond fairly well with what one would expect from qualitative observation. Furthermore it appears interesting that there is a decrease in nearly all parameters measured, volume density of mitochondria, surface density of luminal, basolateral, mitochondrial outer, and mitochondrial cristae membrane between the subcapsular and the juxtamedullary position. The reason for this effect is that in the juxtamedullary sampling position no differentiation between cortical $S_1 + S_2$ and S_3 segments of proximal tubules, contained in the medullary rays of the cortex, has been carried out. There is no possibility of discriminating between the space or "containing volume" of the medullary rays and that of the cortical labyrinth, since on sections no unequivocally distinguishable border between these regions can be diagnosed. The results shown in Tables 6–9 therefore, display a mixture of measurements from both segment populations. Since within the deep cortical region the proportion of cortical S_3 segments is higher, the reduction of subcellular stereological parameters

seems logical. If, on the other hand, a sampling procedure is selected in which a discrimination between $S_1 + S_2$ and S_3 was conducted, no significant difference in quantitative subcellular organization between superficial and deep cortex, with regard to $S_1 + S_2$, can be found (Pfaller and Fischer 1980). The decrease in volume fraction of the tubular lumen (see above) persists also in this type of sampling. This, however, must not necessarily imply that there is no difference in quantitative subcellular organization between the very early and late, or very late parts within the S_1, the S_2, or the S_3 segments of the specific nephron. Differences in quantitative ultrastructure may, in addition, exist between superficial and juxtamedullary nephrons. The existence of such structural gradients along a nephron, especially if subtle, can be demonstrated only by using serial sectioning in combination with morphometric evaluation of the specific nephron transsection profile. A stereological approach, as utilized here, only provides data for the overall organization of structures within the sampling entity. A recent study made in our laboratory (Pfaller and Fischer 1980) shows that such a possibility seems unlikely. Sampling tissue blocks from all over the cortex in a systematic manner, so that all regions, with emphasis on the pole and the midpart of the cortex, as well as on the various depths of the cortex, are equally weighted, delivers surface area estimates on mitochondrial membranes with a total experimental error of less than 15% of the mean value. Since for this experiment, only three animals have been used, the variance among the different sampling positions must be very small. Numerous biochemical investigations based upon fractionation of cells from the whole kidney or its zones, into the subcellular compartments or their membrane fractions, provided information about their corresponding macromolecular constituents. Meanwhile, a number of macromolecular complexes are identified with regard to their topography and can thus be utilized as markers for certain structures. Investigations challenged by the extremely polar construction of proximal tubular cells (Heidrich et al. 1972) demonstrated that the morphologically distinguishable plasma membrane domains – demarcated by the beltlike "tight-junctions" – are also differentiated by the enzymes incorporated or attached to these domains. It clearly could be demonstrated that, for example, alkaline phosphatase and Mg^{2+}-dependent ATPase are exclusively localized at the luminal membrane, whereas the ouabain-sensitive Na- and K-dependent ATPase is confined to only the basolateral membrane (Ernst 1975; Kinne 1979). 5′-nucleotidase, a phosphomonoesterase, however, is distributed over both domains. A correlation between the activities of these enzymes and the surface of the packing material – the membrane – therefore seems plausible. Since the Na-K-ATPase has been recognized as the major protein involved in ATP-dependent solute transport (Blond and Whittam 1964; Schmidt and Dubach 1971) it appears logical to connect basolateral membrane surface with the potential active transport capacity of the respective tubular segment. In addition, we know that the production of ATP fueling the Na-K-ATPase is predominantly carried out by the oxidation of fatty acids and other organic substrates, via oxidative phosphorylation at the mitochondrial cristae membrane-bound respiratory chain. Keeping this in mind, the evaluation of stereological data on membrane surfaces immediately displays a direct interrelationship between basolateral membrane of cells and cristae or mitochondrial inner membrane surface. This is particularly well illustrated by comparing proximal tubular structure of the outer and deep cortical sampling position with that of the outer stripe. The reduction in basolateral membrane area is accompanied by a reduction in mitochondrial inner membrane area of about the same order

of magnitude (Tables 8, 9). A certain connection to the other membrane systems may be assumed for several reasons. Solutes transported transcellularly have to enter proximal tubular cells by diffusion or via carrier-dependent processes and may not always be readily permeable. In addition, a number of substances have to be manipulated by luminal membrane-bound enzymes before cellular uptake is possible. Membrane-bound peptidases will split oligopeptides to free amino acids and disaccharides will be split to monosaccharides via disaccharidases (Silbernagl 1977). The split products will then be transported by the corresponding carrier systems, which are in most cases energized by a sodium gradient (Murer and Hopfer 1974; Ullrich et al. 1979). In the same way as for the Na-K-ATPase a certain amount of membrane must be provided as "packing material" for the carrier system. Furthermore, for substances entering the cell by diffusion, a sufficiently large surface must be available in order to enable effective diffusion. Finally, quite a variety of macromolecules such as lysozyme, albumin, and globulin, still filtered through the glomerular basement membrane, are taken up by proximal tubules via endocytosis which needs a sufficient amount of membrane for wrapping the material to be taken up. This latter process is not evenly represented along the proximal nephron. Morphological evidence for endocytotic processes is confined to the $S_1 + S_2$ segment and is absent in the S_3 segment. This can be supported by stereological data on the volume density of apical vacuoles, which occupy the highest volume fraction within the S_2 segment or proximal tubules of the two cortical sampling positions, as compared to the S_3 segment of proximal nephron or the proximal tubules of sampling 3 (Osom). Furthermore, the endocytic vesicles are paralleled by a relatively large volume fraction of lysosomes (Table 7), a fact which is substantiated by biochemical measurements on single nephrons, where the highest activity of acidic hydrolases is found within the S_2 segment (LeHir et al. 1979, 1980).

6.1.1.2 Outer Stripe of Outer Medulla

It is well established from qualitative observations, that cells of proximal S_3 segments of this zone show long microvilli and therefore possess a large luminal surface per unit of cellular cytoplasm (Table 15). According to the descriptions of many authors (Ericson and Trump 1969; Maunsbach 1973; Tisher 1976) the basolateral surface area should be expected to be relatively small, because of the vanished basolateral cell interdigitations. In fact the basolateral surface area amounts to only 47% of that found in outer cortical $S_1 + S_2$ segments, when referred to a unit of zonal volume which is still unexpectedly high. The surface of mitochondrial cristae membrane is reduced to 57% of that found in the $S_1 + S_2$ segments (Tables 8, 9). When using a unit of proximal tubular cell (unit protoplasm) as a reference, the basolateral surface is reduced by 51% in the outer stripe sampling position, and that of cristae membranes by 42% (Tables 15, 16). This latter fact corresponds well with experiments comparing the function of isolated proximal convoluted parts with that of straight parts, which uncovered remarkable differences regarding glucose transport (Tune and Burg 1971), albumin uptake (Bourdeau and Carone 1974), urea secretion (Kawamura and Kokko 1976), and phosphate transport (Ullrich et al. 1979; Knox et al. 1977; Greger et al. 1977). The most striking functional change between these segments is a decreased salt reabsorptive capacity, which was determined by several investigators (Burg and Orloff 1968; Schafer et al. 1977; Frömter and Gessner 1974a, b; Burg 1976). Ultrastructurally, this finding would be substantiated by a decrease in structures thought to be involv-

ed in reabsorption, the basolateral membrane and mitochondrial cristae membranes. In the case of the rabbit proximal nephron Welling and Welling (1975, 1976) have established a decrease in the luminal membrane, which parallels the reduction in basolateral surface, when comparing S_1 and S_3 segments. Although the methodology applied in this study is not directly comparable to the Welling study, it should be noted that in the case of the rat proximal nephron by no means a one-to-one relationship for luminal and basolateral membranes of proximal nephron cells exists, if a unit volume of cytoplasm or kidney zone is taken as a reference space. The relationship for luminal and basolateral membrane surface is roughly 1:3 for the convoluted part and 1:4 for the straight part. The importance of reduction in reabsorptive capacity is not quite clear. It has often explained by the fact that while losing reabsorptive capacity the proximal tubule gains secretory capability. PAH secretion is several times higher in the straight than in the convoluted part (Tune et al. 1969). In addition, other substances like urea (Kawamura and Kokko 1976), oxalate (Deetjen et al. 1978), prostaglandins (Grantham and Irish 1978), and potassium (Jamison et al. 1976), are excreted at high rates, not to mention a series of pharmacologically used organic substances. The still fairly high surface density for rat proximal S_3 basolateral membrane and mitochondrial inner membrane surface, may be seen in context with secretory processes demanding a definite amount of carriers and metabolic energy as a driving force. Morphological signs for endocytotic processes are missing in cortical and outer stripe S_3 segments, a finding which would be consistent, for example, with a drastically reduced capacity for pinocytotic albumin reabsorption (Carone et al. 1979) and the very low fractional volume of lysosomal structures.

6.1.2 Thin Limb

6.1.2.1 Inner Stripe of Outer Medulla

Kriz et al. (1972) have shown for the first time that short and long loop epithelium in rat kidney differs markedly. This feature was then followed systematically by Schwartz and Venkatachalam (1974), Dieterich et al. (1975), Barrett and Majack (1977), Barrett et al. (1978a, b), and Kriz et al. (1978) for other species. Similarly to the proximal nephron the thin limb may be subdivided into three segments, discernible by qualitative morphological features. Before discussing the quantitative morphology revealed by our stereological analysis, it must be clearly outlined that no differentiation has been performed either for the two nephron populations or for the three segments resembling the loop epithelium. When speaking about the descending part, in fact a combined value of descending limbs from superficial and juxtamedullary nephrons is described. The outer stripe contains not only type 2 epithelium belonging to superficial nephrons characterized by very smooth cell contours, but also type 1 epithelium from juxtamedullary nephrons which make up about 60% of the downward-penetrating nephrons, with extensive basolateral infoldings and a higher number of transsectioned mitochondria. As a result of these features one would expect a relatively high basolateral and mitochondrial inner membrane density as well as a remarkably high mitochondrial volume density per unit volume of inner stripe. The stereological estimates, however, show a low basolateral surface as compared to thin limb segments contained in the inner medulla, but a fair amount of mitochondrial

membrane surface or volume (Tables 8, 9, 15 and 16). The spread measures are small in all cases. The reason for this unexpected result could be seen to some extent in an inadequate qualitative description of type 1 epithelium, which in reality and on average is not as infolded as described in ultrastructural investigations based only on judgement of structures by eye.

6.1.2.2 Inner Medulla

The thin limb segments, descending and ascending, of the inner medulla, resemble a mixture of type 2 and 3 epithelium. Type 3 segments are supposed to exhibit a basolateral cell surface with less infoldings than type 1 epithelium and a low mitochondrial volume fraction. Again these qualitative morphological criteria are not consistent with the stereological data (Tables 8, 9, 15, and 16). For all medullary sampling positions (outermost, midpart, and deep part) the basolateral, the mitochondrial inner, and the luminal membrane surface exceeds that determined for inner stripe thin limb epithelium, regardless of whether or not a unit volume of tubular epithelium or zonal tissue is taken as a reference. Only for the deep inner medulla may a slightly lower figure for the parameters listed above be recognized (Tables 8, 9, 15, and 16). Several explanations may be given for this finding. Comparing inner stripe of outer medulla with the outermost part of inner medulla, a roughly twofold increase in volume fraction is given for both thin limb lumen and epithelium, due to the fact that in the case of inner medulla descending and ascending thin limbs are present. This implicates an increase in mean curvature of cell contours leading to higher basolateral and luminal membrane areas. The slight decline of the parameter's luminal volume, and epithelium and membrane surfaces, toward the innermost part of inner medulla, is certainly due to a reduced number of loops. Despite these reasonable explanations it is doubtful whether qualitative morphological descriptions of the three segments, in terms of infoldings, can be generalized in the way described by Schwartz and Venkatachalam (1974) or Dieterich et al. (1975). Structure function relationships are difficult to ascertain from the recently described stereological data. First of all, only very few concrete data on thin limb transport and metabolism exist for the rat. Slightly more functional data are available for rabbit thin limbs.

From these investigations we know that the thin limb epithelium is poorly permeable. Abramov and Orci (1980) determined a NaCl permeability of 1.7×10^{-6} cm s^{-1}. Furthermore, the configuration of junctional complexes which display all features of "tight" complexes (Staehelin 1974) reduces the probability of paracellular transport routes. This statement is also confirmed by a recent study of Roch-Ramel and Peters (1981), clearly demonstrating high water permeability of descending thin limb only under the condition of overstretching which is contradictory to the findings of Kokko (1974a, b). To infer any correlation with function, in terms of any one of the existing models of the countercurrent concentrating mechanism, on the basis of quantitative data for luminal and basolateral cell surfaces, would be highly speculative and devoid of any firm basis. An interesting phenomenon, however, is the high mitochondrial inner membrane density per unit of cytoplasm within the middle and deep inner medulla, which is only 20% and 30% lower than that determined for the proximal S_3 segment. Consequently it must be questioned why such a high inner membrane density, which at least potentially represents a correlate for ATP production, exists.

The answer again is difficult to give. A proper function of mitochondria within these epithelia seems established, since the PO_2 is in the range of 8–10 mmHg (Cohen 1979) and the critical pressure for mitochondrial work is assumed to cease at values below 1 mmHg. Thus, a correlation may be seen to exist, possibly in context with Ca^{2+} ATPase activity of the thin descending limb (Katz and Doucet 1980). Since Ca^{2+} is provided in reasonable amounts, the high mitochondrial inner membrane density should also be seen in connection with actin myosin or filamin interaction regulating loop diameters during diuresis and antidiuresis. Although at present no experimental evidence for active transport processes existing within this nephron region is given, this specific finding of high mitochondrial membrane surfaces should be cause for a reconsideration of the present passive models of urine concentration.

6.1.3 Distal Nephron

6.1.3.1 Inner Stripe of Outer Medulla

By definition this nephron segment continues the ascending thin limb at an abrupt transition point which is coincident with the border between outer and inner medulla. It penetrates through the inner and outer stripe, reaches the kidney surface in the case of superficial nephrons, and proceeds thereafter toward the deeper cortex to join the collecting ducts. In contrast to the segments (proximal and thin limb) discussed so far, no subsegmentation on the basis of solely morphological features of tubular cells can be described. However, an obvious subsegmentation with regard to the tissue topography exists – the medullary ascending part (MAL), the cortical ascending part (CAL), and the cortical convoluted part (DC). The latter two are sequestered by the macula densa region at the contact side between distal nephron and the vascular pole of the glomerulum from which the nephron originates. Describing the distal nephron in terms of quantitative morphological features reveals differences between the various sampling regions. Utilizing a unit of epithelial cytoplasm as a reference volume, three important transport-related parameters exhibit the highest density for mitochondria and mitochondrial cristae membrane. The basolateral membrane surface is present in about the same amount in the inner stripe and the cortical sampling position, but in a significantly lower amount in the segments contained within the outer stripe. When referring the measurements to a unit volume of kidney zone the situation is identical for basolateral membrane density, but the density of mitochondrial cristae membranes is only 70% of that found for the subcapsular proximal S_2 segments. The reason for this effect is caused by the higher volume fraction of proximal tubular epithelium (47% per unit volume of cortical tissue in comparison to that of the inner stripe distal epithelial volume content which amounts to 28%!). Irrespective of this methodological aspect the stereological finding correlates extremely well with what is known from functional studies. The medullary ascending epithelium is still a part of the Henle loop and, together with the downward-orientated collecting duct, is an integral piece of the countercurrent urine concentration system. The ascending "thick limb" (MAL), poorly permeable to water, is generally accepted as the site of active NaCl reabsorption, setting up the necessary osmotic gradient for water abstraction. This process certainly requires a large amount of outward-orientated pumping sites, presumably Na-K-ATPases. In fact, investigations of Schmidt and Dubach (1971) and Katz et al.

(1979) have substantiated high activities of Na-K-ATPase in the medullary ascending distal nephron, utilizing pieces of microdissected nephrons from the rat. By the same technique the highest activities for succinic dehydrogenase localized at mitochondrial inner membranes and isocitrate dehydrogenase contained in the mitochondrial matrix have been determined (Schmidt and Guder 1976). Despite the fact that there is a correlation between basolateral membrane and Na-K-ATPase activity, it should be pointed out that enzyme activity, on the basis of dry weight, is about 15 times higher in the medullary ascending distal tubule than in the proximal convoluted tubule which possesses a basolateral surface per unit cytoplasm smaller by a factor of only 0.6. This could imply that a lower number of Na-K-ATPase molecules is packed per unit area of membrane of proximal tubules. Whether or not the surface, far exceeding ATPase activity in the proximal tubule, is just necessary in order to handle the larger volume fluxes remains to be elucidated in detail.

6.1.3.2 Outer Stripe of Outer Medulla

Basolateral membrane area of the outer stripe of outer medulla-located ascending distal nephron reveals a 25%, and mitochondrial inner membrane a 40% reduced surface, as compared to the inner stripe part which would indicate a less pronounced active solute transport capacity.

6.1.3.3 Cortex

In contrast to straight segments which largely correspond to the juxtamedullary sampling position, the basolateral surface and mitochondrial cristae membranes again increase to a value found for the inner stripe portions, regardless of whether or not a unit of protoplasm or zone serves as the reference system. Assuming a correlation between Na-K-ATPase basolateral and ATP-forming mitochondrial inner membrane, this finding appears to be contradictory to recently published results of Doucet and Katz (1980) who report highest Na-K-ATPase activity for the distal convolution of rabbit, rat, and mouse. Although it appears at the first glance that structure function correlation does not hold in this case, the opposite is true. Most of the enzyme activity measurements on single microdissected nephron segments are given per unit length, usually per mm of nephron, whereas stereological measures are given per unit of containing volume. Since the fractional volume densities and surface densities as well as length densities of tubules are known, the volume and surface per length of tubule can easily be calculated. Utilizing the unit length as a reference the correlation between enzyme activity and the packing membrane area can again be substantiated. The problem of identical reference systems seems therefore to be of extreme importance. Simply correlating ordinary stereological surface or volume densities with enzyme activities expressed per tubular length is misleading. This also seems to explain the discrepancy between the data elaborated by Schmidt and co-workers and Katz et al. (1979). Schmidt's data are referred to dry weight or fresh section weight directly corresponding to surface density per unit volume of protoplasm. The proof for the correctness of both Na-K-ATPase activity measures is given by the data on distal nephron epithelial volume per unit length (Table 18), which is lower by a factor of 10 in the medullary ascending limb, as compared to the distal convolution, and thus

Table 37

		Number of Na^+ transport sites per mm of tubule	Number of Na^+ transport sites per μm^2 basolateral membrane	Na-K-ATPase activity mol $P_i \cdot mm^{-1} \cdot min^{-1}$ a)	Predicted Na^+ transport capacity mol $\cdot min^{-1} \cdot mm^{-1}$	Experimentally determined Na^+ transport capacity mol $\cdot min^{-1} \cdot mm^{-1}$
Proximal tubule $S_1 + S_2$	Cortex	2.17×10^9	8.8×10^2	4.06×10^{-10}	1.11×10^{-10}	1.02×10^{-10} b)
Proximal tubule S_3	OSOM	1.30×10^9	7.8×10^2	2.59×10^{-10}	0.69×10^{-10}	
Thin limb	ISOM					
	IM					
Distal tubule	ISOM	0.83×10^9	7.3×10^2	2.22×10^{-10}	0.42×10^{-10}	
	OSOM	0.16×10^9	6.8×10^2	3.00×10^{-10}	0.81×10^{-10}	
	Cortex	0.38×10^9	4.5×10^2	5.93×10^{-10}	1.98×10^{-10}	$0.9 - 1.3 \times 10^{-11}$ c)
Collecting duct	Cortex	0.98×10^9	4.0×10^2	0.26×10^{-10}	0.49×10^{-10}	
	OSOM	0.15×10^9	2.7×10^2		0.07×10^{-10}	
	ISOM	0.19×10^9	3.3×10^2		0.10×10^{-10}	
	IM	0.07×10^9	2.3×10^2		0.04×10^{-10}	

a) Katz, et al. (1979)
b) Frömter (1974)
c) Maude (1974)

Statistically significant difference from control

leads to remarkable confusion. As can be seen from Table 37 there is an increase in enzyme activity from the medullary ascending limb toward the distal convolution by a factor of 1.5. The surface per mm of tubule length, however, differs by a factor of 7.6. This could mean a much higher number of enzyme molecules per unit area of basolateral membrane for the medullary ascending limb, if an equal activity is assumed for every Na-K-ATPase molecule. It may, however, also be speculated that the enzyme is evenly distributed per membrane area, and displays higher activity in the medullary portions as compared to other segments due to the ATP available. Measurements performed by Shaver and Stirling (1978) on rabbits suggest 4.1×10^6 binding sites per cell for ^{3}H-labeled ouabain at the medullary ascending limb basolateral membrane. This figure refers to a cell being a cube with 5 μm on edge and every binding site reflecting a transport site. Based upon these figures, and assuming an identical binding capacity for rat medullary ascending limb (inner stripe), the number of transporting sites or Na-K-ATPase molecules would be 8100 per μm^2 of basolateral membrane or 9.3×10^9 per mm of medullary ascending limb. Unfortunately no data on ouabain binding to basolateral membranes of other rabbit medullary ascending distal nephron segments are available and no data exist for rat kidney. If mitochondrial volume and surface densities are referred to a unit length of nephron, exactly the same distribution as described for the basolateral membrane is found. The mitochondrial cristae membranes bear the ATP manufacturing respiratory chain, which was monitored in our study by the marker enzyme cytochrome c-oxidase. Considering the center to center distance of cytochrome a (Reith et al. 1973) the total number of respiratory chain complexes can be calculated and, in combination with the oxygen consumption, the potential amount of ATP being formed. The correlative aspects on this parameter are best illustrated by the cristae membrane density per unit volume of zonal tissue or tubular protoplasm. It clearly can be recognized that the highest membrane surface and ATP formation respectively are confined to the inner stripe ascending distal limb, which seems reasonable since at this segment remarkable amounts of solutes have to be abstracted from the tubular fluid by active transport. Along the subsequent distal segments the dilution capacity becomes less pronounced, which again is in good correlation with the steady decrease in ATP-producing cristae membrane surface density toward the cortical distal convolution. Other experimental findings like the more rapid salt reabsorption of medullary thick ascending limbs (Burg and Bourdeau 1978) would be consistent with quantitative membrane morphology. In this context the medullary ascending part is generally denoted as the site for bulk salt reabsorption, thus establishing high interstitial osmolarity, whereas the cortical straight part and the distal convolution seem to perform the final adjustment of the concentration gradient to the surrounding interstitial fluid. In view of the topographical localization, the functional and quantitative morphological differences seem reasonable. The membraneous (mitochondrial cristae and basolateral membranes) salt reabsorptive machinery creates the outer medullary (inner stripe) interstitial hypertonicity, while the cortical parts contribute to the passive concentration mechanism by elevating the luminal urea concentration (Stephenson 1973a, b; Kokko 1974b; Jamison 1974, 1976). Somewhat surprising is the extensive development of active transport-involved structures of the distal convolution, in comparison to the reabsorbed sodium chloride, which amounts to only one-quarter of that reabsorbed by proximal convolution. The answer is probably given

by the fact that much steeper concentration gradients have to be overcome during sodium reabsorption in the distal convolution. The distal tubular segments in addition are targets of various hormones (Imbert et al. 1975a, b; Chabardes et al. 1975a, b): The medullary part for vasopressin, the cortical for PTH. In addition to proteohormones the distal convoluted part is assumed to be sensitive to the mineralcorticoid aldosterone. According to Schmidt et al. (1975) aldosterone increases Na-K-ATPase activity and thus influences distal convolution reabsorptive capacity. Since elevation of plasma K^+ by oral K^+ administration leads to accelerated conversion of corticosterone to aldosterone and a sustained production and secretion of aldosterone (Boyd et al. 1971), enhanced distal tubular Na^+ reabsorption and K^+ secretion (Wright et al. 1971) occurring in chronic potassium leading or potassium adaptation may be seen in this context. This is further supported by the finding hat aldosterone increases Na-K-ATPase via enzyme induction (Jørgensen 1972). A stereological analysis of the Na-K-ATPase-related basolateral membrane in proximal and distal nephron, however, shows no surface enlargement (W. Pfaller, unpublished results), but a twofold increase in mitochondrial cristae membranes. An identical response was observed following administration of aldosterone (Pfaller et al. 1974). A more recent study of Na-K-ATPase activity during K^+ adaptation on isolated nephrons by Doucet and Katz (1980), defined the cortical and medullary collecting duct as the target site for aldosterone. This finding correlates with data of Wade et al. (1979) describing a 140% increase in basolateral membrane area of principal cells upon the addition of desoxycorticosteroneacetate (DOCA) which has a strong mineralcorticoid component. These quantitative data, however, should be handled with extreme care, because the applied method has not considered the essential border conditions for estimating surface density. The presented data are only valid under the assumption that all basolateral membranes are orientated perpendicular to the section plane, which is certainly incorrect. Whether or not mitochondrial membrane systems are affected by DOCA or aldosterone within this segment remains to be investigated. Elevation in cristae membrane mass as outlined above seems to be substantiated by increased cytochrome c-oxidase activity (Pfaller et al. 1974), and enhanced incorporation of aminoacids (Law and Edelmann 1978) measured on kidney cortex homogenates.

6.1.4 Collecting Duct System

As already mentioned, the early portions of the collecting duct system are closely related to the distal convolution from a functional point of view. Generally the collecting duct system can be devided into the connecting tubule, a cortical, an outer medullary, and an inner medullary portion or segment. A connecting tubule with clear cut borders to the distal convolution and the cortical collecting duct is best developed and identifiable only in the rabbit kidney (Kaissling and Kritz 1979). At present it is unclear whether or not a connecting tubule may be delimited in the rat. Crayen and Thoenes (1975) have shown a gradual transition from the distal tubule to the collecting duct system. A similar situation for man was shown by Myers et al. (1966) and Tisher et al. (1968). In the transient tubular segment of rat an intermingling of different cell types is given. Its beginning is characterized by a mixture of distal tubular cells and intercalated cells, the end comprising intercalated cells and principal cells. Qualitatively and ultrastructurally several special features have to be outlined. As

described by Kaissling and Kritz (1979) in the rat also two types of intercalated cells can be distinguished, a dark and a light type. When discussing the quantitative morphological findings it must be outlined beforehand that the data are not elaborated for each of the different cell types. Volume and surface densities have to be considered as an average over the collecting duct epithelium covering intercalated cells of light and dark appearance according to their frequency of occurrence within the tissue probes. The study was primarily aimed at obtaining baseline data for all functionally important nephron segments. A subdifferentiation of the various collecting duct cells needs a separate and laborious sampling procedure. It should be mentioned that pilot studies on a more detailed analysis of rat collecting duct show the principal cells as the major epithelial constituent, covering more than 70% of the collecting duct epithelium (W. Pfaller, unpublished results). Therefore, the data discussed in the following section mainly reflect the quantitative assembly of principal cells. The mitochondrial volume density is highest in the cortical portions of the collecting duct epithelium and decreases steadily towards the papillary tip. Basolateral surface area is highest in those portions contained in the subcapsular cortex and outer stripe of outer medulla, decreases in the deep cortex, outer medulla, outermost inner medulla, and again increases in the deep medullary parts. In contrast to the proximal and distal nephron, mitochondrial outer and inner membrane surface does not follow the density distribution of the basolateral membrane, but continuously decreases from the subcapsular cortex toward the papillary region. When referred to a unit volume of zonal tissue the values change slightly according to the fractional volume of collecting duct epithelium. This means that the basolateral membrane surface area of the medullary collecting duct portion must have higher values than the cortical or outer stripe portions, whereas the mitochondrial membrane systems – outer and cristae – stay roughly constant along the whole collecting duct. This would imply that there exists no such direct correlation between aerobically formed ATP and basolateral membrane surface. Despite an existing active sodium transport, this surface enlargement seems necessary to enable diffusion of sufficient amounts of water and solutes once the luminal membrane's permeability has been modulated via antidiuretic hormone (ADH) and cAMP.

6.1.5 Absolute Values

The quantitative morphological data discussed so far in connection with functional aspects from micropuncture, microperfusion, or perfusion of isolated nephron segments, are relative values or "concentrations" of volumes and surfaces per unit of containing volume. Since the average volume of the main container, the kidney itself, is known, the absolute values of the sampling strata or reference volumes utilized to calculate the relative values, in other words the various zones, can be easily determined morphometrically (see section "Methods"). All volume and surface densities can then be expressed per standard size kidney. Such figures may be important for both biochemical and physiologic considerations. First of all the physiologist is supplied with data on the absolute size of the urinary space, the nephron epithelium, and the extracellular space under antidiuretic conditions. Since some of the parameters outlined can be determined by other than stereological methods the measures may be utilized for controlling the quality of kidney preparation. This is probably best illustrated by comparing estimates on the vascular space using radiologic and stereological methods.

Rasmussen (1973) has determined renal vascular volume via ^{51}Cr-labeled erythrocytes and ^{125}J-labeled IGM, and determined the following values:

Table 38.

	Rasmussen (1973)	Stereology (present study)
Total kidney	159 µl	139 µl
Cortex	69 µl	69 µl
OSOM + ISOM	81 µl	53 µl
IM	9 µl	6 µl

According to the comparison made in Table 38 the stereological analysis gives an estimate for the vascular space 13% lower than that determined radiologically. Furthermore, electrophysiologic data usually expressed as $\Omega \cdot m^2$ may be transformed to the real membrane surface values either per mm of tubule length per cm^2 of the specific membrane, or per absolute surface of the respective nephron segment membrane system. According to measurements obtained by Frömter (1974) the rat proximal tubular luminal membrane has a resistance of 260 $\Omega \cdot cm^2$, the peritubular or basolateral membrane 92 $\Omega \cdot cm^2$. The real luminal surface has been determined with 62 $mm^2 \cdot cm^{-1}$ for the subcapsular proximal tubule and that of the basolateral cell surface with 37 $mm^2 \cdot cm^{-1}$. With reference to the real membrane surface we now obtain 2.10^4 $\Omega \cdot cm^2$ or conductivities of $5 \cdot 10^{-5}$ S $\cdot cm^{-2}$ and $4.3 \cdot 10^{-4}$ S $\cdot cm^{-2}$. The biochemist is supplied with information that ensures the determination of organelle recovery, for certain subcellular structures like nuclei and mitochondria, after isolation. Furthermore he is provided with information on dissolution or distribution spaces for metabolites or enzymes which are known to be compartmentalized in one of these subcellular components. The exact knowledge of compartment volumes and membrane surfaces bearing specific enzymes may give valuable information concerning the interpretation of enzyme activity measurements obtained from tissue homogenates of the various kidney zones.

The importance of such considerations has already been outlined in discussing the interrelationship between the stereological data and the function of the different nephron segments. With regard to renal and nephron function this is probably best illustrated by the absolute amount of cristae membrane surface, which makes it possible to calculate the number of respiratory chain units since the center to center spacing of cytochrome a is known (Reith et al. 1973). According to the literature there seems to be general agreement upon the fact that this spacing is the same over a variety of cristae membranes from different organs and in different species (Lehninger 1975). The number of cytochrome a molecules or respiratory chains can be calculated as 1.7×10^3 μm^{-2} for mitochondrial cristae membranes. Since the oxygen consumption of 1 µmol cytochrome aa^3 is 5.5 µmol O_2 (Smith et al. 1979) the ATP formed per unit area of mitochondrial cristae membrane and time or per total oxidative phosphorylation surface of the kidney can be calculated. For rat renal oxygen consumption no values are given in the literature unfortunately, but data are available for man and dog where the oxygen consumption is in the range of 2–4 µmol

$O_2 \cdot g^{-1}$ kidney $\cdot$ min^{-1}. Knowing that one mol O_2 yields six mols ATP in oxidative phorphorylation and having calculated 1.06×10^{-8} µmol cytochrome aa_3 (cytochrome c-oxidase) per 3.77 m^2 of cristae surface, for a kidney with a volume of 1320 µl approximately 1 g, 21.04 µmol ATP $\cdot$ min^{-1} should be formed. This value is in good agreement with that of 24 µmol $\cdot$ g^{-1} $\cdot$ min^{-1} reported by Cohen and Kamm (1976) for aerobic ATP formation. From this consideration the absolute surface ATP formation rates for the different nephron segments may be delineated. Thus, for example, the entire proximal nephron epithelium contained within the cortex represented by $S_1 + S_2$ segments should produce at maximum 1.16×10^{-5} mol ATP per min.

Table 39

	ATP µmol · min^{-1}	
Proximal $S_1 + S_2$ epithelium (CORTEX)	11.6	14.2
Proximal S_3 epithelium (OSOM)	2.57	
Thin limb epithelium (ISOM + IM)	0.101	0.101
Medullary ascending distal epithelium (ISOM)	1.632	
Medullary ascending distal epithelium (OSOM)	1.008	5.928
Distal epithelium (CORTEX)	3.29	
Collecting duct epithelium (CORTEX)	0.554	
Collecting duct epithelium (OSOM)	0.084	0.78
Collecting duct epithelium (ISOM)	0.134	
Collecting duct epithelium (IM)	0.038	21.01
Total kidney		21.01

A complete summary of ATP Production rates for the nephron segments is given in Table 39. In addition to this mode of presentation the ATP production can also be expressed per mm of tubule length per minute (Table 40):

All values are calculated under the assumption that oxygen delivery is sufficient to all regions of the kidney. On the basis of ATP formed per mm of proximal tubule

Table 40

		ATP mol min^{-1} · mm^{-1}
Proximal tubule	$S_1 + S_2$ CORTEX	$3.7 \cdot 10^{-11}$
	S_3 OSOM	$2.3 \cdot 10^{-11}$
Thin limb		Not determined
Distal tubule	ISOM	$1.4 \cdot 10^{-11}$
	OSOM	$2.7 \cdot 10^{-11}$
	CORTEX	$6.6 \cdot 10^{-11}$
Collecting duct	CORTEX	$1.62 \cdot 10^{-11}$
	OSOM	$0.24 \cdot 10^{-11}$
	ISOM	$0.32 \cdot 10^{-11}$
	IM	$0.12 \cdot 10^{-11}$

we could check whether or not its amount is sufficient to fuel active Na^+ reabsorption assuming an Na/ATP ratio of 3. For the proximal tubule there exist several direct measurements of this parameter (Frömter 1974; Maude 1974). Frömter concluded that roughly one-third of proximal tubular net Na^+ transport is active and gives a figure of 1.02×10^{-9} mol $\cdot$ cm^{-1} $\cdot$ min^{-1} which would therefore consume 3.4×10^{-10} mol ATP. According to the model calculation the proximal tubule produces 3.7×10^{-10} mol ATP $\cdot$ min^{-1} $\cdot$ cm^{-1}. The metabolic energy produced by proximal tubules thus covers the energy expense of active Na^+ transport and leaves a surplus of ATP in the range of 10%. Determining the whole story on the basis of data given by Maude (1974) for net Na^+ reabsorption, also under the assumption that one-third is transported actively, we end up with 2.3×10^{-10} mol ATP utilized per min and cm of tubule for active Na transport, at a total ATP production of 3.7×10^{-10} mol. This means that a larger surplus of ATP is left, providing phosphorylation energy for other metabolic processes like gluconeogenesis etc., than is calculated from the data given by Frömter. These slight differences are certainly of minor importance since the errors introduced by the experimental procedure might be extensive. Jørgensen (1975) reports an ATP turnover per Na-K-ATPase of 10 000 $\cdot$ min^{-1}. The fact that a unit of Na-K-ATPase has a maximum turnover rate of 10^4 ATP $\cdot$ min^{-1} enables a quantitative analysis of the amount of Na^+ pump sites in our experimental model. Suppose the values of ATP formed per mm tubule length, on the basis of cristae membrane surface contained within this tubule portion, reflect the situation in vivo, then the ratio between ATP formed and the Na-K-ATPase turnover yields the number of maximally active Na^+ transport sites. If we now refer this value to the amount of basolateral surface, the total number of Na^+ pumps per mm of tubule or per unit area of the respective basolateral membrane area can be obtained. Table 37 gives a comprehensive presentation of these interrelationships. The low number of transport sites $2.3–8.8 \times 10^2$ per μm^2 in the peritubular membrane is in striking discrepancy to what we know about ouabain binding sites on the rabbit medullary ascending limb of distal nephron calculated from Shaver and Stirling (1978), which is in the order of 8000, assuming that the peritubular membrane surface per μm^3 of epithelium or cellular volume is comparable to that in the rat. Direct measurements by Deguchi et al. (1977) on freeze-fractured or negatively stained isolated basolateral membranes from rabbit and from rat (Koepsell, personal communication) medulla gives a figure of roughly 13 000–19 000 particles per μm^2 of vesicle membrane, which would correspond to 6000–9000 enzyme molecules, since the stained particles represent dissociated dimers of the enzyme molecule. The numbers of transport sites per μm^2 calculated in Table 37, ranging from 2.3×10^2 in the collecting duct to 8.8×10^2 per μm^2 in the proximal tubule, would imply that every ATPase molecule is working with only one-tenth of its maximum activity. Irrespective of these open questions it should be noted that the number of Na^+ transport sites is of the same order of magnitude per unit area of basolateral membrane (230–880 per μm^2 of basolateral membrane) all over the nephron, with the exception of thin limbs for which no surface per length values have been determined. From this latter feature a correlation between Na-K-ATPase – expressed as Na^+ transport sites – and the basolateral membrane can be delineated, which is quite comparable to the situation above for the mitochondrial cristae membrane. This result would be an expected one if the cytosolic ATP concentration is far below the K_m value. Unfortunately this situation is not met, the cytosolic ATP concentrations in the proximal tubule being about the

same order of magnitude (Guder, personal communication) as found for liver cells (Soboll et al. 1980). The K_m of membrane Na-K-ATPase is 0.32 mmol (Ratanabanangkoon et al. 1973) whereas proximal tubular cytosolic ATP is in the range of 2 mmol/liter. The enzyme therefore is working under conditions of near saturation and would thus be in contradiction to the above interpretation. Whether or not the kinetc characteristics of the Na-K-ATPase determined in vitro can be applied in the described manner is still unanswered.

6.2 The Acutely Injured Kidney Cortex

It is well-known that a number of insults upon the mammalian organism lead to an acute breakdown of renal function. The mechanisms inducing cessation in renal function are usually summarized under the term acute renal failure (ARF) and are always paralleled by severe morphological alterations of proximal tubular epithelium, also known as acute tubular necrosis. We have seen in the preceeding chapters that renal function is unequivocally linked to definite tissue and cell structures. Therefore, the question must be put forward as to whether the numerous functional disturbances during the initiation and maintenance of acute renal failure are a consequence of structural changes of tubular cells or vice verse. Also, the interrelationship between structure and function, once acute renal failure is established and maintained, may be questioned. Detailed information on this question provides, or may provide, the opportunity of gaining access firstly to the chronology of disturbances leading to, and secondly to the mechanisms responsible for, the onset of ARF. Experimental models form the basis for most considerations of the pathophysiologic processes of ARF, with clinical correlates being drawn where available, since more detailed model studies have been performed over the last few years.

6.2.1 The $HgCl_2$ Model

One of the oldest experimental models is intoxication with $HgCl_2$. As shown in results obtained following subcutaneous administration of a low dose $HgCl_2$, glomerular filtration rate decreases within the first 6 h after the intoxication by roughly 30%. At this interval the first morphological changes become apparent. They are confined mainly to the proximal nephron. The stereological analysis confines the changes to a decrease in both luminal and basolateral membrane surface (Table 35) per unit of cytoplasm. As early as 30 min after mercury administration, morphological alterations can be revealed by the stereological analysis. At this time the extracellular space has increased by about 40% above the control value. This increase persists for the whole experimental interval studied. Such an effect has not been recognized in the numerous studies on $HgCl_2$-induced renal injury reported earlier (Oliver et al. 1951; Rodin and Crowson 1962; Gritzka and Trump 1968; McDowell et al. 1976; Ganote et al. 1975). The reason for this effect could be seen in an immediate change in capillary wall permeability to larger molecules like albumin. This assumption seems to be supported by observations of Pinter G. (personal cummunication 1980) who measured enhanced lymph production utilizing a similar experimental protocol. The qualitative morphological findings described in the section on results are fairly consistent with those

reported earlier (McDowell et al. 1976). The quantitative morphological evaluation reveals that there is no swelling of proximal tubular mitochondria as reported by others (McDowell et al. 1976; Ganote et al. 1975), but an increase in lysosomal volume fraction for the cortical S_3 segment of the proximal tubule (Table 33). The most striking result is the decrease of luminal, basolateral, and mitochondrial cristae membrane surface (Table 35) per unit volume of cytoplasm for both the S_2 and S_3 segments of proximal tubule. Since there exist, as we know from the previous chapter, specific biochemical parameters for every one of the affected structures and we have postulated an interrelationship between these, the morphological result must be paralleled by a loss in activity of alkaline phosphatase, Na-K-ATPase, 5′-nucleotidase and cytochrome c-oxidase. Indeed, a diminished Na-K-ATPase activity is found which correlates to the measured reduction of the membrane surface area (Fig. 16). Alkaline phosphatase and 5′-nucleotidase activity, however, is not affected. This latter result does not contradict what has been stated about structure function correlation. Enzyme activity has been measured on kidney cortex homogenates and luminal membranes sludged off the cell's luminal surface may stay active in the tubular lumen over a relatively long time, so that the enzyme activity measured does not reflect the real situation given for the enzyme-bearing structures. Diminution of proximal basolateral membrane surface is substantiated not only by reduced Na-K-ATPase activity but also by increased fractional Na excretion and an elevated output of urine with low osmolarity. This would imply that both Na^+ and volume reabsorption is lower than under control conditions. The cristae membrane surface reduction of 43%, when related to a unit of cytoplasm, is substantiated by a loss in cytochrome c-oxidase activity (Fig. 17) and lower ATP content per mg kidney cortex protein (Fig. 18). The decrease of P/O ratio, cytochrome c-oxidase activity, and mitochondrial cristae membrane is of about the same order of magnitude (Fig. 18). The combined decrease of activity and membrane surface must thus be interpreted as a loss in membrane mass. The increased lysosomal volume fraction could possibly be evaluated as a sign for the occurrence of increased autophagic activity related to membrane degradation. A similar result was described by Fowler and Woods (1977) after oral methyl mercury administration and interpreted as a detoxification response to mercury. The lysosomes were assumed to arise from binding of mercury to the acidic lipoprotein component of lysosomes (Goldstone and Koenig 1969; Nordberg et al. 1974) and/or by internalization of a mercury binding protein. This latter aspect would be supported by the drastically increased volume fraction of apical-coated vacuoles which can be considered to be a morphological correlate of enhanced endocytotic mechanism (Table 33). In the 24-h interval some of the described changes are even more pronounced. Stereological analysis of cortical tissue reveals 14% of the proximal tubular epithelium to be necrotic. The majority of the proximal tubules, however, are comprised of cells with various states of injury. It should be noted in this context that none of the necrotic cells entered a stereological analysis at the ultrastructural level, since the principle of geometric similarity was not fulfilled. Only normally looking cells, and those exhibiting injury up to state 4b according to the classification of Trump and colleagues (Mergner et al. 1976; Trump et al. 1974; Glaumann et al. 1977), were analyzed. Surprisingly for all these cells no remarkable additional quantitative morphological changes can be verified, although in comparison to the 6-h interval the corresponding marker enzymes (Na-K-ATPase, alkaline phosphatase, cytochrome c-oxidase) show an additional loss of activity (Figs. 16, 17). The most drastic enhancement in

functional alteration is found for mitochondria isolated from kidneys 24 h after mercury administration. At this stage the P/O ratio is only 0.66 and the respiratory control index close to 1. The oxygen consumption in state three is reduced, which indicates inhibition of mitochondrial respiration and oxidative phosphorylation. The latter seems supported by a low kidney cortex ATP content (Fig. 18). Mercury was monitored in kidney cortex over the whole treatment interval in order to correlate severity of cell injury and renal dysfunction with the amount accumulated. Interestingly peak tissue Hg is reached within 1 hour after injection and declines toward the 24-h experimental interval (Fig. 23). Calcium concentrations measured from the same samples, however, show significant elevation as compared to controls 6 h after $HgCl_2$ and correlate with the first detectable ultrastructural and mitochondrial damage (Fig. 10). Calcium reaches the highest concentrations at 24 h where at least in necrotic, but also in sublethally injured cells, significant amounts of mitochondrial flocculent densities can be recognized, which are usually considered to be a morphological expression of damaged mitochondria and are brought about by the formation of Ca^{2+} complexes (Glaumann et al. 1977). This seems to illustrate that the events leading to tubular injury must be triggered fairly soon after administration and it appears questionable whether or not the alterations found are all due to a direct effect of Hg^{2+} by binding to membranes or enzymes. In order to clarify this latter point other parameters must be considered. It is likely that the decrease is body temperature which can be measured on $HgCl_2$-treated conscious rats lower renal cortical perfusion remarkably. Evidence for such mechanisms is given by studies recording outer cortical blood flow and systemic blood pressure which are dependent on body temperature (Deetjen and Silbernagl 1972). A decreased blood flow may at least potentially lead to hypoxic conditions for a number of tubular cells and thus induce changes in proximal tubular ionic homeostasis via reduced ATP production. This hypoxia effect will be augmented by increased O_2 affinity at a decreased body temperature. Although it is difficult to experimentally prove such a statement, several indirect sources of information are obtainable which seem to support this interpretation. The first source of information is provided from studies on oxygen binding to rat erythrocytes during $HgCl_2$ treatment. Six hours after mercury erythrocyte 2,3-diphosphoglycerate (2,3-DPG) concentration is elevated by 12% when compared to controls, despite an acidosis of the experimental animals, which will counteract 2,3-DPG formation (Pfaller et al. 1978). This result could be seen at least potentially to be analogous to some human diseases which are paralleled by tissue hypoxia, like anemia, where an increase in 2,3-DPG seems to compensate for the reduced O_2-transport capacity of erythrocytes or generalized hypoxia (Humpeler et al. 1974). A reduction in body temperature of 2 °C would, in addition to reduced cortical perfusion, lead to an increased O_2 affinity and therefore enhance hypoxic conditions. Experimental evidence for reduced outer cortical perfusion in $HgCl_2$ intoxication is provided by studies of Hsu et al. (1977). The mercury, which in addition may have bound to basolateral or luminal membrane, can at least transiently inhibit enzymes like Na-K-ATPase and alkaline phosphatase, and thus contribute to changes in intracellular ionic composition which may trigger changes in mitochondrial function. Mercury bound to the luminal membrane (Goldstone and Koenig 1969; Nordberg et al. 1974) seems to stimulate endocytosis and autophagy and may thereby gain access to cytoplasmic binding sites. A very likely site for such a binding is reduced glutathione (GSH) and the enzymes glutathione-reductase, peroxidase, and synthase. The data in Fig. 21 clearly show GSH depletion 24 h after $HgCl_2$ paralleled by a sub-

stantial loss of activity of GSH reductase and peroxidase (Pfaller et al., 1981). The GSH system is known to be the most important scavenger system for superoxide anions produced during cell metabolism and protects cellular compounds, especially lipids, from free radical formation and auto-oxidation. Indeed, enhanced lipid peroxidation can be determined for this experimental interval in the form of elevated malonyldialdehyde levels in kidney cortex homogenates and isolated mitochondria (Gstraunthaler and Pfaller, to be published). This finding is supported by the fact that the other systems eliminating O_2^-, the superoxide dismutase and catalase, also display reduced activity (Gstraunthaler and Pfaller, to be published). No significant change for GSH could be found 6 h after $HgCl_2$, whereas GSH reductase and peroxidase show a decrease in activity. The loss in membrane mass may therefore be due to disintegration of membranes by enhanced lipid peroxidation. Another possibility for explaining membrane disintegration and loss in surface area would be an activation of phospholipase A_2 by elevated intracellular Ca^{2+}, a hypothesis which is favored by several authors in context with ischemic cell injury (Smith et al. 1980). Since reduction of cellular tocopherol, another antiauto-oxidative substance, is reported to stimulate mitochondrial phospholipase A_2 (Pappu et al. 1978), it could be concluded that in addition to, or instead of Ca^{2+}, GSH might regulate phospholipase A_2 activity and produce an augmented membrane disintegration.

6.2.2 The Maleic Acid Model

Normally, maleic acid-induced renal injury is utilized to simulate experimentally a Fanconi syndrome, characterized by glucosuria aminoaciduria, phosphaturia, and bicarbonaturia. Generally, this syndrome is assumed to result from blockade of essential SH groups (Whorthen and Good 1958) a fact which is confined to maleic acid (Morgan and Friedmann 1938) and of course also to the heavy metal mercury. It may therefore be assumed that the spectrum of changes, the morphological as well as the functional, are similar to those found in mercury ARF. As shown in the results, intraperitoneally administered maleic acid produces structural alterations of proximal tubuli within such a short interval as 2 h. The major part of our attention was focused upon the question of whether or not a correlation between structure or changed structure and the related functional features exists in the case of maleic acid treatment. As can be seen in detail in the chapter dealing with results, similar to $HgCl_2$ intoxication this model is also associated with a marked decrease in gross renal function, which is illustrated by a decrease in GFR, a decrease in Na^+ reabsorption, and just as in the $HgCl_2$ ARF, by an increased urine flow. These findings are in good agreement with the measured changes of biochemical parameters. Two hours after maleic acid the Na-K-ATPase activity, as well as the cytochrome c-oxidase, are diminished. The latter result corresponds well with a reduction in cristae membrane surface area determined for all cortical nephron segments (Tables 34, 36) and is further substantiated by the altered resporatory activity determined on mitochondria isolated from kidney cortex 2 h after maleate administration (Fig. 17). In contrast to structure function correlation on the normal kidney, and in contrast to the effects discussed above for the $HgCl_2$ model, the reduction in Na-K-ATPase activity and the related basolateral membrane are not very pronounced. No statistically significant difference from controls can be found. There is however, a tendency

toward a decrease for both parameters, the enzyme activity and the membrane surface. On the other hand, the extreme sensitivity of mitochondria, relative to other cellular components, is clearly outlined. Tissue glutathione concentrations are decreased in a similar way to the mercury model. The interpretation, namely that depletion in glutathione would stimulate lipid peroxidation and thus induce membrane loss, seems to be valied for this model also since the glutathione peroxidase activity (Gstraunthaler and Pfaller, to be published) is significantly depressed. Glutathione peroxidase is the only enzyme which can prevent the accumulation of hydroperoxides (Chance et al. 1978). As in the mercury model a decrease in body temperature of conscious rats was revealed. The drop in temperature is extreme and amounts to about 6 °C within the 2-h treatment time. In analogy to the interpretation given above for $HgCl_2$-induced ARF, this would lead to a drastically elevated oxygen affinity and, in combination with reduced renal cortical perfusion, to hypoxia, diminished ATP production, and thus to changes in intracellular ion concentrations. This is brought about by accumulation of maleate in the cytoplasm and mitochondria thus lowering the CoA pool (Angielski et al. 1976). Na-K-ATPase could be blocked very early via maleate binding on the membranes outer site but also via the latter mechanisms. The occurrence of vacuolar structures in the apex of proximal tubular cells could be seen as enhanced pinocytotic activity following binding of maleate to the luminal membrane. The two models of renal injury discussed, have been assumed to be a consequence of toxic events. As shown, there are in addition several disturbances which are related to hemodynamic alterations. In order to determine the degree of cellular damage following a primary disturbance in renal hemodynamics, kidneys were injured ischemically.

6.2.3 The Ischemic Model Without Blood Reflow

This type of injury has been extensively studied with respect to qualitative morphological alterations (Glaumann et al. 1975, 1977; Reimer et al. 1972; Venkatachalam et al. 1978) which shall not be discussed here. The quantitative morphological changes (see section on results) display some very interesting features. At the light optical level a raise in proximal epithelial volume density, at the expense of the distal and collecting duct lumen, is the most prominent finding when using a unit volume of cortical tissue as a reference. At the subcellular level, utilizing a unit of cytoplasm as the reference value, we find a decrease in mitochondrial and lysosomal volume density. This might appear somewhat surprising and seems in striking contrast to qualitative observations, reporting a mitochondrial swelling. Keeping in mind the remarkable volume increase of the "container", the tubular cytoplasm or epithelium (Table 32), the measured density of 23% could very well be compatible with swelling. In fact, this finding means that the cytoplasm undergoes a far larger volume increase than the mitochondrial compartment. When the mitochondrial volume density of controls as well as of ischemic kidneys is referred to a unit of cortex it can be recognized that the volume fraction stays unaltered. The description of swollen mitochondria is therefore not adequate. Instead of swelling a change in shape occurs which is supported by a reduced mitochondrial outer membrane surface, which indicates that the mitochondria are less irregularly shaped than usual. The luminal membrane is decreased by a factor of 10, the basolateral membrane by a factor of 2, which also applies for cristae membrane

area. Considering the above-mentioned increase in reference space, the changes are less pronounced relative to a unit of cortex. Certainly an inadequate supply with oxygen and metabolic substrates is the initial, major biochemical aberration in ischemic ARF. The proximal nephron in particular is dependent on oxidative processes for generating ATP, whereas the distal tubule and the collecting duct are able to synthesize ATP under conditions of limited O_2 supply (Schmidt and Guder 1976; Stoff and Epstein 1976). Therefore, energy demanding functions of the proximal tubule are much more susceptible to hypoxia than those of the distal tubule and lack ATP, necessary for the maintenance of structural integrity, which must lead to structural changes. As with the models discussed above, the altered structural parameter corresponds to changes in functions being localized there. The changed functions are documented by a fall in Na-K-ATPase, alkaline phosphatase, and cytochrome c-oxidase activity and are further supported by a remarkable loss in all adenine nucleotides (Figs. 16, 17, 18). Enhancement of anaerobic metabolism during the time of ceased oxygen supply is documented by the accumulation of lactate (Fig. 19). The extremely reduced P/O ratio determined from isolated mitochondria substantiates the experimental findings. Despite the dramatically disturbed metabolism the relative concentration of the adenine nucleotides, as expressed in terms of the number of anhydride-bound phosphate per adenosine moiety, the energy charge, has not decreased below a value incompatible with cellular viability for all proximal tubular cells. This is of importance when investigating renal cortical structure and function after blood reflow.

6.2.4 Ischemia with Blood Reflow

Renal artery clamping with subsequent blood reflow is one of the most widely used and investigated ARF models. The renal functional aspects are reviewed in several recent publications (Oken 1976; Stein et al. 1978; Flamenbaum and Wilson 1978). The severity of cellular damage depends on the period of ischemia (Venkatachalam et al. 1978, Glaumann et al. 1975). After a 45-min clamping and 45-min reflow period, renal function displays all features characteristic for ARF. GFR is only 25% of the control and fractional Na^+ excretion is elevated to 10% of GFR. This latter feature seems to be well explained by a reduction in the activity of cytochrome c-oxidase together with the packing cristae membrane of all cortical nephron segments. This ischemia and reflow period is obviously not sufficient to drastically damage the basolateral membrane system and the Na-K-ATPase. Although there is a decrease in both parameters the changes are not very pronounced. Since mitochondria isolated from cortex still exhibit reduced P/O ratios and the cortical ATP, ADP, and AMP level is significantly lower than under control conditions (Figs. 17, 18), it must be concluded that the functional changes revealed for this model are mainly linked to disturbed mitochondrial respiration and phosphorylation. When evaluating the tissue assembly at light microscopic level (sampling level 1) an enlarged volume density of tubular lumina is apparent (Table 32). The rarefication of the brushborder contributes to this effect only in part. The increased luminal volume is more likely to be caused by obstructive processes which take place in deeper nephron segments or by drastically reduced proximal tubular volume reabsorption. A somewhat surprising result was the fact that renal cortical tissue has lost 50% of its glutathione during the reflow period; whether or not this is linked to enhanced peroxidative processes as in the $HgCl_2$ model cannot be answered at present.

6.2.5 The Hypothermia Model

To what extent hemodynamic alterations contribute to the toxic ARF models may be ascertained when the whole set of parameters physiologic, biochemical, and morphological is determined in an experimental model, using hypothermia as the only insult to induce renal injury. This specific experiment in fact shows that most of the quantitative morphological changes revealed in the ischemic and nephrotoxic injuries are present (Tables 32–36). With regard to renal functional parameters a decrease in GFR and an increase in fractional Na^+ is detected (Fig. 22). These changes, in context with reduced Na-K-ATPase, cytochrome c-oxidase activity, and a fall in mitochondrial respiratory activity (Figs. 17, 18), are fairly comparable to those found in the other models. In contrast to the results for the other experimental protocol, tissue ATP levels are elevated above the control value. Several mechanisms could explain this finding. Together with reduced oxidative phosphorylation capacity the ATP hydrolysis is diminished. First: The amount of reduction in structural equivalents – basolateral and mitochondrial cristae membrane – may contribute to decreased Na-K-ATPase activity to a lesser extent than the fall in body temperature. Second: Respiratory chain enzymes and Na-K-ATPase may respond differently to a fall in temperature. Na-K-ATPase is indeed more susceptible to temperature changes and therefore ATP accumulates despite a reduction in oxidative phosphorylation capacity of mitochondrial cristae membranes. The high lactate levels measured indicate a stimulated anaerobic glycolysis, which, at least to a small extent, can contribute to elevation of ATP. Of course the argument could also be raised that lowered body temperature has a protective effect in the development of injury. That such an argument is not valid may be seen from the nephrotoxic $HgCl_2$ model under rewarming conditions, where the structural and functional changes are less severe than under conditions of no rewarming. In order to clarify which of the postulated pathogenetic sources is the predominant one, the hypoxic or the nephrotoxic, $HgCl_2$ intoxication should be carried out at constant body temperature.

6.2.6 The $HgCl_2$ Model – 6 Hours After $HgCl_2$ and Counterheating

In the event that the hypoxic component induced via the lowered body temperature is a predominant pathogenetic factor, the changes in all parameters determined should be very subtle or missing. As can be seen from the results GFR is indeed not decreased to the same extent as in usual $HgCl_2$ intoxication. The cellular damage, as expressed by volume and surface density values, reveals some differences in comparison to the $HgCl_2$ ARF model without counterheating. The loss in luminal and basolateral membrane mass is less pronounced after $HgCl_2$ and counterheating in both the proximal $S_1 + S_2$ and S_3 segment. In contrast to our expectation, the mitochondrial cristae membrane system of proximal tubules displays an identical change to that found with the $HgCl_2$ treatment without rewarming when compared to the controls, although the qualitative morphological appearance of the cells is quite comparable to the normal situation (Fig. 18). The respiratory function of isolated mitochondria characterized by the P/O ratio is not different from that of the non-rewarmed group. The same applies for the activity of the cytochrome c-oxidase. Considering all these findings the following explanation could be delineated. Evidence for participation of a hemodynamic

mechanism in the very early phase of $HgCl_2$-induced ARF seems to be supported by the fact that under rewarming conditions a higher GFR is found. This seems to prevent some of the early cell injury effects. Since changes of mitochondrial structure and function under conditions of rewarming are identical to those without rewarming, toxic mechanisms must be assumed to be predominant with regard to damage of this system. There is, however, still a slight chance that hypoxia participates in mitochondrial injury, via a direct and early action of mercury on the oxygen transport and binding capacity of erythrocytes, which has not been investigated under rewarming conditions. Irrespective of the pathogenetic aspects stressed in the discussion of kidney injury or ARF models, it must be stated that under conditions of cell damage a close correlation between structure and function is also maintained. The application of a careful quantitative morphological analysis therefore seems to be a valuable tool for revealing basic principles in cell and tissue function, and seems to prove the statement that every biologic function must have a clearly defined structural basis.

7 Summary

The problem concerning if, and to what extent, the architecture of the kidney and especially that of the smallest units – the nephrons – correlate with functional properties has been investigated. Most of the functional data on renal and nephron function deal with transport mechanisms, therefore in the present study the subcellular structures interrelated to transport have been quantified by means of stereology. The sampling procedure of the stereological analysis was carried out in a way which enabled representative estimates of the various portions of the nephrons and their specific subsegments to be obtained. Mean values and spread measures of volume densities of nuclei, lysosomes, and mitochondria contained within a unit of the respective nephron segment, are given.

Furthermore, membrane surface densities per unit of epithelium like the luminal membrane, the basolateral or peritubular membrane, and the mitochondrial membrane have been determined for the various nephron portions. The highest basolateral or peritubular membrane density per cell is related to the thick ascending limb of Henle's loop, the early distal nephron, contained in the inner stripe of outer medulla. A basolateral surface density of the same size is found in the distal convoluted portion of the renal cortex. Mitochondria display their highest cellular volume density within the early distal nephron in the inner stripe of outer medulla and are lowest in papillary collecting ducts. In addition to densities or concentrations per unit of cell or tissue the absolute values for volumes and surfaces can also be given. Expressed in an absolute form, the luminal membrane of proximal tubules amounts to 4.9 m^2, that of basolateral to 1.2 m^2, and that of mitochondrial cristae membranes to 2.5 m^2. Although the total volume of distal nephrons per standard rat kidney is only 130 μl, as compared to the proximal nephrons with 550 μl, their basolateral membrane amounts to 0.6 m^2. If function, as stated dogmatically, is intimately linked to structure, changes in function must be paralleled by changes in structure. For this reason the rat kidney was injured by the toxins $HgCl_2$ and maleic acid, and by clamping the renal artery for 1 h and lowering the body temperature to 30 °C over a period of 2 h. In all cases the reabsorption of sodium is reduced. This effect is combined with a

decrease in activity of the Na-K-ATPase representing the mechanism for removing Na^+ from the nephron lumen into the blood and being localized on the basolateral membrane. In addition, the respiratory activity and the phosporylation capacity of mitochondria is reduced. These effects are linked to a diminuation of luminal, basolateral, and mitochondrial cristae membranes, and clearly illustrate that the close correlation of structure and function, with respect to transport mechanisms, persists also under the condition of cell damage.

References

Abramov M, Orci L (1980) On the "tightness" of the rabbit descending limb of the loop of Henle – physiological and morphological evidence. Int J Biochem 12:23

Angielski S, Pempkowiak L, Gmaj P, Hoppe A, Nowicka C (1976) The effect of maleate and lithium on renal function and metabolism. Curr Probl Clin Biochem 6:142

Aronson NN, Touster O (1974) Isolation of rat liver plasma membrane fragments in isotonic sucrose. Methods Enzymol 31:90

Baines AD, DeRouffignac C (1969) Functional heterogeneity of nephrons. II. Filtration rates, intraluminal flow velocities and fractional water reabsorption. Pfluegers Arch 308:260

Barrett JM, Majack RA (1977) The ultrastructural organization of long and short nephrons in the kidney of the rodent (Octodon degus). Anat Rec 187:530

Barrett JM, Kriz W, Kaissling B, DeRouffignac C (1978a) The ultrastructure of the nephrons of the desert rodent (Psammomys obesus) kidney. I. Thin limb of Henle of short looped nephrons. Am J Anat 151:487

Barrett JM, Kriz W, Kaissling B, DeRouffignac C (1978b) The ultrastructure of the nephrons of the desert rodent (Psammomys obesus) kidney. II. Thin limbs of Henle of long looped nephrons. Am J Anat 151:499

Bell RD, Keyl MJ, Parry WL (1970) Experimental study of sites of lymph formation in the canine kidney. Invest Urol 8:356

Bergmeyer HU, Bernt E, Schmidt F, Stark H (1974) In: Bergmeyer HU (ed) Methoden der enzymatischen Analyse, vol. II. Verlag Chemie, Weinheim, s 1241

Bessey OA, Lowry HO, Broch MJ (1946) A method for measuring alkaline phosphatase activity. J Biol Chem 164:321

Blond DM, Whittam R (1964) The regulation of kidney respiration by sodium and potassium ions. Biochem J 92:158

Bohman SO (1974) The ultrastructure of the rat renal medulla as observed after improved fixation methods. J Ultrastruct Res 47:329

Bourdeau JE, Carone FA (1974) Protein handling by the renal tubule. Nephron 13:22

Bowman W (1842) On the structure and use of the Malphigian bodies of the kidney, with observations on the circulation through the gland. Philos Trans R Soc Lond 1:57

Boyd JE, Palmore P, Mulrow PJ (1971) Role of potassium in the control of aldosterone secretion in the rat. Endocrinology 88:556

Braus H (1929) Anatomie des Menschen. Springer, Berlin Heidelberg New York

Brehe IE, Burch H (1976) Enzymatic assay for glutathione. Anal Biochem 74:184

Buffon GLL (1977) Essai d'arithmetique morale. Suppl Hist Natur (Paris) 4

Burg MB, Bourdeau JE (1978) Function of the thick ascending limb of Henle's loop. In: Vogel HG, Ullrich KJ (eds) New aspects of renal function. Excerpta Medica, Amsterdam Oxford (Workshop conferences Hoechst, Vol VI, p 91)

Burg M, Orloff J (1968) Control of fluid absorption in the renal proximal tubule. J Clin Invest 47:2016

Burg M (1976) The renal handling of sodium chloride. In: Brenner BM, Rector FC Jr (eds) The kidney, vol 1. Saunders, Philadelphia London Toronto, p 272

Chabardès D, Imbert M, Clique A, Montégut M, Morel F (1975a) PTH sensitive adenyl cyclase activity in different segments of the rabbit nephron. Pfluegers Arch 354:229

Carlberg I, Mannervik B (1975) Purification and characterization of the Flavoenzyme glutathione reductase from rat liver. J Biol Chem 250:5475

Carone FA, Peterson DA, Oparie S, Pullman TN (1979) Renal tubular transport and catabolism of proteins and peptides. Kidney Int 16:271

Chabardès D, Imbert-Teboul M, Montégùt M, Clique A, Morel F (1975b) Catecholamine sensitive adenylate cyclase activity in different segments of the rabbit nephron. Pfluegers Arch 361:9

Chalkley HW (1943) Methods for quantitative morphological analysis of tissue. J Natl Cancer Res 4:47

Chance B, Boveris A, Nakase Y, Sies H (1978) Hydroperoxide metabolism. An overview. In: Sies H, Wendel E (eds) Functions of glutathione in liver and kidney, vol 3. Springer, Berlin Heidelberg New York, p 93

Chappell E (1964) The oxidation of citrate, isocitrate and cis-aconitate by isolated mitochondria. Biochem J 90:225

Cohen JJ (1979) Is the function of the renal papilla coupled exclusively to an anaerobic pattern of metabolism? Am J Phsiol 236:F423

Cohen JJ, Kamm DE (1976) Renal metabolism: relation to renal function. In: Brenner BM, Rector FC (eds) The kidney, vol 1. Saunders, Philadelphia London Toronto, p 126

Crayen M, Thoenes E (1975) Architektur und cytologische Charakterisierung des distalen Tubulus der Rattenniere. Fortschr Zool 23:279

Crofton MW (1885) Probability. In: Encyclopedia Britannica, 9th edn, vol 19, p 768

Deetjen P, Silbernagl S (1972) Some new developments in continuous microperfusion. Yale J Biol Med 45:301

Deetjen P, Greger R, Lang F (1978) Renal elimination of endogenous organic adics. In: Vogel HG, Ullrich KJ (eds) New aspects of renal function. Excerpta Medica Amsterdam Oxford (Workshop Conferences Hoechst, vol VI, p 51)

Deguchi N, Jørgensen PL, Maunsbach AB (1977) Ultrastructure of the sodium pump. Comparison of thin sectioning, negative staining, and freeze-fracture of purified, membrane-bound (Na-K)-ATPase. J Cell Biol 75:619

Delesse MA (1847) Procédeé méchanique pour déterminer la composition des roches. CR Acad Sci (Paris) 25:544

Dieterich HJ, Barrett JM, Kriz W, Bulhoff JP (1975) The ultrastructure of the thin loop limbs of the mouse kidney. Anat Embryol (Berl) 147:1

Doucet A, Katz AI (1980) Renal potassium adaptation: Na-K-ATPase activity along the nephron after chronic potassium loading. Am J Physiol 238:F380

Duffin RJ, Meussner RA, Rhines FN (1953) Statistics of particle measurement and of particle growth. Technical Report 52, C.I.T. AF8A – TR 32. Carnegie Institute of Technology, Pittsburgh

Ericson JLE, Trump BF (1969) Electron microscopy of the uriniferous tubules. In: Rouiller C, Muller AF (eds) The kidney, vol. 1. Academic Press, New York London p 351

Ernst SA (1975) Transport ATPase cytochemistry: ultrastructural localization of potassium-dependent and potassium-independent phosphatase activities in rat kidney cortex. J Cell Biol 66:586

Flamenbaum W, Wilson D (1978) Models of acute renal failure. In: Proc VIIth int congr nephrol. Karger, Basel München Paris London New York Sydney, p 687

Fowler BA, Woods JS (1977) Ultrastructural and biochemical changes in renal mitochondria during chronic oral methyl mercury exposure. Exp Mol Pathol 27:412

Frömter E (1974) Electrophysiology and isotonic fluid absorption of proximal tubules of mammalian kidney. In: Thurau K (ed) Kidney and urinary tract physiology, vol. 6. University Park Press, Baltimore, p 2

Frömter E, Geßner K (1974a) Free flow potential profile along rat kidney proximal tubule. Pfluegers Arch 351:69

Frömter E, Geßner K (1974b) Active transport potentials. Membrane diffusion potentials and streaming potentials across rat kidney proximal tubule. Pfluegers Arch 251:85

Ganote CE, Reimer KA, Jennings RB (1975) Acute mercuric chloride toxicity. An electron microscopic and metabolic study. Lab Invest 31:633

Glagolev AA (1933) On the geometrical methods of quantitative mineralogic analysis of rocks. Trans Inst Econ Min (Moscow) 59:1

Glaumann B, Glaumann H, Berezesky IK, Trump BF (1975) Studies on the pathogenesis of ischemic cell injury. II. Morphological changes of the pars convoluta (P_1 and P_2) of the proximal tubule of the rat kidney made ischemic in vivo. Virchows Arch [Cell Pathol] 19:281

Glaumann B, Glaumann H, Trump BF (1977) Studies on cellular recovery from injury. Ultrastructural studies on the recovery of the pars recta of the proximal tubule (P_3 segment) of rat kidney from temporary ischemia. Virchows Arch [Cell Pathol] 25:281

Goldstone A, Koenig H (1969) Lysosomal lipoproteins and enzymes characteristics and biosynthesis. J Cell Biol 43:44

Grantham JJ, Irish JM III (1978) Organic acid transport and fluid secretion in the pars recta (PST) of the proximal tubule. In: Vogel HG, Ullrich KJ (eds) New aspects of renal function, vol VI. Oxford: Excerpta Medica Amsterdam, p 83

Greger R, Lang F, Marchand G, Knox GF (1977) Site of renal phosphate reabsorption. Micropuncture and microinfusion study. Pfluegers Arch 369:111

Gritzka TL, Trump BF (1968) Renal tubular lesions caused by mercuric chloride. Electron microscopic observations. Degeneration of the pars recta. Am J Pathol 52:1225

Gstraunthaler G, Pfaller W (to be published) Superoxide anion metabolism in acute renal failure. Renal Physiology

Gundersen HJG (1977) Notes on the estimation of the numerical density of arbitrary profiles: the edge effect. J Microsc 111:219

Heidenhain R (1874) Mikroskopische Beiträge zur Anatomie und Physiologie der Nieren. Arch Mikrosk Anat Entwicklungsmech 10:1

Heidrich HG, Kinne R, Kinne-Safran E, Hannig K (1972) The polarity of the proximal tubule cell in rat kidney. Different surface charges for the basal infoldings. J Cell Biol 54:232

Hennig A (1956) Bestimmung der Oberfläche beliebig geformter Körper mit besonderer Anwendung auf Körperhaufen im mikroskopischen Bereich. Mikroskopie 11:1

Higashimara E, DuBose TD, Kokko JP (1978) Direct examination of chloride transport across papillary collecting duct of the rat. Am J Physiol 235:F219

Horikawa E (1954) On a new method of representation of the mixture of several austhenite grain sizes. Tetsu To Hagane 40:991

Hsu CH, Kurtz TW, Rosenzweig J, Weller JM (1977) Renal hemodynamics in $HgCl_2$-induced acute renal failure. Nephron 18:326

Humpeler E, Amor H, Braunsteiner H (1974) Unterschiedliche Sauerstoffaffinität des Hämoglobins bei Anämien verschiedener Ätiologie. Blut 29:382

Hyrtl J (1863) Über die Injektionen der Wirbeltiernieren und deren Ergebnisse. Sitzungsber Akad Wiss Wien Math-Naturwiss Kl Abt I 47:146

Hyrtl J (1892) Das Nierenbecken der Säugetiere und des Menschen. Denkschr Akad Wiss Wien 31:107

Imbert M, Chabardés D, Montègut M, Clique A, Morel F (1975a) Adenylate cyclase activity along the rabbit nephron as measured in single isolated segments. Pfluegers Arch 354:213

Imbert M, Chabardés D, Montègut M, Clique A, Morel F (1975b) Vasopressine dependent adenylate cyclase in single segments of rabbit kidney tubule. Pfluegers Arch 357:173

Jacobsen NO (1975) Enzyme histochemical observations on the segmentation of the proximal tubules in the kidney of the female rat. Histochemistry 43:11

Jamison RL, Lacy FB, Pennell PJ, Sanjana VM (1976) Potassium secretion by the descending limb logy, vol VI. Butterworths London, University Park Press, Baltimore, p 199

Jamison RL (1976) Urinary concentration and dilution. In: Brenner BM, Rector FC (eds) The kidney, vol 1. Saunders, Philadelphia London Toronto, p 199

Jamison RL, Lacy FB, Pennell PJ, Sanjana VM (1976) Potassium secretion by the descending limb or pars recta of the juxtamedullary nephron in vivo. Kidney Int 9:323

Javorek D, Gruber W, Bergmeyer HU (1974) Adenosine-5′-triphosphate. In: Bergmeyer HU (ed) Methoden der enzymatischen Analyse, vol II. Verlag Chemie, Weinheim, p 2147

Jørgensen PL (1972) The role of aldosterone in the regulation of (Na-K)-ATPase in rat kidney. J Steroid Biochem 3:181

Jørgensen PL (1975) Isolation and characterization of the components of the sodium pump. Q Rev Biophys 7:239

Kaissling B, Kriz W (1979) Structural analysis of the rabbit kidney. In: Brodal A, Hild W, Van Limborgh J, Ortmann R, Schiebler TH, Tödury G, Wolff E (eds) Advances in anatomy, embryology and cell biology, vol 56. Springer, Berlin Heidelberg New York, p 1

Katz AI, Doucet A (1980) Calcium activated adenosine-triphosphatase along the rabbit nephron. Int J Biochem 12:125

Katz AI, Doucet A, Morel F (1979) Na-K-ATPase activity along the rabbit, rat and mouse nephron. Am J Physiol 237:F114

Kawamura S, Kokko JP (1976) Urea secretion by the straight segement of the proximal tubule. J Clin Invest 58:604

Kinne R (1979) Metabolic correlates of tubular transport. In: Giebisch G, Tosteson DC, Ussing HH (eds) Membrane transport in biology, vol 4. Springer, Berlin Heidelberg New York, p 529

Knox FG, Haas JA, Berndt T, Marchand GR, Youngsberg SP (1977) Phosphate transport in superficial and deep nephrons in phosphate-loaded rats. Am J Physiol 233:F150

Kokko JP (1974a) Urea transport in the proximal tubule and the descending limb of Henle. J Clin Invest 51:1999

Kokko JP (1974b) Membrane characteristics governing salt and water transport in the loop of Henle. Fed Proc 33:25

Kriz W (1967) Der architektonische und funktionelle Aufbau der Rattenniere. Z Zellforsch 82:495

Kriz W, Schnerman J, Dieterich HJ (1972) Differences in the morphology of descending limbs of short and long loops of Henle in the rat kidney. In: Wirz H, Spinelli F (eds) Recent advances in renal physiology. Karger, Basel, p 140

Kriz W, Kaissling B, Psczolla M (1978) Morphological characterization of the cells in Henle's loop and the distal tubule. In: Vogel HG, Ullrich KJ (eds) New aspects of the renal function. Excerpta Medica, Amsterdam Oxford (Workshop conferences Hoechst, vol VI, p 67)

Law PY, Edelmann SI (1978) Effect of aldosterone on incorporation of amino acids into renal medullary proteins. J Membr Biol 41:15

LeHir M, Dubach UC, Schmidt U (1979) Quantitative distribution of lysosomal hydrolases in the rat nephron. Histochemistry 63:245

LeHir M, Dubach UC, Guder WG (1980) Distribution of acid hydrolases in the nephron of renal and diabetic rats. J Biochem (Tokyo) 12:41

Lehninger AL (1975) Biochemistry. Worth, New York

Loud AV (1968) A quantitative stereological description of the ultrastructure of normal rat liver parenchymal cells. J Cell Biol 37:27

Maude DL (1974) Mechanisms of tubular transport of salt and water. In: Thurau K (ed) Kidney and urinary tract physiology, vol 6. University Park Press, Baltimore, p 40

Maunsbach AB (1966) Observations on the segmentation of the proximal tubule in the rat kidney. J Ultrastruct Res 16:239

Maunsbach AB (1973) Ultrastructure of the proximal tubule. In: Orloff J, Berliner RW (eds) Handbook of Physiology, vol 8. Williams and Wilkins, Baltimore, p 31

McDowell M, Nagle RB, Zalme RC, McNeil J, Flamenbaum W, Trump BF (1976) Studies on the pathophysiology of acute renal failure. I. Correlation of ultrastructure and function in the proximal tubule of the rat following administration of mercuric chloride. Virchows Arch [Cell Pathol] 22:173

Mergner WJ, Chang SM, Trump BF (1976) Studies on the pathogenesis of ischemic cell injury. V. Morphologic changes of the pars convoluta (P_1 and P_2) of the proximal tubule of rat kidney made ischemic in vitro. Virchows Arch [Cell Pathol] 21:211

Morgan EJ, Friedmann E (1938) CXVI. Maleic acid as inhibitor of enzyme reactions induced by SH-compounds. Biochem J 32:862

Murer H, Hopfer U (1974) Demonstration of electrogenic Na^+-dependent D-glucose transport in intestinal brush border membranes. Proc Nat Acad Sci USA 71:484

Myers CE, Bulger RE, Tisher CC, Trump BF (1966) Human renal ultrastructure. IV. Collecting duct of healthy individuals. Lab Invest 15:1921

Noll F (1974) Bestimmung mit LDH, GPT and NAD. In: Bergmeyer HU (ed) Methoden der enzymatischen Analyse, Bd II. Verlag Chemie, Weinheim, p 152. 1 (1521)

Nordberg M, Trojanowska B, Nordberg GF (1974) Studies on metal binding proteins of low molecular weight from renal tissue of rabbits exposed to cadium or mercury. Environ Physiol Biochem 4:149

Oken DE (1976) Local mechanisms in the pathogenesis of acute renal failure. Kidney Int 10:94

Oliver JR (1952) Urinary system. In: Lansing AI (ed) Problems of ageing. Williams & Wilkins, Baltimore, p 631

Oliver J, McDowell M, Tracy A (1951) The pathogenesis of acute renal failure associated with traumatic and toxic injury. Renal ischemia, nephrotoxic damage and the ischemic episode. J Clin Invest 30:1307

Osgood RW, Reineck HJ, Stein JH (1978) Further studies of segmental sodium transport in the rat during expansion of the extracellular fluid volume. J Clin Invest 82:311

Pappu AS, Fatterpaker P, Sreenivasan A (1978) Phospholipase A_2 of rat liver mitochondria in vitamin E deficiency. Biochem J 172:349

Peter K (1909) Untersuchungen über Bau und Entwicklung der Niere, vol 1, 2. G Fischer, Jena

Pfaller W, Fischer WM (1980) Sampling for morphometry of mitochondrial membranes. Vth international Congress for Stereology, Salzburg/Austria Sept 3–8, 1979; Mikroskopie:37 (Suppl), 173

Pfaller W, Trump BF (1980) Glycogen deposition in distal tubular cells during $HgCl_2$ induced acute renal failure. Virchows Arch [Cell Pathol] 32:281

Pfaller W, Fischer WM, Stieder N, Wurnig H, Deetjen P (1974) Morphologic changes of cortical nephron cells in potassium-adapted rats. Lab Invest 31:678

Pfaller W, Humpeler E, Deetjen P (1978) Morphometrische und biochemische Untersuchungen zur Entstehung des durch $HgCl_2$ ausgelösten akuten Nierenversagens. 62. Meeting of the German Society of Pathology, Vienna

Pfaller W, Rittinger M, Fischer WM (1979) A concept for stereological investigation of rat kidney. Microsc Acta 82:137

Pfaller W, Gstraunthaler G, Deetjen P (1981) Biochemical aspects of cell injury in acute renal failure.Tel Aviv Symposium on Acute Renal Failure June 16–18, 1981

Pfaller W, Trifilis A, Smith MW, Kahng MW, Trump BF (to be published) Pathogenesis of $HgCl_2$-induced acute renal failure: A combined morphometric and biochemical analysis. Lab Invest

Potter EL (1952) Pathology of the Fetus and the Newborn. Year Book Medical Publishers, Chicago

Rasmussen SN (1973) Intrarenal red cell and plasma volumes in the non-diuretic rat. Determination by means of ^{51}Cr-labelled red cells and ^{125}I-γM-immunoglobulin. Pfluegers Arch 342:61

Ratanabanangkoon K, Dixon JF, Hokein LE (1973) Studies on the characterization of the sodium-potassium transport adenosintriphosphatase. XI. Comparison of kinetic properties of the purified with the impure membrane-bound enzyme from squalus-acanthias. Arch Biochem Biophys 156:342

Reimer KA, Ganote CE, Jennings RB (1972) Alteration in renal cortex following ischemic injury. III. Ultrastructure of proximal tubules after ischemia or autolysis. Lab Invest 26:347

Reith A, Brediezka D, Nolte J, Staudte HW (1973) The inner membrane of mitochondria under influence of triiodothyronine and riboflavin deficiency in heart muscle and liver of the rat. A quantitative electron microscopic and biochemical study. Exp Cell Res 77:1

Rittinger M (1980) Quantitative Morphologie der Rattenniere. PhD dissertation, University of Innsbruck

Roch-Ramel F, Peters G (1981) Renal transport of urea. In: Greger R, Leng F, Silbernagl S (eds) Renal transport or organic substances. Springer, Berlin Heidelberg New York, p 134

Rodin AE, Crowson CN (1962) Mercury nephrotoxicity in the rat. 1. Factors influencing the localization of the tubular lesion. Am J Pathol 41:297

Rollhäuser H, Kriz W, Heinke W (1964) Das Gefäßsystem der Rattenniere. Z Zellforsch 64:381

Rosiwal A (1898) Über geometrische Gesteinsanalysen. Verh K.K. Geol Reichsanst Wien 143

Sachs L (1969) Statistische Auswertungsmethoden. Springer, Berlin Heidelberg New York, p 723

Saltykov SA (1958) Stereometric metallography, 2nd edn. State publishing House for Metals and Sciences, Moscow

Schafer JA, Patlak CS, Andreoli TE (1977) Fluid absorption and active and passive ion flows in the rabbit superficial pars recta. Am J Physiol 233:F154

Schmidt U, Dubach UC (1971) Quantitative Histochemie am Nephron. Prog Histochem Cytochem 2:185

Schmidt U, Schmidt J, Schmid H, Dubach UC (1975) Sodium- and potassium-activated ATPase. A possible target of aldosterone. J Clin Invest 55:655

Schmidt U, Guder W (1976) Sites of enzyme activity along the nephron. Kidney Int 9:233

Schmidt-Nielsen B, Reinking L (1980) Pulsatile urine flow and fluid reabsorption in papillary collecting ducts of the hamster kidney with intact renal pelyis. In: XXVII int. congress of physiological sciences, vol XIV. Hungarian Physiologic Society, Budapest, p 687

Schwartz MM, Venkatachalam MA (1974) Structural differences in thin limbs of Henle: Physiological implications. Kidney Int 6:103

Sendroy AL, Dillon RT, v Slyke DD (1934) Studies of gas and electrolyte equilibria in blood: Solubility of carbon dioxide at 38° in water, salt solution, serum and blood cells. J Biol Chem 105:597

Shaver JLF, Stirling C (1978) Ouabain binding to renal tubules of the rabbit. J Cell Biol 76:278
Silbernagl S (1977) The role of brush border enzymes in tubular reabsorption of disaccharides. A microperfusion study in rat kidney. Pfluegers Arch 371:141
Silva P, Torretti J, Hayslett JP, Epstein FH (1976) Relation between Na-K-ATPase and respiratory rate in the rat kidney. Am J Physiol 230:1432
Singer TH (1974) Determination of the activity of succinate, NADH, choline and -glycerophosphate dehydrogenase. In: Glick D (ed) Methods of biochemical analysis, vol 22. John Wiley & Sons, New York, p 123
Smith CS, Guttman L (1953) Measurement of internal boundaries in three-dimensional structures by random sectioning. Trans AIME 197:81
Smith MW, Collan Y, Kahng MW, Trump BF (1979) Changes in mitochondrial lipids of rat kidney during ischemia. Biochim Biophys Acta 618:192
Smith L, Davis HC, Nava ME (1980) Reaction of cytochrome-c-oxidase with endogenous and exogenous cytochrome-c. Biochemistry 19:4261
Soboll S, Akerboom TPM, Schwenke WD, Haase R, Sies H (1980) Mitochondrial and cytosolic ATP/ADP ratios in isolated hepatocytes. Biochem J 192:951
Staehelin LA (1974) Structure and function of intercellular junctions. Int Rev Cytol 39:191
Stein JH, Osgood RW, Kunau RT (1976) Direct measurement of papillary collecting duct sodium transport in the rat. J Clin Invest 58:767
Stein JH, Lifschitz MD, Barnes LK (1978) Current concepts on the pathophysiology of acute renal failure. Am J Physiol 234:F171
Stephenson JL (1973a) Concentrating engines and the kidney. I. Central core model of the renal medulla. Biophys J 13:512
Stephenson JL (1973b) Concentrating engines and the kidney. II. Multisolute central core system. Biophys J 13:546
Stoff JS, Epstein FH (1976) Recent advances in renal tubular biochemistry. Ann Rev Physiol 38:46
Tisher CC (1976) Anatomy of the kidney. In: Brenner BM, Rector FC (eds) The kidney, vol 1. Philadelphia London Toronto, p 3
Tisher CC, Bulger RE, Trump BF (1968) Human renal ultrastructure. III. The distal tubule in healthy individuals. Lab Invest 18:655
Tomkeieff SI (1945) Linear intercepts, areas and volumes. Nature 155:24
Trueta J, Bareley AE, Daniel PM, Franklin KJ, Prichard MML (1947) Studies of the renal circulation. vol VI. Thomas, Springfield, p 39
Trump BF, Strum JM, Bulger RE (1974) Studies on the pathogenesis of ischemic cell injury. I. Relation between ion and water shifts and cell ultrastructure in rat kidney slices during swelling at 0–4 °C. Virchows Arch [Cell Pathol]16:1
Tune B, Burg M (1971) Glucose transport by proximal tubules. Am J Physiol 221:580
Tune B, Burg M, Patlak C (1969) Characteristics of p-aminohippurate transport in proximal renal tubules. Am J Physiol 217:1057
Ullrich KJ, Frömter E, Murer H (1979) Prinzipien des epithelialen Transportes in Niere und Darm. Klin Wochenschr 57:977
Underwood EE (1968) Particle size distribution. In: DeHoff RT, Rhines FN (eds) Quantitative Microscopy. McGraw Hill, New York, p 149
Van Slyke DD, Sendroy AL, Dillon RT (1928) Studies of gas and electrolyte equilibria in blood: Solubility and physical state of uncombined oxygen in blood. J Biol Chem 78:765
Venkatachalam MA, Bernard DB, Donohoe JF, Levinsky GL (1978) Ischemic damage and repair in the rat proximal tubule: differences among the S_1, S_2 and S_3 segments. Kidney Int 14:31
Von Möllendorff W (1930) Der Exkretionsapparat. In: v Möllendorff W (ed) Handbuch der mikroskopischen Anatomie des Menschen, vol VII/1. Springer, Berlin Heidelberg New York, p 1
Vurek GG, Pegram SE (1966) A fluorimetric method for the determination of naogram quantities of inulin. Anal Biochem 16:409
Wade JB, O'Neil RG, Pryor JL, Boulpaep EL (1979) Modulation of cell membrane area in renal collecting tubules by corticosteroid hormones. J Cell Biol 81:415
Weibel ER (1963) Morphometry of the human lung. Springer, Berlin Heidelberg New York
Welling LW, Welling DJ (1975) Surface areas of brush border and lateral cell walls in the rabbit proximal nephron. Kidney Int 8:343

Welling LW, Welling DJ (1976) Shape of epithelial cells and intercellular channels in the rabbit proximal nephron. Kidney Int 9:385
Wharton DC, Tzagoloff A (1967) Cytochrome oxidase from beef heart mitochondria. Methods Enzymol 10:245
Whorthen HG, Good RA (1958) The de Toni-Fanconi syndrome with cystinosis. Am J Dis Child 95:653
Wright FS, Giebisch G (1978) Renal potassium transport: contributions of individual nephron segments and populations. Am J Physiol 235:F515
Wright FS, Strieder N, Fowler NB, Giebisch G (1971) Potassium secretion by distal tubule after potassium adaptation. Am J Physiol 221:437

Other Reviews of Interest in this Series

Volume 60

R. Hildebrand: Nuclear Volume and Cellular Metabolism.
1980. 12 figures, 11 tables. VII, 54 pages
ISBN 3-540-09796-1

Volume 61

H. Korr: Proliferation of Different Cell Types in the Brain.
1980. 21 figures, 1 table. VII, 72 pages
ISBN 3-540-09899-2

Volume 62

B. Brown Gould: Organization of Afferents from the Brain Stem Nuclei to the Cerebellar Cortex in the Cat.
1980. 10 figures, 2 tables. VIII, 90 pages
ISBN 3-540-09960-3

Volume 63

G.H. Rager: Development of the Retinotectal Projection in the Chicken.
1980. 66 figures, 4 tables. VII, 92 pages
ISBN 3-540-10121-7

Volume 64

A. Brodal, K. Kawamura: Olivocerebellar Projection: A Review.
1980. 45 figures. VII, 140 pages
ISBN 3-540-10305-8

Volume 65

E. Pannese: The Satellite Cells of the Sensory Ganglia.
1981. 30 figures. IX, 111 pages
ISBN 3-540-10219-1

Volume 66

H.-M. Schmidt: Die Artikulationsflächen der menschlichen Sprunggelenke.
1981. 45 figures. VIII, 81 pages
ISBN 3-540-10306-6

Volume 67

H. Wolburg: Axonal Transport, Degeneration and Regeneration in the Visual System of the Goldfish.
1981. 28 figures. IX, 94 pages
ISBN 3-540-10336-8

Volume 68

A.A.M. Gribnau, L.G.M. Geijsberts: Developmental Stages in the Rhesus Monkey (Macaca mulatta).
1981. 27 figures. VI, 84 pages
ISBN 3-540-10469-0

Volume 69

L. Záborszky: Afferent Connections of the Medical Basal Hypothalamus.
1981. 31 figures, approx. 9 tables. Approx. 120 pages
ISBN 3-540-11076-3

Springer-Verlag
Berlin
Heidelberg
New York

A.G. Brown

Organization in the Spinal Cord

The Anatomy and Physiology of Identified Neurones

1981. 148 figures, approx. 2 tables. XII, 244 pages
ISBN 3-540-10549-2

The successful introduction of Horseradish Peroxidase (HRP) as a neurone marker has generated a mass of data on the spinal cord, leading to a considerable revision of previously accepted neurophysiological ideas. Although some results from the use of this method have been published in scientific journals, the restrictions they impose on space, format and numbers of illustrations led the author of this monograph to undertake its publication to allow extended coverage and discussion of results in one place.

Organization in the Spinal Cord is not just a text on spinal cord anatomy and physiology, it is also a description of results obtained using the intracellular injection of HRP, together with other complementary experiments on selected axons and neurones, specifically on the larger cutaneous axons and dorsal horn neurones and on the larger muscle afferent fibers and motoneurones. This book presents a sufficient amount of new material for review and assessment to suggest that the time has come for a complete rethinking of structural-functional relationships in the mammalian central nervous system. *Organization in the Spinal Cord* will help make neurobiologists aware of the value of working with identified neurones, while providing anatomists, physiologists, pharmacologists and developmental biologists with invaluable information on normal structural-functional relationships in the spinal cord.

Springer-Verlag
Berlin
Heidelberg
New York